THE HYDROGENATION OF CINNAMALDEHYDE OVER SILICA SUPPORTED COPPER AND MODIFIED COPPER CATALYSTS

By

ALAN CHAMBERS

A THESIS SUBMITTED FOR THE DEGREE OF

DOCTOR OF PHILOSOPHY OF THE UNIVERSITY OF GLASGOW

DEPARTMENT OF CHEMISTRY, JANUARY 1994

ProQuest LLC.
789 East Eisenhower Parkway
P.O. Box 1346
Ann Arbor, MI 48106 – 1346

This thesis is dedicated to my Mum and Dad without whose help I would not have been able to start my PhD never mind complete it.

"…. what a catalyst you turned out to be"

The Jam "Eton Rifles"

ACKNOWLEDGEMENTS

I should like to thank my supervisors, Professor G. Webb and Doctor Diane Stirling, for their continual help and advice during the past three years. Special thanks should be given to Diane for her enthusiasm towards the project.

Thanks also to Doctor Tom Baird and Vicky Yates for their help with the electron micrographs and to Doctor David Jackson for work carried out at I.C.I. Billingham. I am indebted to the Science and Engineering Research Council for providing the funding for this project.

Great thanks are due to the Technical Staff at the University and to the many people that have shared the same research rooms as myself during my Ph.D for their help, encouragement and general "patter". Among these special thanks must go to Isobel Matheson and Colin Park for their help in producing this thesis.

SUMMARY

A series of silica supported copper and modified copper catalysts has been prepared, characterised and used for the hydrogenation of cinnamaldehyde. Supported copper catalysts were doped with V, Pd or Ru to investigate their effects on the catalytic activity and selectivity.

The catalysts were prepared by impregnation of preformed silica pellets with metal salts of the appropriate ions. The metal components of the catalysts were as follows:-

Cu/SiO_2	$Cu/V/SiO_2$	$Cu/V/Pd/SiO_2$
$Cu/Pd/SiO_2$	$Cu/Ru/SiO_2$	V/SiO_2.

The copper, palladium and ruthenium contents of the catalysts were varied. Grace and PQ silicas were used. These silicas were supplied by I.C.I.

The catalysts were characterised using temperature programmed reduction (TPR) studies and the copper metal dispersions were calculated by following the decomposition of N_2O over the reduced catalysts. Selected catalysts were also characterised by hot stage x-ray diffraction (XRD), transmission electron microscopy (TEM) and mercury porosimetry.

TPR studies of copper oxide supported on Grace and PQ silica showed that the TPR profile could be drastically altered by varying

1. copper metal content
2. the silica support
3. the procedure for calcination of the precursors.

The reduction temperature was found to increase with increasing copper metal content and extra high temperature peaks were sometimes observed.

The reduction temperature of the TPR profiles was lowered and reduction took place over a narrower temperature range when the higher surface area Grace silica was used as a support rather than PQ silica.

Calcination of the uncalcined supported precursors in flowing air rather than in a muffle oven also resulted in a lowering of the reduction temperature. The silica supported CuO and V_2O_5 calcined catalyst precursor was found to reduce concomitantly at the temperature normally found for the supported CuO although supported V_2O_5 itself reduced at much higher temperatures. Generally addition of palladium to the supported copper oxide lowered the reduction temperature while a new low temperature reduction peak emerged when ruthenium was added to supported CuO.

The copper metal dispersion was highest in the copper oxide on Grace silica catalysts. The V_2O_5 had no effect on the copper metal dispersion but the addition of palladium generally increased the dispersion. Increasing the content of ruthenium chloride in the catalyst precursor resulted in a decrease in the copper metal dispersion in the reduced catalyst. Dispersion was improved for copper by calcining the catalyst precursors in flowing air rather than in a muffle oven, and also by calcining at lower temperatures.

Although in the hydrogenation of cinnamaldehyde, selective reduction of the carbon-carbon double bond was generally favoured, optimisation of the preparative variables resulted in the production of Cu/SiO_2 catalysts which were selective for the production of cinnamyl alcohol from cinnamaldehyde. The rate of hydrogenation was found to be

greater on the Grace supported copper than on its PQ counterpart. However, the Grace supported copper metal catalysts always selectively hydrogenated the carbon-carbon double bond in the cinnamaldehyde to form hydrocinnamaldehyde. The addition of palladium to the catalysts also increased the hydrogenation rate, forming mainly hydrocinnamaldehyde. Selectivity to cinnamyl alcohol was induced by adding $RuCl_3$ to the supported copper catalyst precursor. Addition of V_2O_5 to the supported copper catalysts resulted in a loss of activity.

Generally the catalysts which showed high activities were less selective for cinnamyl alcohol formation. These catalysts also were found to reduce at lower temperatures in the TPR profiles and have the higher copper metal dispersions.

The variations in the hydrogenation properties of each of the catalysts was assigned to a combination of the following factors:-

1. the addition of an extra metal
2. the copper metal particle size
3. metal-support interactions.

The results were interpreted in terms of a concerted mechanism in which phenyl propanol was formed by the successive hydrogenation of hydrocinnamaldehyde and cinnamyl alcohol.

Page

Page

Chapter 1

INTRODUCTION

1.1 GENERAL INTRODUCTION

1.1.1 Catalysis

It was first noticed in the early part of the 19th century that a number of chemical reactions were affected by trace amounts of substances which did not appear to be used up in the course of the reaction (1). Traces of acid brought about the hydrolysis of starch and low concentrations of some metal ions (although at this point in time they had not been identified as such) affected the decomposition of hydrogen peroxide. Amongst the most startling effects, however, were those shown by the noble metals, platinum and palladium.

Michael Faraday was one of the first to use a noble metal as a catalyst in a reaction when he used it to sustain the oxidation of ethanol vapour. J. W. Döbereiner discovered that platinum could bring about the oxidation of hydrogen (2).

At the time those discoveries were being made, however, there was no attempt to link them to chemical reactivity due to the extent of available knowledge and it was not until 1836 that some rationalisation of the findings took place. It was J. J. Berzelius who first coined the words "Catalytic Power" and "Catalysis" and he defined the power of the catalyst as being that which is able to "awake the affinities, which are asleep at this temperature, by their mere presence and not by their own affinity." It was not until 1894, however, that Ostwald gave us the modern concept of catalysis as a method of controlling the rate and the

direction of a chemical reaction (3).

The best definition of a catalyst is "a catalyst is a substance which increases the rate of attainment of equilibrium of a reacting system without causing any great alteration to the free energy changes involved" (4).

Catalysis is a purely kinetic process in which the rates of both forward and reverse reactions are equally affected. A catalyst, therefore, can only alter the rate of a chemical reaction that is thermodynamically feasible, that is, a reaction which involves a decrease in free energy. It is incorrect to say that the catalyst should remain unchanged at the end of the reaction as, in practice, catalysts are sintered, eroded, etched or covered in residues left behind by the reacting molecules. The rate enhancement by catalysis is realised by a lowering of the activation energy of the reaction, achieved through the transitory adsorption (almost always chemisorption) of one or more reactants onto the surface of the catalyst.

Catalysts these days are highly important in the chemical industry, being involved in the "cracking" process to form fuel from the residual oil left after the fractional distillation process. The reforming process involves the use of catalysts to increase the octane rating of various hydrocarbons in order to produce a superior quality fuel. Catalysts are also used extensively in the petrochemical and fine chemicals industry.

1.1.2 Hydrogenation Reactions

The addition of hydrogen across a multiple bond is one of the easiest and most studied catalysed reactions. The process whereby hydrogen is added across a multiple bond is known as hydrogenation. Metals are good catalysts for hydrogenation and are used in a variety of physical forms, wires, gauzes, finely divided metal powders or most commonly when supported on a carrier.

A supported metal catalyst usually contains more than 80% w/w carrier. The purpose of the carrier is to act as a means of increasing the dispersion of the supported metal, giving the resulting catalyst physical and mechanical properties superior to those of the unsupported metal (5). Supported copper, for example, is an active hydrogenation catalyst whereas the unsupported metal is ineffective (6). Supported copper catalysts have been used extensively in this capacity for reactions that demand a high degree of selectivity such as in the partial hydrogenation of vegetable oils or fragrant substances (7, 8). For oils and fatty acids the main objective is to decrease the concentration of conjugated, unsaturated molecules, which are sensitive to oxidation, without reaching saturation. In perfumery the synthesis of fragrances requires the selective formation of allylic alcohols from α,β-unsaturated aldehydes or ketones. However, despite the reported high activity of copper catalysts for the hydrogenation of carbonyl bonds compared with carbon-carbon double bonds (9) surprisingly low selectivity was found in the hydrogenation of α,β-unsaturated aldehydes or ketones (10).

This thesis is concerned with trying to develop supported copper catalysts that will selectively hydrogenate α,β-unsaturated aldehydes to the corresponding allylic alcohol. The hydrogenation of cinnamaldehyde (3-phenyl prop-2-enone) has been chosen as a test reaction. The reaction was carried out in the liquid phase. This reaction has been studied extensively in the past and the factors that affect selectivity are described in this chapter.

1.1.3 Selective Hydrogenation

The selectivity of a catalyst to preferentially catalyse one of several thermodynamically possible reactions is an important feature of heterogeneous catalysis. The ability of a catalyst to selectively hydrogenate either a carbon-carbon double bond or a carbon-oxygen double bond has been investigated in this project. In the hydrogenation of cinnamaldehyde, if it is assumed that the benzene ring is not hydrogenated and no other reactions occur, there are three possible products (Figure 1.1).

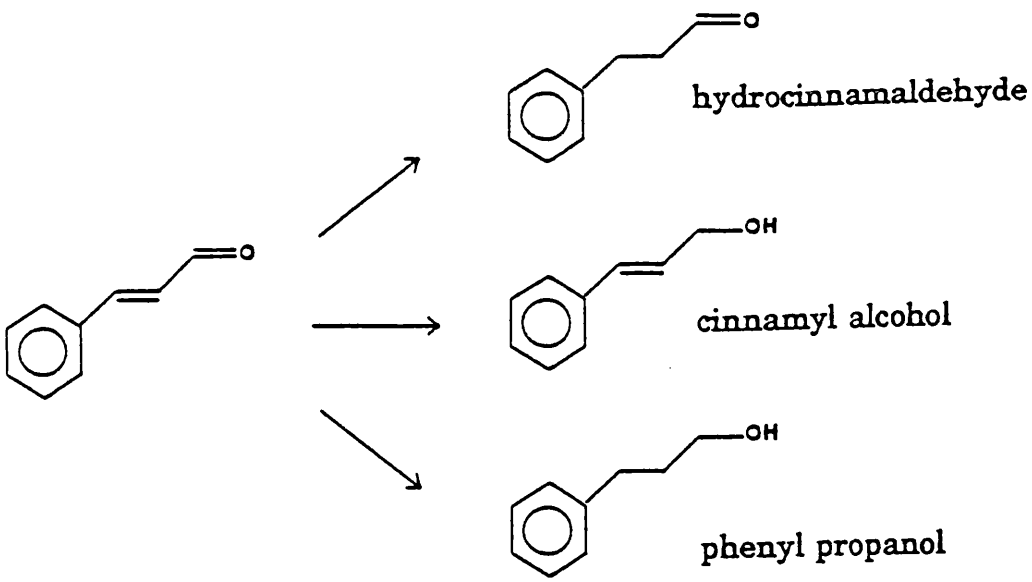

Figure 1.1 Possible Products of Cinnamaldehyde Hydrogenation.

The selectivity for the product cinnamyl alcohol is the fraction that it constitutes of the total products.

1.1.4 Diffusion Limitations

The reaction between molecules adsorbed on the surface of a catalyst, or between adsorbed and gaseous molecules, may be broken down into five basic steps.

1. Transport of reactants to the catalyst.
2. Adsorption of the reactants on the catalyst.
3. Reaction on the catalyst involving one or more adsorbed reactant.
4. Desorption of the products from the catalyst.
5. Transport of products away from the catalyst.

Any one of these five steps can be rate determining. Steps 2, 3 and 4 can be regarded as jointly constituting the catalytic reaction. Step 1, however, is a physical process whereby the reactants are brought through the gaseous or liquid phase surrounding the solid catalyst to the active sites on the catalyst surface. This is a diffusion process, and the phenomenon is called mass transport or mass transfer. Step 5 is the corresponding process for getting products away from the surface. When either step 1 or 5 is slower than the catalytic rate itself, the rate is determined by the rate of arrival of reactants (or removal of products) and the rate is said to be diffusion or mass transport limited.

Reactions where a liquid phase is present, as in this study, are far more likely to become diffusion limited than those where only gaseous reactants are present. Reactions where diffusion limitations are present can be recognised by the following characteristics.

1. The rate is proportional to the catalyst weight raised to a power less than unity, which in the limit may be zero.
2. The rate is increased by better agitation of the liquid with respect to the catalyst.
3. The apparent activation energy may be as low as 10 - 15 kJ mol^{-1}.

Reactions whose rate is not governed by diffusion limitations show the following features.

1. The rate is proportional to the catalyst weight.
2. The rate is unaffected by better agitation although it is often found that a minimum rate of stirring or shaking has to be exceeded

before the liquid surface begins to break up and, thus, before reasonable rates of reaction are observed.

3. The apparent activation energy is usually in excess of 25 kJ mol^{-1}.

Owing to the low solubility of hydrogen in most liquids it is almost always the transport of hydrogen to the catalyst that will limit the reaction rate rather than the diffusion of organic molecules to the catalyst surface. The concentration of dissolved hydrogen can be increased by using a solvent with a high solubility for hydrogen, or by using low temperatures and high pressures. This minimises the chance of diffusion becoming the slowest step in the whole process. Other methods recommended to avoid diffusion limitation are low catalyst weights and good agitation of the reaction mixture.

1.2 SELECTIVE HYDROGENATION REACTIONS

The hydrogenation of αβ-unsaturated aldehydes has been studied extensively in the past. The selectivity towards unsaturated alcohol is governed by the nature of the metal itself but other features can be utilised to increase selectivity, namely

1. The metal particle size
2. The effect of promoters
3. The support and metal support interactions

These will all be discussed in this section.

Much of the previous work for this reaction has centred on copper supported on chromia (copper chromite) and it is useful here to give a brief summary of copper chromite as a selective hydrogenation catalyst.

1.2.1 Copper Chromite

Copper based catalysts are used in a wide variety of high added value, low volume processes as well as large scale processes such as methanol synthesis. The most widely used copper catalysts, apart from those used in making methanol, are supported on chromia, the so-called copper chromite system. Copper chromite is often the catalyst of choice for selective hydrogenations of one functional group in the presence of another and is extensively used throughout the chemical industry for a wide range of reductions, including the hydrogenation of esters, unsaturated aldehydes, nitriles, fatty acids and dienes (9, 11, 12, 13). The selectivities of different copper containing catalysts were shown to be practically

independent of the type of catalyst, therefore it was ascribed to the copper part (14). The form of copper that contributes most to the activity is a topic under constant discussion (14, 15). However, it is generally thought that the active species is metallic copper formed during hydrogenation at pressures greater than 10 atmospheres, in accordance with the theory suggested by Rabes and Schenk (16).

It has been shown that some reactive species (H^*), different from those of hydroxyl groups, are present in the bulk of the cubic spinel phases obtained by the reduction of copper chromite catalysts (17, 18). These H^* species were considered to be responsible for hydrogenation of dienes in the absence of gaseous hydrogen. For isopropene, the hydrogen content of the solid was varied and controlled by isoprene hydrogenation reaction. In this instance copper chromite functioned as a reservoir for hydrogen in a manner similar to that observed for hydrogen bronzes such as $LaNi_5$ or $PtWO_3$ (19, 20). It has also been shown, by using isoprene deuteration , that the H^* species has a very important catalytic role since it is directly involved in the hydrogenation process occurring under molecular hydrogen flow (21). The catalytic site for hydrogenation was formed by the association of a H^* species with a cuprous ion in an octahedral environment (22).

The activity of copper chromite catalysts has been studied by following the reaction mechanism of isoprene hydrogenation using deuterium as a tracer atom (23). Figure 1.2 illustrates the variation in product distribution obtained by the authors in the isoprene hydrogenation

reaction and the general reaction network is shown in Figure 1.3.

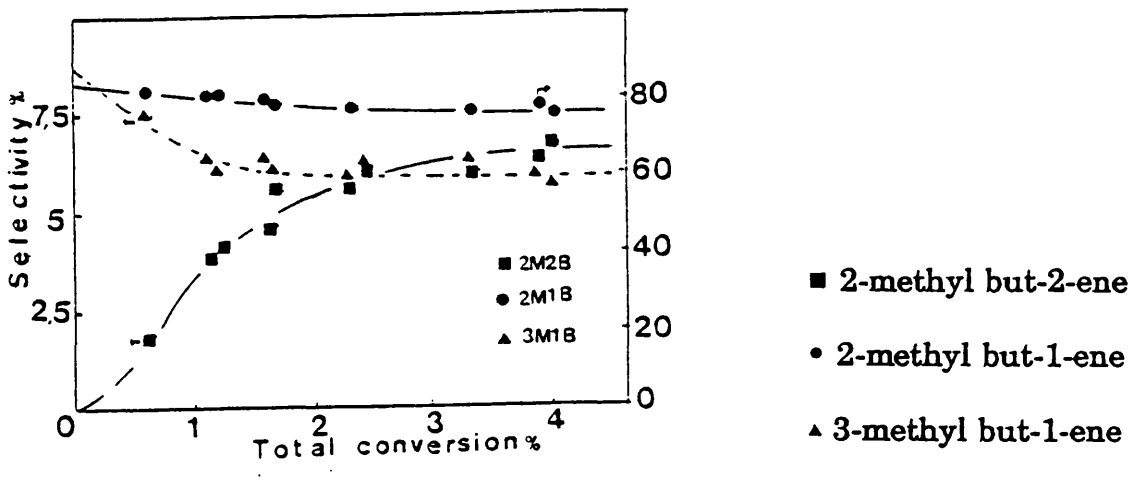

Figure 1.2 Isoprene Hydrogenation: Selectivities versus total Conversion.

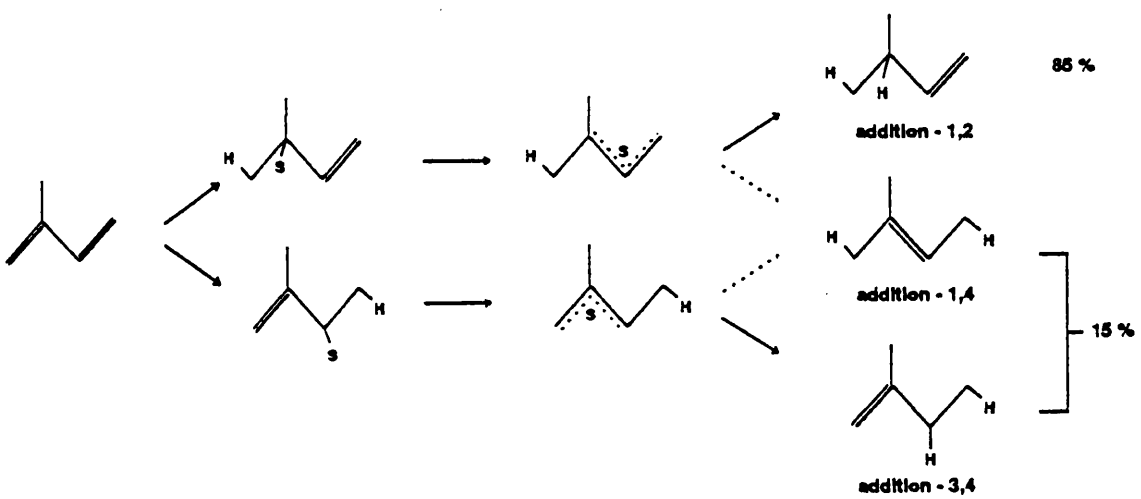

Figure 1.3 General Reaction Network for Isoprene Hydrogenation.

Analysis of the isoprene hydrogenation pattern suggested that the reaction selectivity was essentially governed by three different effects which are listed in order of decreasing importance

a) steric hindrance of substituent groups

b) electronic effects

c) formation of conjugated intermediates

This was characteristic of a nucleophilic attack with the nucleophile being a hydride ion.

Further problems were apparent when attempting to hydrogenate carbonyl bonds. Jenck and Germaine (9) studied the competitive hydrogenation of aldehydes, ketones and olefins over copper chromite catalysts. They proposed a general scale of reactivity

$$C{=}O \text{ (aldehyde)} > C{=}O \text{ (ketone)} > C{=}C.$$

Reactivity of acyclic olefins obeys Lebedev's rule

$$\text{i.e. } -CH{=}CH_2 > -CH{=}CH- > C{=}CH-.$$

This scale of reactivity was extended to non-conjugated carbonyl compounds and, as expected, high enol selectivity was obtained when an unhindered carbonyl bond was associated with an unhindered carbon-carbon double bond. However this prediction broke down with the hydrogenation of conjugated carbonyl systems where low functional group and monohydrogenation selectivity was found (Table 1.1).

Table 1.1 Crotonaldehyde Hydrogenation.

Total conversion %	Butanal mole %	2-Buten-1-ol mole %	1-Butanol mole %
0.1	84.5	15.5	-
0.2	87.0	13.0	-
0.4	88.3	11.7	-
1.2	91.1	9.1	-
1.6	93.5	6.5	-
2.1	92.2	7.8	-
3.2	92.7	7.3	-
10.2	91.8	7.2	2.0
20.5	88.6	6.6	4.9
25.5	88.0	6.1	5.9
38.6	86.2	6.8	7.0
49.0	78.2	6.0	15.2

Functional group selectivity in the hydrogenation of conjugated carbonyls is influenced by the same factors as that of dienes and they react in a slightly similar way (Figure 1.4).

However high polarisation of the conjugated carbonyl system leads to a selective attack on carbons 2 and 4 by a hydride ion (10) (Figure 1.5).

In all these reactions the formation of a 1-enol was never detected. This suggested that only 3,4 or 1,2-hydrogenation routes were possible. However a 1-enol is easily isomerised and therefore the existence of a 1,4-hydrogenation pathway cannot be ruled out.

Functional group selectivity in these reactions was governed by the following effects, listed in order of decreasing importance as

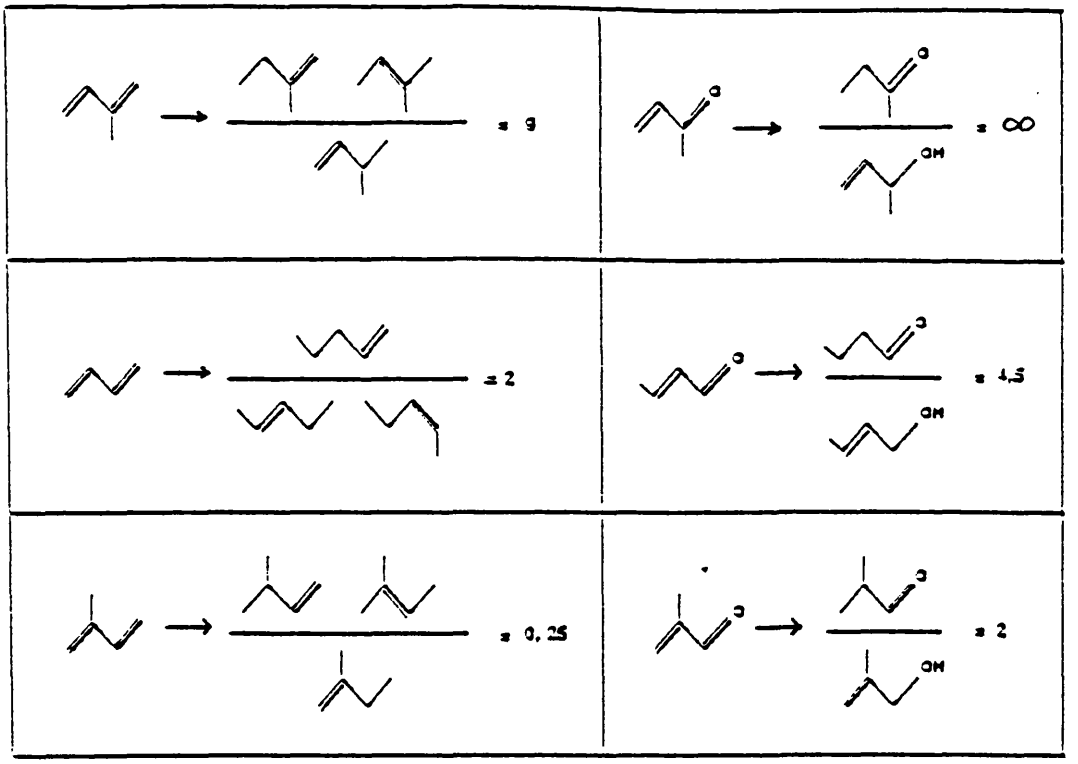

Figure 1.4 Functional Group Selectivity: Comparison of Conjugated Carbonyls with Dienes.

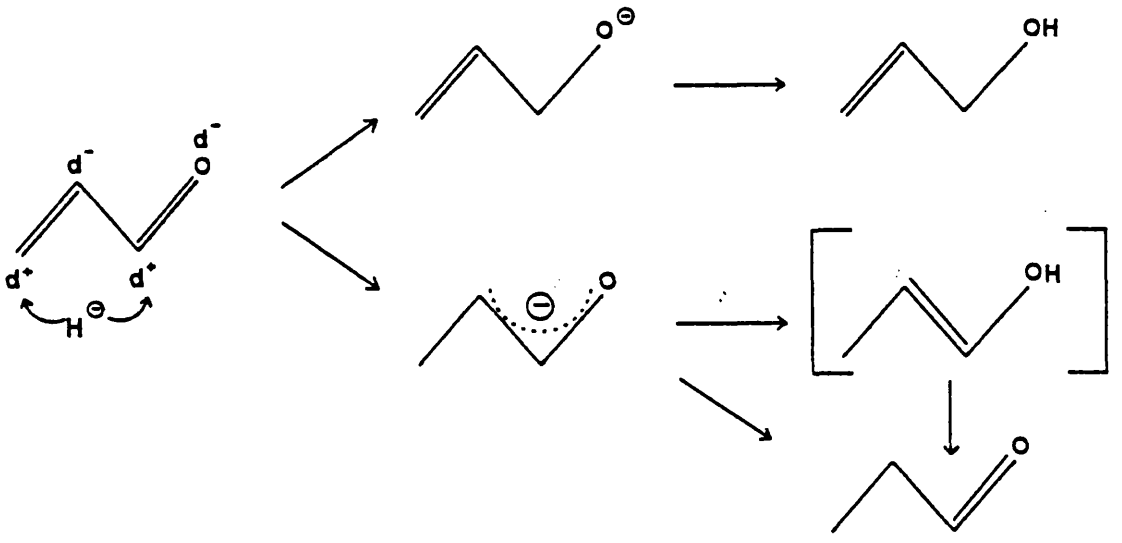

Figure 1.5 General Reaction Network for a Hydride Ion Attack on a Conjugated Carbonyl.

a) polarisation of the conjugated system

b) steric hindrance

c) electronic effects

d) formation of conjugated intermediates.

The effects of steric hindrance can be seen in the hydrogenation of methyl vinyl ketone where 2-butanone is formed almost exclusively (Figure 1.4). The difference in the hydrogenation of crotonaldehyde and methacrolein (Figure 1.4) was related to electronic effects. The aldehyde was the preferred product but in the case of methacrolein more enol was found to be present. The presence of a methyl group on carbon number 4, as in crotonaldehyde, enhanced the delocalisation of π electrons, whereas if the methyl group was on carbon 3, as in methacrolein, a slight decrease was expected. More saturated aldehyde would therefore be expected for crotonaldehyde hydrogenation.

The low monohydrogenation activity of conjugated carbonyl systems on copper chromite has been attributed to the high activity or strong adsorption of the allylic alcohols which were formed as primary products. It has been proposed (10, 23, 24) that surface copper ions in an octahedral environment may be the precursors (C site) of the active sites in copper chromite. After reduction, the hydrogenation site (CH site) consisted of a $Cu^{+}H^{-}$ pair containing two anionic vacancies (Figure 1.6).

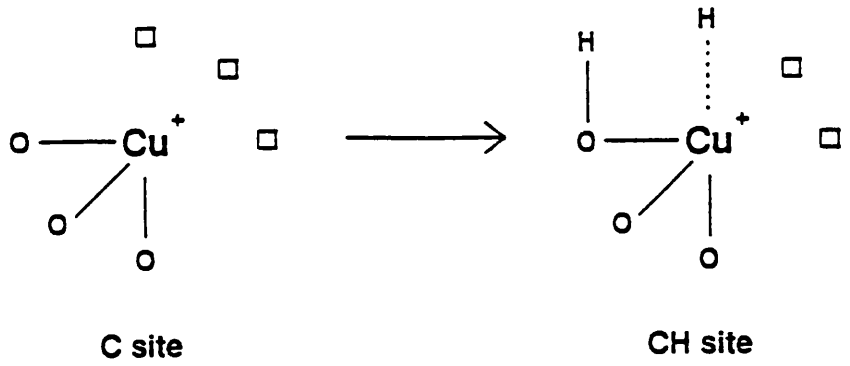

Figure 1.6 C Site and CH Site for Hydrogenation.

This weak electrophilic, active site will only adsorb strong nucleophilic reagents. Thus isolated ethylenic bonds were unreactive, whereas conjugated dienes, polar carbonyl compounds and allylic alcohols were sufficiently nucleophilic to interact with these active sites. It therefore followed that the monohydrogenation selectivity for dienes was very high but was low for conjugated carbonyls.

With copper chromite catalysts, allylic alcohols were isomerised and dehydroxylated as well as being hydrogenated. Since these reactions did not occur on copper hydride, it was proposed that the active site for these reactions may be a chromium ion associated with a hydride ion and two anionic vacancies as shown (25) (Figure 1.7).

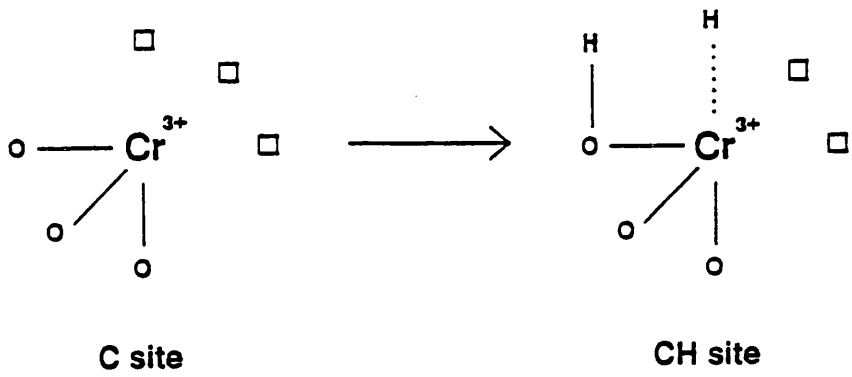

Figure 1.7 C Site and CH Site for Isomerisation.

Thus copper chromite consisted of two active metallic ions, Cu^{+} and Cr^{3+}, with a number of hydride groups located either in a vacancy associated with a single ion or in a shared bimetallic vacancy (BMV) (26). The copper ion was said to be responsible for addition reactions while the chromium ion was involved in other reactions such as nucleophilic substitution (Figure 1.8).

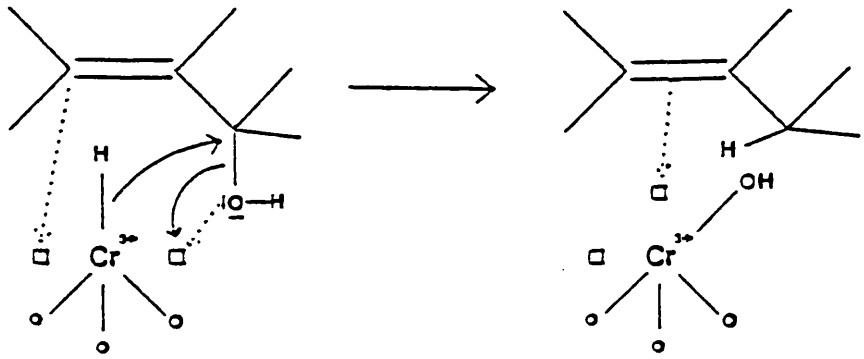

Hydro - dehydroxylation mechanism (Sn 2)

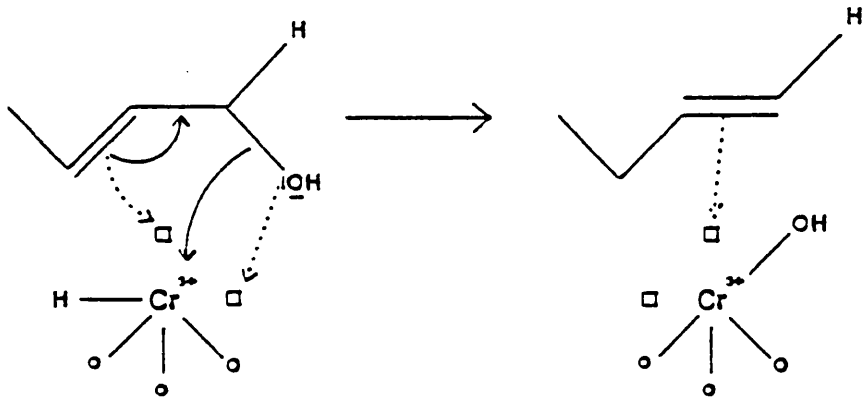

Hydro - dehydroxylation mechanism (Sn 2')

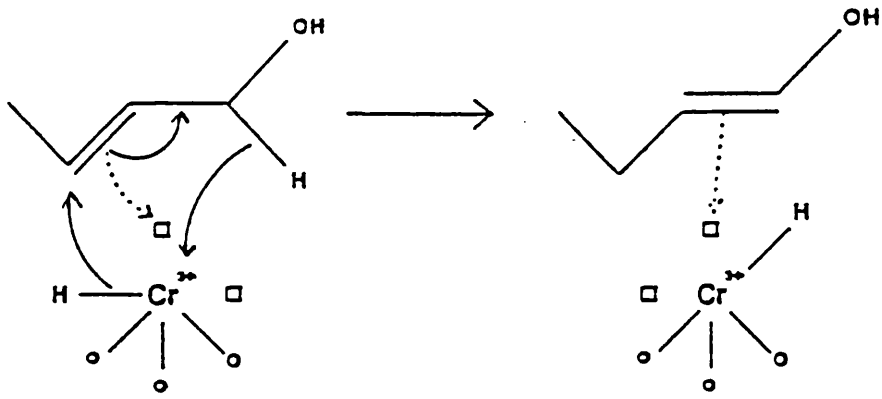

Isomerisation mechanism (Sn 2')

Figure 1.8 Possible Reactions on Cr Active Sites.

1.2.2 Promoter Effects

Supported platinum catalysts have been shown to exhibit similar properties to those of copper chromite catalysts in hydrogenation reactions. Hydrogenation of α,β-unsaturated aldehydes into saturated aldehydes and alcohols is readily achieved using supported platinum catalysts under mild conditions (114) but selective hydrogenation to unsaturated alcohol is generally poor. The selectivity of platinum metals can be improved however by the addition of Brønsted or Lewis bases (27, 28, 29), but the reasons for these promoting effects are not yet known. High selectivity can be induced by the addition of promoters such as iron(III) chloride and tin (IV) chloride. Galvagno *et al* (30) studied the effect of addition of metal chlorides to supported platinum catalysts in the hydrogenation of cinnamaldehyde.

Addition of the metal chlorides, to a commercial 10% Pt/C catalyst and a 2.12% Pt/Nylon catalyst was found to strongly modify the reaction pathway. While the kinetics of the overall disappearance of cinnamaldehyde always remained first order with respect to the organic substrate, the absolute value of the rate constant and the relative composition of the reaction products changed with the amount and chemical nature of the metal chlorides. It should be noted that the effect of additives was similar on both the supports used. A summary of the results obtained is shown in table 1.2.

Table 1.2 The Effect of the Addition of Metal Chlorides to Supported Platinum Catalysts on the Selectivity to Cinnamyl Alcohol (S_{COL}) in Cinnamaldehyde Hydrogenation.

Additive	Rate ($s^{-1}(gPt)^{-1}$)	S_{COL} %
none	0.8×10^{-4}	< 10
NaCl	0.8×10^{-4}	< 10
$CaCl_2$	1.7×10^{-4}	< 10
$AlCl_3$	1.8×10^{-4}	< 10
$CoCl_2$	8.4×10^{-4}	25
$SeCl_4$	2.6×10^{-4}	64
$FeCl_3$	24×10^{-4}	74
$SnCl_4$	100×10^{-4}	75
$GeCl_4$	178×10^{-4}	94

The results refer to the amount of additive which gave the highest cinnamyl alcohol yields. The results show that the catalytic behaviour of platinum towards the hydrogenation of cinnamaldehyde can be drastically modified by the addition of metal chlorides. The largest effect was observed on addition of $SnCl_4$, $GeCl_4$ or $FeCl_3$. Small amounts of these additives raise the catalytic activity of the noble metal, while higher concentrations were found to deactivate the catalyst (Figure 1.9).

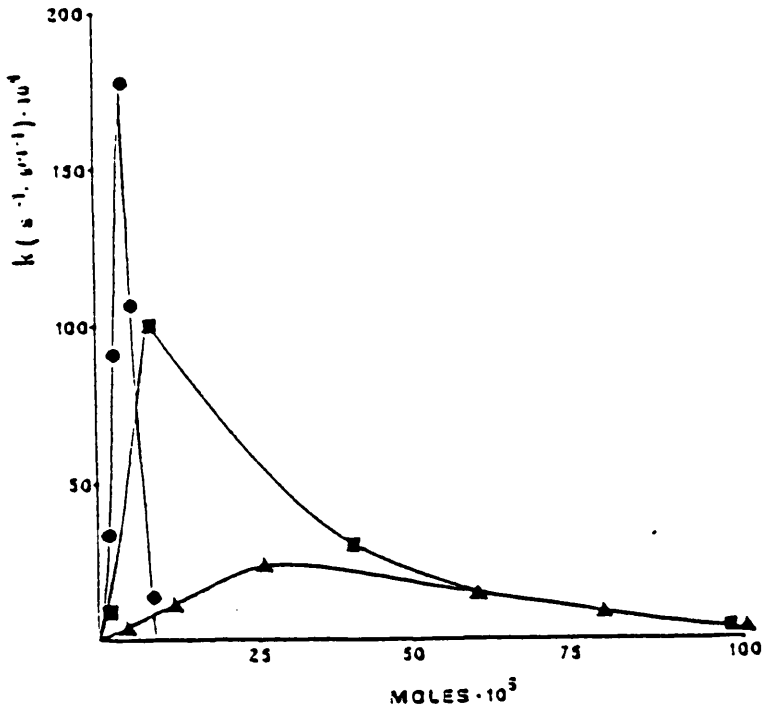

Figure 1.9 The Effect of Addition of Metal Chlorides on the Reaction Rate Constant; ● $GeCl_4$ ■ $SnCl_4$ ▲ $FeCl_3$.

Energy dispersive X-ray emission analysis (EDX) on a similar supported platinum/iron chloride system (39) shows bimetallic particles in which iron is associated with platinum.

Clearly the presence of iron, tin or germanium atoms on the surface of the platinum enhances selectivity to an unsaturated alcohol. It has been proposed that the addition of these promoters modify the course of the reaction through two main effects (31), one being on the reactant and the other on the noble metal.

An electron transfer from the promoter metal to platinum increases the electron density on the platinum. This results in a lower probability of the carbon-carbon bond being activated, as this involves an electron

transfer of π electrons to the metal d-band as a first step. This, however, does not account for the enhancement of the rate of the carbonyl bond hydrogenation and its subsequent decrease in rate as more promoter is added.

The electron deficient promoter atoms act as Lewis adsorption sites for the cinnamaldehyde molecules. The carbonyl group adsorbs via donation of a lone pair of electrons from the oxygen atom (Figure 1.10).

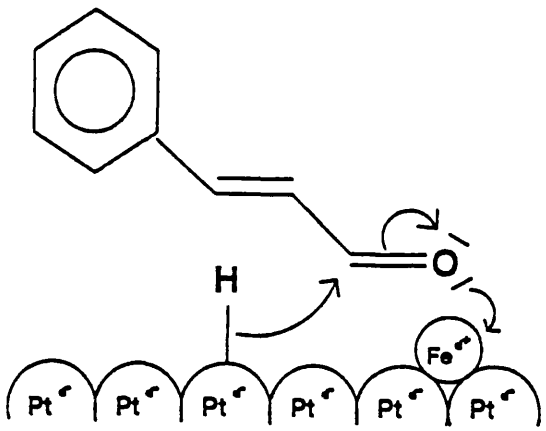

Figure 1.10 Possible Mechanism of Iron Enhancing Selectivity to Unsaturated Alcohol on a Platinum Surface.

The polarisation of the carbonyl group enhances its reactivity towards a weak nucleophilic agent such as chemisorbed hydrogen (Figure 1.10). This dual site mechanism can account for the volcano shaped activity curves (Figure 1.9). The selectivity towards cinnamyl alcohol formation and the rate of reaction increases as more promoter atoms cover

the platinum surface until an optimal surface composition is attained. At higher coverages the rate decreases, and the catalyst eventually becomes inactive for a monolayer coverage. Thus, at low additive concentrations, the activation of the cinnamaldehyde prevails but the above mentioned "poisoning effect" would prevail at higher concentrations.

With the exception of $SeCl_4$ it is interesting to note that higher selectivities were found on the more active systems. Moreover, the catalytic activity and selectivity to cinnamyl alcohol showed a general tendency to increase with the electronegativity of the metal cation. However, no clear correlation has been found between the electronegativity values reported in the literature and the catalytic performance.

It should be noted that the promoting action is not related to the presence of chlorine in this case. Chlorine, however, has been shown to have an effect in these types of reactions (32, 33, 34, 35, 36). Nitta *et al* (36) studied the activities of two kinds of silica supported cobalt catalysts, one with and one without residual chlorine. The catalysts were prepared from cobalt chloride and cobalt nitrate, respectively. Both catalysts had similar cobalt particle sizes but the catalyst prepared from cobalt chloride showed a higher selectivity towards cinnamyl alcohol in the hydrogenation of cinnamaldehyde (Table 1.3).

Table 1.3 The Effects of the Starting Co Salt on the Selectivity to Cinnamyl Alcohol in the Hydrogenation of Cinnamaldehyde.

Co salt	S^0_{COL}	S^{50}_{COL}
Chloride	94	93
Nitrate	81	77

S^0_{COL} - Initial selectivity to cinnamyl alcohol

S^{50}_{COL} - Selectivity to cinnamyl alcohol at 50% conversion.

The activities of the two catalysts were compared in the hydrogenation of cinnamyl alcohol (C=C bond) and hydrocinnamaldehyde. As shown in Table 1.4, the hydrogenation of the carbon-carbon double bond on the catalyst prepared from cobalt chloride was strongly depressed compared to the reaction of the carbonyl bond. This explains the higher selectivity of the chloride compared with the nitrate precursor catalyst in the hydrogenation reaction.

Table 1.4 Comparison of Individual Hydrogenation Rates of C=C and C=O Double Bonds Over Co/SiO_2 Catalysts With and Without Residual Chlorine.

Catalyst	Rate (C=C) mmol $min^{-1}g^{-1}$	Rate (C=O) mmol $min^{-1}g^{-1}$	Rate (C=C)/ Rate (C=O)
Prepared from cobalt nitrate	2.8	0.18	15.5
Prepared from cobalt chloride	0.041	0.082	0.5

From Table 1.4 we can see that although the chloride precursor was more selective towards unsaturated alcohol than the nitrate precursor, the catalyst prepared from chloride had a lower activity. It is possible that the chloride is acting as a poison.

A poison is a substance which is much more strongly adsorbed on the catalyst surface than the reactants, and it therefore denies the reactants access to the active sites. It is possible that the chlorine here is being selectively adsorbed on the sites where the carbon-carbon bond hydrogenation occurs thereby suppressing this reaction in favour of the hydrogenation of the carbonyl bond. Metallic catalysts are particularly sensitive to poisons, especially to compounds of sulphur and nitrogen containing lone pairs of electrons which form strong donor bonds to the metal surface.

The effect of the presence of sulphur on the activity and selectivity of an alumina supported copper catalyst was examined using the selective hydrogenation of crotonaldehyde by Rochester *et al* (37). They found that copper/alumina in the absence of sulphur poisons produced preferentially 1-butanol whereas catalysts pre-dosed with a suitable amount of thiophene shifted the product distribution towards formation of crotyl alcohol. The results of this study showed that the catalyst was partially poisoned by thiophene. The thiophene selectively poisons sites responsible for the hydrogenation of the carbon-carbon double bond.

1.2.3 Particle Size

Metal particle size has been found to have a marked effect on the hydrogenation of cinnamaldehyde. In general it has been shown that a large metal particle size increases the selectivity to cinnamyl alcohol (38, 39, 40). Richard, Fouilloux and Gallezot (40) studied the effects of the particle size using two graphite supported platinum catalysts. The platinum loading of these catalysts was 3.6 wt %. The first catalyst, Pt/G1, was reduced in flowing hydrogen at 573 K while the second, Pt/G2, was reduced by heating Pt/G1 in flowing hydrogen up to 773 K then under vacuum up to 1173 K. The metal dispersions of the catalysts were studied by Transmission Electron Microscopy (TEM). TEM showed that the above treatment resulted in a smaller dispersion and larger metal particle size in Pt/G2 (Table 1.5). This in turn led to a higher initial selectivity towards cinnamyl alcohol, S^0_{COL}, when the catalysts were used to hydrogenate cinnamaldehyde (Table 1.5).

Table 1.5 The Effect of Metal Particle Size on the Selectivity To Cinnamyl Alcohol (S^0_{COL}).

Catalyst	Average Particle Size (nm)	S^0_{COL}
Pt/G1	1.3	72
Pt/G2	5	91

This can be interpreted in terms of a steric effect whereby the adsorbed planar cinnamaldehyde molecule is not parallel to the flat

surface of the facetted platinum particles in Pt/G2 (Figure 1.11). Indeed the aromatic ring which is not chemically bonded to the surface, must lie at a distance exceeding 0.3 nm because there is an energy barrier which prevents it from approaching closer to the surface (41). Therefore the molecule is tilted with the carbonyl extremity closer to the surface than the carbon-carbon double bond. Thus we can expect the carbon-carbon double bond to be activated less easily than the carbonyl bond, therefore accounting for the higher selectivity of Pt/G2. In contrast, there are no steric constraints for the approach and adsorption of both the carbon-carbon double bond and the carbonyl bond on particles smaller than 2 - 3 nm, as in Pt/G1, because the phenyl group lies beside the metal surface, as indicated in Figure 1.11. It follows therefore that Pt/G1 is not as selective towards cinnamyl alcohol as Pt/G2.

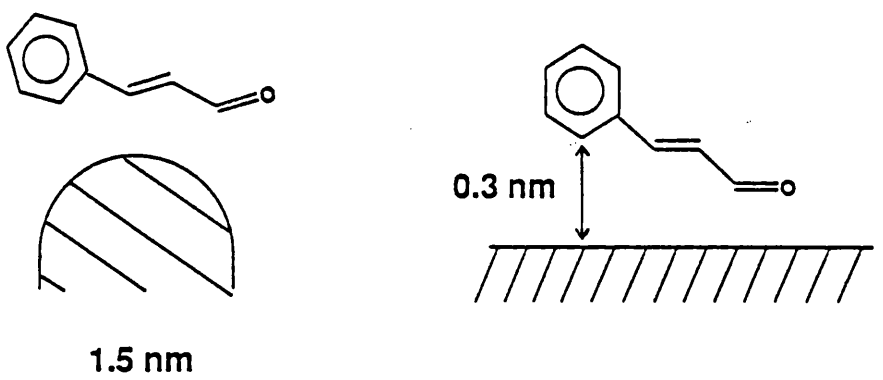

Figure 1.11 The Effect of Particle Size on the Approach of Cinnamaldehyde to the Surface.

This phenomenon is not exclusive to supported platinum catalysts. Similar effects have been observed using supported ruthenium catalysts (38). It has also been shown that pretreatment of a Raney-copper/cadmium catalyst in hydrogen or nitrogen at approximately 573 K prior to use for the hydrogenation of crotonaldehyde leads to an increase in the mean crystallite size of copper and an increase in the selectivity to crotyl alcohol (42). Silica supported cobalt catalysts exhibit the same particle size effects as shown by Nitta *et al* (43). In that study it was shown that the degree of reduction and the mean crystallite size of cobalt increased almost linearly with an increase in the reduction temperature of the catalysts. The selectivities from cinnamaldehyde to cinnamyl alcohol also increased with increasing reduction temperature and thus from an increased metal particle size.

1.2.4 Effects of The Support

The traditional view of the role of the support in any heterogeneous catalysis reaction is that of an inert carrier of the active component. The literature on supported metal catalysts in the period from 1950 to 1970 contains numerous references to apparent variations in catalytic activity with the nature of the support employed. One example is the work done on the dehydrogenation of cyclohexane over variously supported platinum catalysts by Nehring and Dreger (44). Some of their results are shown in Table 1.6.

Table 1.6 Dehydrogenation of Cyclohexane at 773 K Catalysed by Platinum on Various Supports (44).

Support	C_6H_6 %	Gaseous Products %	C_6H_{12} %
TiO_2	76	3	21
Al_2O_3	60	3	37
MgO	32	22	46
SiO_2	23	20	57
C	55	14	31

From Table 1.6 we can see that different supports give different results, with the highest yield of benzene being given using a titania support. Observations like these gave rise to a feeling that there might be some way in which the catalytic properties of metal particles could be affected by the support with which they were in contact.

Metal-support interactions have been shown to alter activity and selectivity of catalysts in hydrogenation reactions (40, 98). For instance, platinum and ruthenium catalysts supported on graphite have been shown to give higher selectivities towards unsaturated alcohol in the hydrogenation of cinnamaldehyde than those supported on charcoal (40). The particle sizes were the same on the two supports so the higher selectivities of the catalysts supported on graphite were attributed to the support. It was shown (45, 46) that graphite acts as an electron-donating macroligand, increasing the electron density of platinum particles anchored on graphite steps. This was evidenced by an expansion of the

platinum lattice and by a decrease of the $K_{T/B}$, the ratio of the adsorption coefficients of toluene and benzene. This ratio is a good probe for the electronic structure of metals since toluene is a better electron donor than benzene (47). The good selectivity of the graphite supported metals was attributed to the reduced ability of the metal particles to hydrogenate the carbon-carbon double bond of the cinnamaldehyde molecule. This is due to the fact that the first step in the activation of the carbon-carbon double bond involved the transfer of π electrons to the metal d-band. This is unlikely to occur if there is a high electron density on the metal.

Delk and Vavere (98) studied the hydrogenation of 2-methyl butanal over copper catalysts supported on titania and silica. They found that under a wide variety of conditions a high alcohol yield was obtained with the silica supported copper. This was not the case, however, with the titania catalysts, where much poorer yields of the alcohol 2-methyl butanol were obtained. Furthermore, although the reduction temperature had no effect on the activity of the silica catalysts it had a profound effect on the titania catalysts. The titania catalysts were also much more easily reduced than their silica counterparts. They concluded that a metal-support interaction was invoked by the reduction treatment leading to partial reduction of the support.

1.3 THE CATALYSTS

In this section the choice of the components of the catalysts is explained.

1.3.1 Support Materials

It has long been established that in heterogeneous catalysis the best catalysts for hydrogenation reactions are those of the Group VIII metals (48). Most of these metal catalysts are used on a support. This provides a means of dispersing a metal, such as platinum, for its most effective use, or a means of improving the mechanical strength of an inherently weak catalyst. The support, however, can sometimes contribute towards the catalytic activity. For example, it is generally accepted that on reforming catalysts skeletal isomerisation occurs according to a bifunctional mechanism, where dehydrogenation reactions take place on the metallic function (usually platinum) while isomerisation reactions take place on the acidic support (49). Also, in the hydrogenation of cinnamaldehyde over copper chromite it has been proposed that the chromia support is responsible for hydro-dehydroxylation and isomerisation reactions leading to products such as phenyl propane (24).

The selection of a support is based on it having certain desirable characteristics, namely:-

1. Economic

The cost is lowered by dispersing expensive metals, such as platinum, on a support.

2. Mechanical

The support should:-

(a) give the catalysts mechanical strength.

(b) optimise bulk density.

(c) provide a heat sink or heat source.

(d) dilute an overactive phase.

3. Geometric

The support should:-

(a) increase the surface area (high surface area is usually but not always desirable).

(b) optimise the porosity of a catalyst (high area implies fine pores, but relatively small pores, around 2 nm, may become plugged in catalyst preparation, especially if high loadings are sought).

(c) optimise crystal and particle size.

(d) allow the catalyst particles to adopt the most favourable configurations.

4. Chemical

The support should:-

(a) be inert to undesired reactions.

(b) be stable under reaction and regeneration conditions.

(c) react with the catalyst to improve specific activity.

5. Deactivation

The support should:-

(a) stabilise the catalyst against sintering.

(b) minimise poisoning (50).

Obviously no support can fulfil and optimise all these requirements. In this study silica was chosen as the support material.

1.3.2 Silica

Pure silica, SiO_2, occurs in only two forms, quartz and cristobalite. The silicon is always tetrahedrally bound to four oxygen atoms, but the bonds have considerable ionic character. In cristobalite the silicon atoms are arranged in the same manner as the carbon atoms in diamond with the oxygen atoms midway between each pair. In quartz there are helices so that enantiomorphic crystals occur, and these may be easily recognised and separated mechanically (51).

Kieselguhr is the only natural silica of commercial importance. Kieselguhr is a naturally occurring, finely divided silica consisting of the skeletal remains of diatoms. Depending on the deposit, it typically contains small amounts of alumina and iron as part of the skeletal structure. It is inexpensive, but it must usually be purified by acid treatment for use in catalysts. The surface area is usually in the range of 20 - 40 m^2g^{-1} and a rather broad range of particle sizes exists, mostly in the order of 100 nm or more (52).

Synthetic silicas are generally preferred in commercial applications

since porosity and surface area can be controlled by the preparation conditions, for example, pH of precipitation, calcination time, temperature and atmosphere. Commercial grade silicas are generally classified according to the way in which they are prepared, as either silica gels, colloidal silicas or fume silicas.

1. Silica Gels

   These consist of three dimensional networks of contiguous particles of colloidal silica. Silica gels usually have a high surface area, as high as about 700 m^2g^{-1}. The average pore diameter is correspondingly very low, typically in the range 2.5 to 4 nm.

2. Colloidal Silicas

   A variety of colloidal silicas are available containing up to 40 wt % SiO_2 in the form of spherical non-porous particles. The colloid is stabilised by ammonium or sodium ions.

3. Fume (Pyrogenic) Silica

   These are finely divided, non-porous and highly pure silica powders, e.g. Cabosil and Aerosil. They are manufactured from high purity $SiCl_4$, which is hydrolysed in an oxygen/hydrogen flame. The HCl that is formed is adsorbed on the silica surface, but can be removed by subsequent high temperature calcination. Particle sizes are about 40 - 50 nm and surface areas about 200 - 400 m^2g^{-1} (52).

High surface area silicas, prepared either as gels or via the pyrogenic route, are x-ray amorphous and reasonably stable up to temperatures of 800 K. However, significant surface area losses, due to

the collapse of the internal pore structure, are observed on heating above 800 K.

Silica is relatively unreactive towards Cl_2, H_2, acids and most metals at ordinary or slightly elevated temperatures, but is attacked by F_2, gaseous HF, alkaline hydroxides and fused carbonyls (53).

The surface of silica is characterised by silanol groups (-SiOH). The hydroxyl groups attached to the surface silicon atoms will not be exactly equidistant from each other since the silicon atoms on the surface of amorphous silica are not in a regular geometrical arrangement. The hydroxyl groups are therefore not all equivalent in their behaviour in adsorption or in chemical reactions. Several types of surface hydroxyls are shown in Figure 1.12.

It is generally accepted that on the smooth, heat stabilised amorphous silica that is fully hydroxylated there are 4 - 5 SiOH groups nm^{-2} which remain when the sample is dried at 398 - 423 K (54).

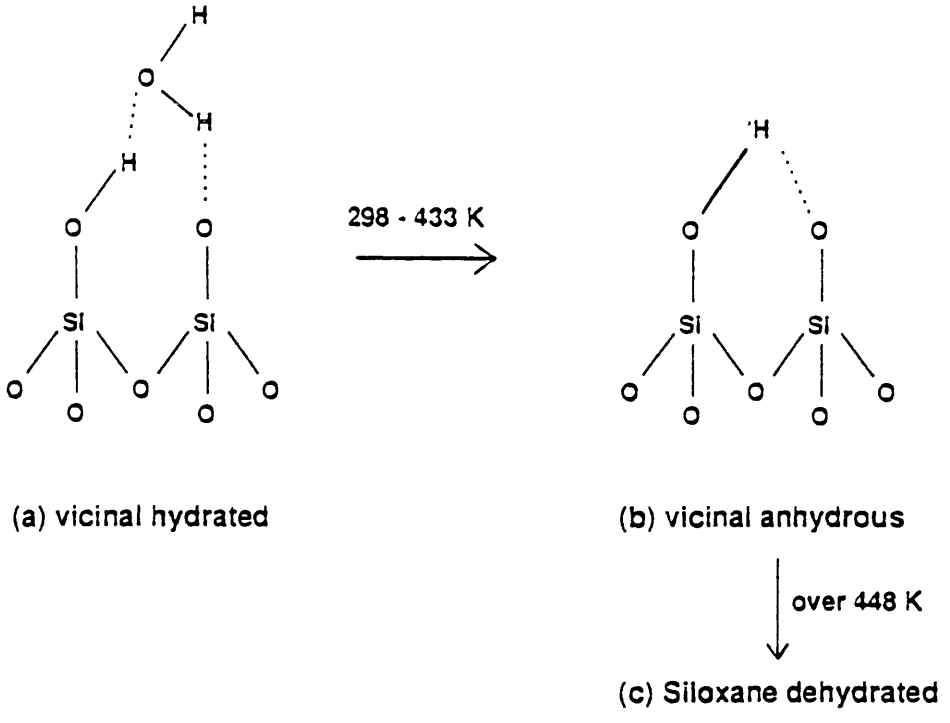

Figure 1.12 Surface Hydroxyls.

1.3.3 Metal-Support Interactions

The concept of a metal-support interaction is one of the oldest in heterogeneous catalysis. In 1935, Adadurov proposed that metals would be polarised by the surfaces of oxides containing highly charged cations. Although this idea does not appear to have received further attention it is probably the first specific suggestion of how the catalytic properties of a metal might be influenced by the support.

Boudart and Deja-Maridassou (55) and Bond and Burch (56) have emphasised the need to distinguish between apparent (or indirect) and real metal-support effects. Apparent metal-support effects include inhibition of reduction of the metal by the support, specific particle size effects (i.e. cluster size, epitaxial growth of the metal on the support or particle morphology), bifunctionality, spillover and effects of support action as a source or sink of catalytic poisons. Only if all these and related complications can be eliminated is it possible to study real metal-support interactions that may be attributed to geometric and electronic effects.

Early isolated observations generated the idea that a real metal-support interaction could be electronic in character. Schwab (57) and Szabo and Solymosi (58), working independently, produced the first convincing evidence for the transfer of electrons between metal particles and their support. The driving force for the transfer was the difference in energy between the two Fermi levels which can be altered by changing the semiconducting character of the support. Systems, including Ni/Al_2O_3, Ni/TiO_2 and Ni/Cr_2O_3, where the support was doped with ions of a greater

or lesser valency were examined for formic acid decomposition and systematic, but frequently somewhat small, differences in activation energy were observed (58). The materials that were used in this work could not at the time be assessed by surface analysis techniques now routinely applied and there is a strong possibility that the formation of an alloy might have been a complicating factor in some of the systems examined. However, this work was important in that it strongly suggested that electron movement between metal and support was a real possibility and that, therefore, a metal-support interaction could have an electronic basis. This idea has been proposed as an explanation of the strange effects observed (59, 60, 61) when metals on TiO_2 and related oxides are reduced in hydrogen at high temperature.

Traditionally, catalytic activity is taken to be determined by geometric as well as by electronic factors, and it is possible that the support may affect this factor too. Thus the support may influence particle shape. This is most likely to occur through differences in interfacial energy where the metal and the support are in contact. A high interfacial energy will cause the metal to wet the support and to spread so as to maximise the area of contact, giving for example hemispherical particles or two-dimensional islands. A low interfacial energy will tend to result in minimum contact between the two phases, and particles which are clearly three-dimensional may result. As a result of this effect the support may determine the crystal habit of the metal particle. It is generally agreed that for very small particles the icosahedron is a more

stable arrangement than octahedra or face centred cubic (fcc) structures (62). Where the interfacial energy at the metal-support junction is large, this may override the energy difference between icosahedra and fcc structures, thus encouraging the formation of the latter. Conversely when it is small, the added stability of the icosahedra may be the determining factor and particles of this form might be detected. Yacaman *et al* obtained results by electron microscopy to back up this theory and also observed that the magnitude of the interaction as deduced from the particle shape is also a function of metal loading (63).

The support may also affect the proportion of the metal which is finally aggregated into particles. Cations of the base metals of Group VIII tend to react with alumina and silica forming reducible aluminates and silicates. This is not a serious problem provided that the active metal surface area and the degree of reduction are measured. However, the effect of the unreduced metal cations on or in the support on the behaviour of the reduced metal through electron transfer has to be considered (64). There is also evidence (65, 66, 67) that certain supports, especially Al_2O_3, tend to stabilise intermediate oxidation states such as Rh^{I}, Pt^{III} and Re^{IV} as well as retarding reduction because of a strong interaction with the metal precursor. At low concentrations, Cu^{I} appears to be stabilised on alumina and silica (68, 69). Metal-support interactions of this kind can have an important influence on catalytic activity on insulator supports. However it is possible to state with some conviction that the direct influence of insulator oxide supports upon the geometric or electronic

properties of small metal particles is usually small.

In summary, apparent metal-support interactions may arise through the operation of a specific particle size effect, bifunctionality, spillover or through the support acting as a source or sink of a catalytic poison. Deliberately added promoters constitute an additional complication. Real interactions not due to these or similar causes may be attributed either to electronic or geometric effects, or to the creation of phases which contain the active component in a form which is hard to reduce.

The term strong metal-support interaction (SMSI) was coined by Tauster *et al* (59, 60, 61, 70) to describe the interaction "consisting of a covalent bond between the metal atoms of the supported phase and cations of the support".

The existence of such an interaction was proposed to account for the fact that, after reduction at elevated temperatures, Group VIII metals on transition metal oxide supports lost the ability to adsorb hydrogen or carbon monoxide gas. This suppression of chemisorption is now accepted as conclusive evidence that a SMSI exists. However it is often the case that contaminated metal surfaces may not be able to adsorb hydrogen or carbon monoxide as strongly as a clean surface (71, 72, 73) so the state of the surface must be ascertained before assigning the suppression of chemisorption to metal-support interactions.

1.3.4 Hydrogen Spillover

The phenomenon of hydrogen spillover has been described as "an apparent metal-support interaction" by Burch and Bond (56). It involves the dissociative adsorption of molecular hydrogen on metal sites. The atomic hydrogen so-formed migrates to another phase of the catalyst which contains hydrogen acceptor sites but which could not adsorb hydrogen directly under identical conditions. A schematic diagram of hydrogen spillover is shown in Figure 1.13.

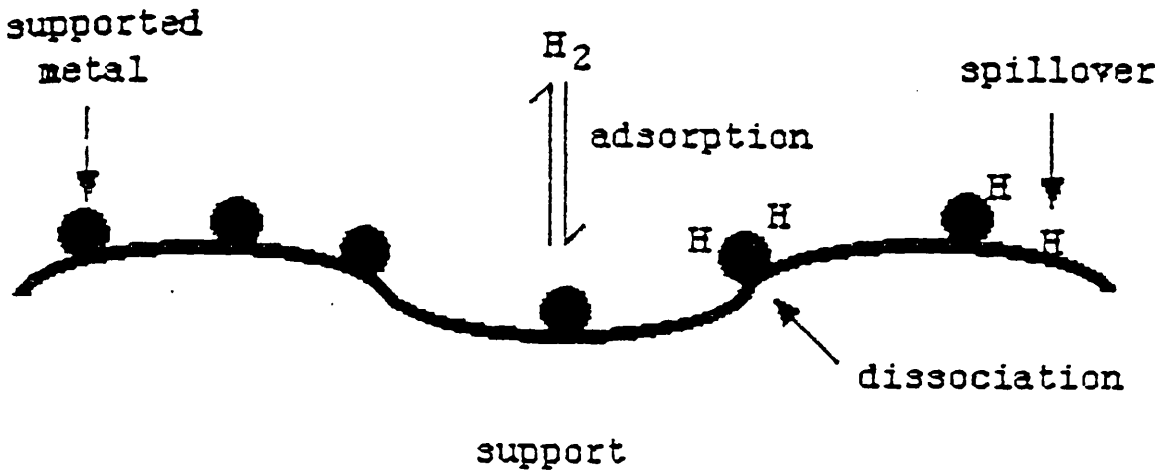

Figure 1.13 Hydrogen Spillover.

Spillover was first noticed in the 1950s (75) when it was observed by Kuriacose that the decomposition of GeH_4 on a Ge film was increased by contact with a Pt wire used to measure the conductivity. Taylor proposed that the wire provided a "porthole" for the recombination of hydrogen atoms to hydrogen molecules (76).

The first direct experimental evidence for spillover was presented by Khoobiar, in 1964, who documented that the formation of tungsten bronzes (H_xWO_3) was possible at room temperature for a mechanical mixture of WO_3 with Pt/Al_2O_3 (77). Sinfelt and Lucchesi postulated that reaction intermediates (presumably H) had migrated from Pt/SiO_2 on to Al_2O_3 during ethene hydrogenation (78).

It is generally accepted that spillover depends on at least two prerequisites: a source of a spillage species such as a Group VIII metal and an acceptor such as an oxide or active carbon. The phenomenon of hydrogen spillover is believed to take place via surface rather than gas phase transport of hydrogen species (79).

Most of the earlier work on hydrogen spillover was concerned with enhanced H_2 adsorption (80, 81) at atmospheric pressure and temperatures of around 573 K. The hydrogen adsorption was expressed as the H/Mt ratio where H stands for the H atomic species adsorbed per total number of metallic atoms, Mt. Values of H/Pt as high as 64 and 68 for Pt/Al_2O_3 and Pt/SiO_2 catalysts respectively, have been quoted by Altham and Webb (82).

It has been shown that metal content above 0.8% does not influence the spillover process. When the metal loadings are less than 0.00008% no spillover occurs.

Hydrogen spillover on to irreducible oxides such as Al_2O_3 and SiO_2 does not seem to initiate reduction even at temperatures as high as 773 K. The exchange of deuterium with surface hydroxyl groups can be

used to measure the extent of hydrogen spillover on these supports (83). The spillover does not appear to be greater than 1 % of the surface and is therefore far less than the number of surface hydroxyls (84). When hydrogen spills over on to reducible oxides such as MoO_3 and V_2O_5, hydrogen metal bronzes can be formed at or just above ambient temperature (85). A further description of the formation, structure and reactivity of hydrogen bronzes is given in the next section.

Lenz and Conner (86) found that silica could be activated using hydrogen spillover without direct contact between the silica and the supported metal. Hydrogenation and exchange activity was induced which was found to be independent of the metal. The induced catalytic activity was an activated process, which required high temperatures and long contact times. The hydrogenation mechanism was found to be similar to that on metal oxides and, as such, the molecular identity of the reacting hydrogen was retained.

1.3.5 Hydrogen Metal Bronzes

The term bronze was originally used by Wohler (87) in 1825 to describe Na_xWO_3, but is now used to describe a variety of crystalline phases of transition metal oxides.

Hydrogen metal bronzes can be formed from metal oxides with an incomplete d shell and for which the nd electron energy is higher than the (n+1)p electron energy (88). Examples of oxides which form hydrogen metal bronzes are molybdenum(VI) oxide, MoO_3, tungsten(VI) oxide, WO_3

and vanadium oxide, V_2O_5.

The addition of small quantities of metal catalysts, such as Pt or Pd, has been shown to dramatically lower the temperature of the reduction of oxides such as MoO_3, WO_3 and V_2O_5 (89, 107). For example, for Pd/MoO_3 the reduction temperature of MoO_3 is lowered by 400 K by formation of atomic hydrogen on the palladium which then spills over on to the MoO_3 resulting in its reduction. The atomic hydrogen produced by spillover can diffuse inside the host lattice, with or without the help of a catalyst and lead to the formation of hydrogen metal bronzes. Hydrogen bronzes provide a mechanism for storing and releasing hydrogen and therefore have the potential to control selectivity and activity in hydrogenation reactions (21).

1.3.6 The Choice of Catalysts

The main objective of this work was to try to increase the selectivity to unsaturated alcohols in the hydrogenation of cinnamaldehyde using silica supported copper catalysts and modified silica supported catalysts. The following catalysts were used:-

Cu/SiO_2 $Cu/V/SiO_2$ $Cu/Ru/SiO_2$

$Cu/Pd/SiO_2$ $Cu/V/Pd/SiO_2$ V/SiO_2.

Metal loadings were varied.

Currently, copper is widely used as a hydrogenation catalyst when it is supported on chromia (see Section 1.2.1). However, chromia based catalysts are likely to be phased out during the next few years owing to

their toxicity. Copper has been chosen in this study for the following reasons:-

1. Copper is the non-toxic component of copper chromite. Furthermore, it has been proposed that the active site for addition of hydrogen in the copper chromite catalysed hydrogenation of cinnamaldehyde to allylic alcohol is a copper site (24) while the chromium is involved in other reactions which decrease selectivity towards allylic alcohol. (See Section 1.2.1).
2. A number of investigations using supported platinum and ruthenium catalysts (40, 38) have shown that a large metal particle size can increase the yield of allylic alcohol in the hydrogenation of cinnamaldehyde. (See Section 1.2.3). High metal loadings have been used to achieve a large metal particle size. However, this requirement for high metal loadings results in supported platinum catalysts being expensive to operate on a commercial scale. High loaded copper catalysts on a relatively inert support such as silica would provide a viable, inexpensive alternative to the supported platinum system.

Catalyst precursors containing vanadium oxide (V_2O_5) were also prepared. Vanadium oxide (V_2O_5) can be reduced to a mixed valence metal oxide bronze that contains the metal in the original oxidation state and a lower state (Section 1.3.5). Hydrogen bronzes provide a mechanism for storing and releasing hydrogen and therefore have the potential to control selectivity and activity in hydrogenation reactions (21).

Palladium was also chosen as a modifier for the supported copper catalysts. Palladium catalysts generally give predominantly, as the initial step, preferential hydrogenation of the carbon-carbon double bond in conjugated carbonyl systems (90). However, palladium may function differently when used as a modifier to copper. Palladium was used in trace quantities as a modifier for copper in our work. Small amounts of palladium have been shown to have a marked effect on the reduction of copper oxide (94) and with its known capacity to adsorb hydrogen, palladium may further modify the selectivity of the copper catalysts.

Both palladium nitrate and palladium chloride were used as catalyst precursors to examine the effect which any residual chlorine would have on the reaction. Nitta *et al* found that higher selectivities to unsaturated alcohols were obtained for cobalt on silica catalysts when they were prepared from chloride rather than nitrate precursors (36).

Trace amounts of ruthenium were added to the catalysts as modified supported ruthenium catalysts have been shown to have the capacity to selectively hydrogenate α,β-unsaturated aldehydes to allylic alcohols (38).

The catalysts were all supported on silica. By using silica it was hoped to avoid the isomerisation and nucleophilic substitution reactions that occurred when the reaction was studied using copper supported on chromia. Silica is also non-toxic. The known toxicity of many chromium salts is likely to result in the phasing out of copper chromite catalysts in the next few years.

Palladium was also chosen as a modifier for the supported copper catalysts. Palladium catalysts generally give predominantly, as the initial step, preferential hydrogenation of the carbon-carbon double bond in conjugated carbonyl systems (90). However, palladium may function differently when used as a modifier to copper. Palladium was used in trace quantities as a modifier for copper in our work. Small amounts of palladium have been shown to have a marked effect on the reduction of copper oxide (94) and with its known capacity to adsorb hydrogen, palladium may further modify the selectivity of the copper catalysts.

Both palladium nitrate and palladium chloride were used as catalyst precursors to examine the effect which any residual chloride would have on the reaction. Nitta *et al* found that higher selectivities to unsaturated alcohols were obtained for cobalt on silica catalysts when they were prepared from chloride rather than nitrate precursors (36).

Trace amounts of ruthenium were added to the catalysts as modified supported ruthenium catalysts have been shown to have the capacity to selectively hydrogenate α,β-unsaturated aldehydes to allylic alcohols (38).

The catalysts were all supported on silica. By using silica it was hoped to avoid the isomerisation and nucleophilic substitution reactions that occurred when the reaction was studied using copper supported on chromia. Silica is also non-toxic. The known toxicity of many chromium salts is likely to result in the phasing out of copper chromite catalysts in the next few years.

1.4 CHARACTERISATION OF CATALYSTS

An understanding of the physical and chemical characteristics of a catalyst is invaluable when investigating its reaction chemistry. A wide range of analytical techniques were therefore used to establish a detailed knowledge of the catalysts' physiochemical properties. These techniques are described in this section but the actual experimental procedure is detailed in the experimental chapter.

1.4.1 The BET Method

Adsorption measurements have a variety of uses and applications, but perhaps the most important in catalysis is in determining the surface areas of catalysts. The Brunauer-Emmett-Teller (BET) method is used to measure the total accessible surface area of a catalyst. The BET theory is an extension of the Langmuir model of monolayer physical adsorption on surfaces to multilayer adsorption. Adsorption in the first layer is assumed to take place on a surface of uniform site energy. Multilayer adsorption then occurs on the first layer of molecules and approaches infinite thickness as the equilibrium vapour pressure approaches saturation vapour pressure ($p \rightarrow p^0$). Summation of the amount adsorbed in all layers gives the isotherm equation:

$$\frac{V}{V_m} = \frac{Cp/p^o}{(1 - p/p^o)\,[1 + (C - 1)p/p^o}$$

where V = volume of gas adsorbed at the equilibrium relative pressure p/p°

V_m= the value of V at monolayer coverage

C = constant related to the heat of adsorption of the gas on the solid

p°= the saturation vapour pressure.

The BET equation is usually expressed in the form

$$\frac{p}{V(p^o - p)} = \frac{1}{V_m C} + \frac{(C-1)p}{(V_m C)p^o}$$

A plot of p/V(p°-p) against p/p° is linear, thus allowing the determination of V_m. The surface area of the adsorbing solid can then be computed from V_m and knowledge of the physical dimensions of single molecules.

1.4.2 Mercury Porosimetry

Mercury porosimetry indicates the volume of liquid mercury (non-wetting) forced under pressure into the pores and extruded from the pores as the pressure is released. Mercury enters or intrudes pores in response to their size and to the applied pressure. The applied pressure must overcome the surface tension of mercury which opposes its entrance into pores. Mercury has a contact angle greater than 90° with most materials and this causes it to resist wetting the solid and entering into pore spaces in the absence of an externally applied pressure.

A series of pore volume readings for a given applied pressure can be used to derive the pore size distribution for samples by virtue of the Young-Laplace equation:-

$$p = (4\gamma\cos\Theta)/d$$

where Θ = the contact angle (140° for mercury)

d = the pore diameter

γ = the surface tension of the penetrating liquid

p = the pressure

Pore volume (cm^3g^{-1}) can then be plotted against $\log_{10}$(pore diameter). The plot is cumulative, hence at any given pressure, the pore volume will be equivalent to the total number of pores filled.

1.4.3 Temperature Programmed Reduction

When the temperature of an oxidised catalyst is increased linearly in a stream of hydrogen, containing inert gas, hydrogen will be absorbed as a function of the temperature/reactivity relationship of the oxidised species. This technique is called temperature programmed reduction (TPR). TPR is highly sensitive and hydrogen uptakes during the reduction of 1 µmol can be readily detected (91). It does not depend on any specific property of the material under investigation other than the sample being reducible and it is eminently suitable for studying low-loaded, highly dispersed systems which cannot be analysed by more direct methods of structural analysis, for example x-ray diffraction. TPR permits a "fingerprint" of catalyst reduction to be obtained, clearly indicating support-metal interactions, metal dispersion and the valency of the metal oxide on the support surface. These factors are important in determining the ultimate catalytic activity and hence TPR can be used as a quality

control method for catalyst performance analysis.

The term TPR was first described by Robertson *et al* (92) and since then a number of publications on the TPR technique have appeared (91, 93, 94, 95, 96). TPR has been applied successfully to study the influence of support materials, variables during the preparation stage of the catalyst precursors and the application of promoters on the reducibility of the catalyst surface.

A typical reduction profile, as shown in Figure 1.14, consists of a series of peaks. Each peak represents a distinct reduction process involving particular chemical components of the catalyst being studied. The position of a peak in the profile is determined by the chemical nature and environment of the chemical component, and the area of the peak reflects the concentration of that component present in the catalyst.

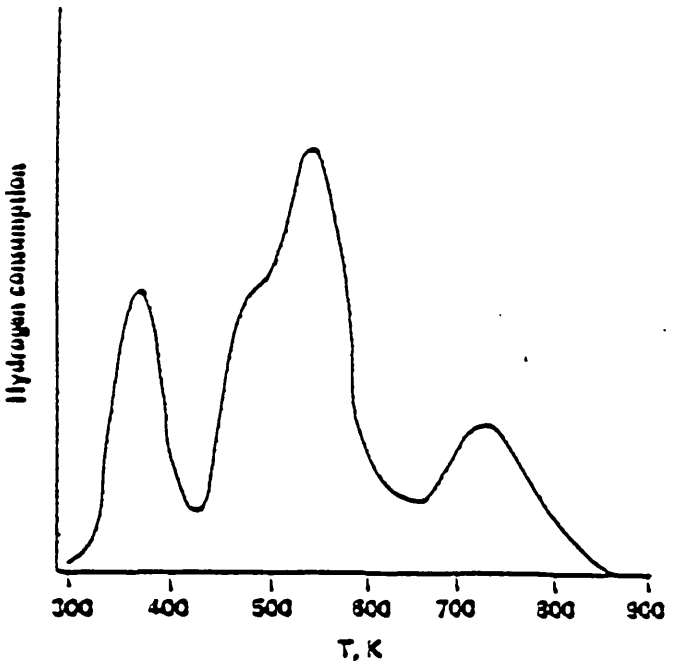

Figure 1.14 Typical Reduction Profile.

Silica-supported copper oxide has been studied using TPR (92) and it was found that for a 0.75 % weight copper loaded catalyst the position of the TPR maximum of the reduction peak was lowered by about 70 K to 570 K compared with that of a reduction performed on bulk copper oxide. The support in this case appeared to be enhancing the reactivity of the oxide in the reduction by acting as a dispersing agent. The TPR of copper oxide, obtained from the calcination of the same copper nitrate that was used as the catalyst precursor, showed a single reduction peak at roughly 640 K (92).

Metal-support interactions have been observed on silica supported copper catalysts (97) that were prepared by an ion exchange method. Three TPR peaks were observed at roughly 555 K, 673 K and 1000 K. The low temperature and high temperature peaks were interpreted as arising from the reduction of Cu^{2+} interacting strongly with the silica surface in a stepwise fashion to Cu^{0} through Cu^{+}. Isolated Cu^{2+} ions weakly interacting with the silica surface were responsible for the peak at 673 K.

Catalysts of 1 - 4 % weight copper supported on silica and titania have been studied by Delk and Vavere (98). For 1 % copper on silica the main reduction peak was found at 500 K with a shoulder at 550 K. This lower temperature compared with that found by Robertson et al (92) can be explained by the greater flow rate of gas used by Delk compared to Robertson (95 ml min^{-1} compared to 10 ml min^{-1}). The copper reduced at a much lower temperature on the titania support compared to the silica. The 1 % copper on titania sample showed a reduction peak at 403 K with

a small shoulder at 493 K. This shoulder becomes a peak in the 4 % copper on titania sample. The hydrogen consumption for both the silica and titania samples were consistent with the complete reduction of Cu^{2+} to Cu^0. The low temperature peak in the titania samples was caused by an anomalous metal-support interaction and was ascribed to reduction of a Cu^{2+} species in intimate contact with the titania support.

The effects of adding small amounts of palladium to copper oxide were observed using TPR by Gentry *et al* (99). Gentry's TPR profiles for palladium doped copper oxide samples are shown in Figure 1.15.

At low levels of palladium doping, 0.01 to 0.2% palladium, the TPR profiles appear as a major peak with a high temperature shoulder. As palladium content is increased within this range, both the shoulder and peak move to a lower temperature. It was proposed that this promoting influence of palladium, towards reduction, may arise in two ways. Palladium ions may distort the copper oxide lattice to produce potential copper nucleation sites such that reduction occurs at a lower temperature but does not involve the preferential reduction of palladium ions. Bulk palladium oxide, however, is easily reduced at room temperature and this suggested the preferential reduction of palladium ions to form palladium nucleation sites.

The emergence of a new low temperature peak in the catalysts with loadings above 0.5% palladium supported the mechanism involving the preferential reduction of palladium ions. The results indicated that Pd^{2+} did not reduce immediately on contact with hydrogen at room temperature

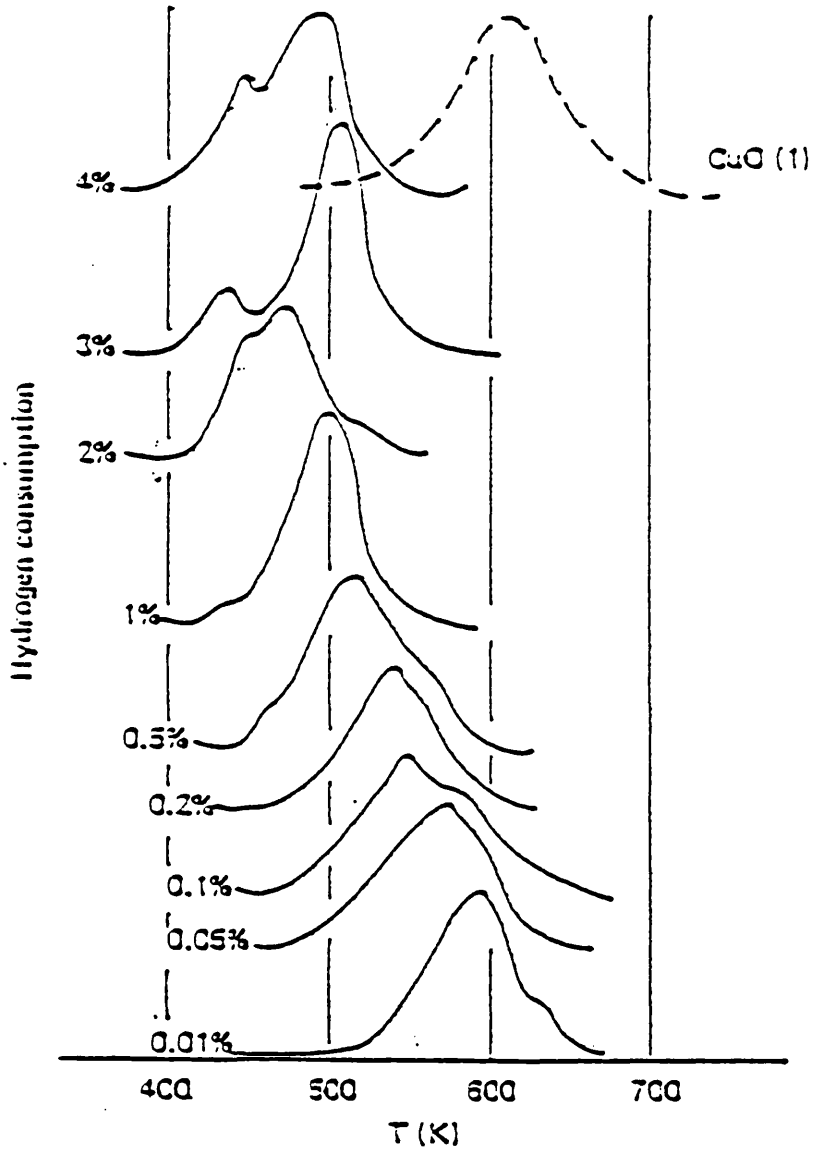

Figure 1.15 TPR Profiles for CuO Doped with x mol % of Palladium.

but was reduced to Pd^0 simultaneously with the reduction of some Cu^{2+} to Cu^0 in the low temperature peak of the TPR profile. Therefore, it was proposed that the promoting influence of palladium arose from the preferential reduction of Pd^{2+}, together with some Cu^{2+} reduction, leading to the production of palladium rich nucleation sites.

TPR profiles of ruthenium doped copper oxides have been shown to be similar to those of palladium doped copper oxide (94) in that the reduction temperature is reduced. Gentry *et al* found a low temperature peak at 440 K which they assigned to the reduction of ruthenium(II) oxide.

In a study of ruthenium on silica, Koopman *et al* (106) showed that upon oxidation at room temperature, catalysts prepared by direct reduction of ruthenium(III) chloride on silica ($RuCl_3/SiO_2$) oxidised first on the surface, then by bulk oxidation. This behaviour differed substantially from that of catalysts prepared by calcination of $RuCl_3/SiO_2$ at high temperature, followed by reduction. The TPR of catalysts prepared in this way showed a single reduction peak at 450 K.

Catalysts based on vanadium and bulk vanadium oxides have also been studied by TPR (100, 101, 102, 103, 104, 105). Roozeboom *et al* (101) obtained a TPR profile for pure V_2O_5 and found one single reduction peak at 803 K, but Bosch *et al* (100) obtained profiles consisting of three or four peaks between 900 and 1100 K in which only the first two peaks were resolved. They concluded that the reduction probably proceeds as follows:

$$V_2O_5 \rightarrow 1/3\ V_6O_{13} \rightarrow 2\ VO_2 \rightarrow V_2O_3$$

The last two peaks were taken collectively to be representing the

last step. Bond *et al* (105) obtained similar results as Bosch *et al*. The materials used by Roozeboom and by Bosch were the commercial oxide V_2O_5, so the discrepancy in their results can only be attributed to differing experimental conditions. Roozeboom used a reducing gas of 66 % hydrogen/nitrogen in his experiments. This was a very high concentration of hydrogen and although the concentration of hydrogen was not stated by Bosch it was presumably much lower. If it was indeed lower, then the shift of the peak to higher temperatures observed by Bosch *et al* was in the right direction.

A combination of Raman spectroscopy and TPR was used by Roozeboom *et al* (101) for qualitative and quantitative structural analysis, respectively, of supported vanadium(V) oxide catalysts. The TPR profiles of silica supported vanadium(V) oxide are shown in Figure 1.16.

Two peaks were observed, one at approximately 700 K and one at approximately 750 K. The low temperature peak was assigned to some surface phase or phases such as a two-dimensional octahedral polyvanadate species or a tetrahedral vanadate species. These low temperature surface species had been observed on vanadium(V) oxide supported on alumina (101). The high temperature peak was assigned to crystalline vanadium(V) oxide.

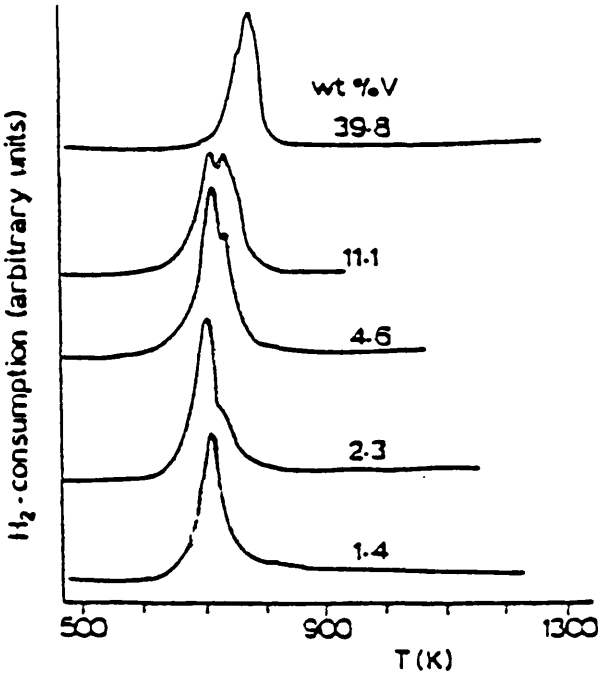

Figure 1.16 TPR Profiles of Impregnated Vanadium(V) Oxide/Silica.

Wu has shown (107) that a small amount of palladium leads to a significant decrease in the reduction temperature of bulk vanadium(V) oxide and that the reduction temperature decreased with increasing palladium content.

1.4.4 Copper Metal Surface Area Determination

Special procedures have been devised for measuring the extent of the metallic part of the surface in addition to the well known methods developed for the determination of the total surface area and the pore volume distribution of heterogeneous catalysts. Traditionally metal surface areas have been determined by chemisorption of a suitable adsorbate. Both carbon monoxide and hydrogen have been used to measure copper surface area although neither adsorbate is thought to

provide accurate results (108). The reaction of nitrous oxide has been used to measure metal surface areas for both pure and supported copper catalysts (109, 110, 111, 112, 115). The methods are based on the decomposition of a nitrous oxide molecule on a copper surface which is accompanied by the liberation of one nitrogen molecule according to:-

$$N_2O(g) + 2\ Cu(s) \rightarrow N_2(g) + (Cu\text{-}O\text{-}Cu)_s \qquad [1]$$

where the subscript s signifies surface atoms. It has been shown (113), using ultra violet photoelectron spectroscopy (UPS), that after oxidation with N_2O, at temperatures below 373 K, the surface copper is primarily in the Cu(I) oxidation state. Several different experimental methods have been used to follow the extent of the reaction [1]. Osigna *et al* (110) and Dell *et al* (109) determined the amount of nitrogen formed by freezing the excess of N_2O and measuring the residual nitrogen pressure using a conventional volumetric adsorption apparatus. Scholten (111) used microkatharometric and mass spectroscopic methods. Dvork and Pasek (112) employed a pulse chromatographic method. Scholten defined the fractional surface coverage Θ as being equal to giving a surface stoichiometry of $Cu_s/O_{ads} = 2$. They did so because on this basis a coverage of $\Theta = 1$ then results when copper reacts with N_2O at 363 K, the temperature they employed to measure free copper surface areas of catalysts. In this study Scholten's definition of Θ is used, namely that $\Theta = 1$ for $Cu_s/O_{ads} = 2$.

1.4.5 X-Ray Diffraction and Transmission Electron Microscopy

Two other methods for the characterisation of catalysts used in this study are x-ray diffraction (XRD) and transmission electron microscopy (TEM). In XRD a narrow beam of monochromatic x-rays is directed onto a rotating powdered sample set at the centre of a circular camera and the resulting diffraction pattern from the different crystal planes of the crystallites is recorded on a strip of film. XRD gives information on the bulk crystallographic structure of catalysts.

Electron microscopy is an extremely versatile technique capable of providing structural information over a wide range of magnification. In this study TEM was used to measure particle sizes of the reduced catalysts.

Chapter 2

OBJECTIVES

OBJECTIVES OF THE PRESENT STUDY

Selective reduction reactions are widely used in the manufacture of fine chemicals and chemical intermediates. Hydrogenations are carried out homogeneously using catalysts such as formic acid, formaldehyde, sodium dithionite, bisulphite or polysulphide or heterogeneously using supported group VIII metal catalysts such as palladium, platinum, nickel or cobalt. Increasingly, safety, health and environmental considerations render these processes less than ideal and many will have to be replaced in the near future. Production of the strategically important compounds aniline (low cost production of which is essential to polyurethane manufacture) and Koch acid (a key intermediate in dyestuffs manufacture), depend upon the use of nickel catalysts. These need to be replaced frequently due to by-product formation and poisoning and their disposal will become increasingly more expensive. Currently, the only feasible alternative catalyst in aniline manufacture is copper chromite. It has become clear that such copper chromite systems have the ability to compete in areas of catalysis which are at present dominated by precious metals and nickel. It is extremely likely that within the next decade the use of copper chromite will be phased out due to environmental legislation. Therefore there is now a large commercial incentive to develop novel catalysts as replacements for these nickel and copper chromite systems. Copper based catalysts inherently have the required characteristics but need the addition of suitable modifiers to be viable as direct replacements.

The aim of this work was to establish the scientific foundations for

the development of such modified copper catalysts based on environmentally safe supports for use in selective hydrogenation reactions.

The selective hydrogenation of α,β-unsaturated carbonyl compounds to their corresponding unsaturated alcohols is an important step in the preparation of various fine chemicals such as fragrances for the perfumery industry. The main objective of this work was to try to increase the selectivity to unsaturated alcohol in cinnamaldehyde hydrogenation using silica supported copper catalysts and modified silica supported copper catalysts. It was intended that a study of the hydrogenation of cinnamaldehyde using these catalysts would reveal the main chemical and physical factors that affect selectivity to cinnamyl alcohol, namely

1. the addition of another metal to the copper catalyst
2. the metal particle size
3. metal-support interactions.

In order to achieve this objective the catalysts and their precursors were characterised using temperature programmed, spectroscopic, chemisorption and diffraction techniques prior to the study of their reaction chemistry.

Chapter 3

EXPERIMENTAL

3.1 INTRODUCTION

A range of silica supported catalysts were prepared, characterised and tested for their selectivity in the hydrogenation of cinnamaldehyde. The catalysts were prepared using a wet impregnation method, the metal precursors being impregnated onto a silica support. The catalysts were then oven dried at 393 K and calcined at either 623 or 723 K.

Several methods were used for the characterisation of the catalysts. Atomic absorption, temperature programmed reduction (TPR) and nitrous oxide chemisorption techniques were carried out at Glasgow. X-ray diffraction (XRD), mercury porosimetry and BET surface area measurements were carried out at ICI Katalco.

The catalysts were then tested for hydrogenation activity using a specially designed liquid phase hydrogenation reactor and the results were analysed by gas chromatography (GC).

3.2 PREPARATION OF CATALYSTS

3.2.1 Industrial Catalysts

Several catalysts were prepared at ICI Katalco in Billingham.

Copper nitrate ($Cu(NO_3)_2.3H_2O$), ammonium metavanadate ($NH_4V_2O_5$) and palladium nitrate ($Pd(NO_3)_2$) (ICI C & P Ltd.) were used for the preparation of the catalysts in this study. The supports used were PQ silica and Grace silica. The catalyst precursors had been prepared using a wet impregnation method.

(a) Copper oxide/Silica PQ (ICI CuO/SiO_2/PQ *a*)

A known weight (200 g) of PQ silica was placed in a round bottomed flask and copper nitrate (110 g), dissolved in water (200 ml), was added. The flask was connected to a rotary evaporator and the excess water was removed.

(b) Copper oxide/Silica Grace (ICI CuO/SiO_2/Grace *a*)

Copper nitrate (110 g) was impregnated on Grace silica (200 g) as in (a).

(c) Copper oxide/Silica PQ (ICI CuO/SiO_2/PQ *b*)

Copper nitrate (55 g) was impregnated on PQ silica (200 g) as in (a).

(d) Copper oxide/Silica Grace (ICI CuO/SiO_2/Grace *b*)

Copper nitrate (55 g) was impregnated on Grace silica as in (a).

(e) Vanadium pentoxide/Silica PQ (V_2O_5/SiO_2)

Ammonium metavanadate (50 g) was dissolved in water (1000 ml) and PQ silica (200 g) was dipped in the solution for thirty minutes. The ammonium metavanadate on silica was then drained, oven dried at 393 K and calcined in a muffle oven at 723 K for three hours.

(f) Copper oxide/Vanadium pentoxide/Silica PQ ($CuO/V_2O_5/SiO_2$)

Copper nitrate (27 g) was dissolved in water (75 ml) and impregnated on previously made vanadium pentoxide/silica (e) (50 g).

(g) Copper oxide/Palladium oxide/Vanadium pentoxide/Silica PQ ($CuO/V_2O_5/PdO/SiO_2$)

Copper nitrate (27 g) and palladium nitrate (0.03 g) were dissolved in water (75 ml) and impregnated on previously made vanadium pentoxide/ silica (e) (50 g).

After impregnation the catalyst precursors (a, b, c, d, f and g) were oven dried at 393 K and then calcined in a muffle oven at 723 K for three hours.

3.2.2 Catalysts

Several catalysts were prepared in the Catalysis Laboratory in the University of Glasgow.

Copper nitrate ($Cu(NO_3)_2.3H_2O$), palladium nitrate ($Pd(NO_3)_2$),

palladium chloride ($PdCl_2$) and ruthenium chloride ($RuCl_3$) (Aldrich) were used for the preparation of the catalysts used in this study. The supports used were ICI PQ Silica and ICI Grace Silica.

The catalyst precursors were prepared using a similar wet impregnation technique as described above (3.2.1).

(a) G.U. Copper oxide/Silica PQ (GU CuO/SiO_2)

Copper nitrate (27 g) was dissolved in water (75 ml) and impregnated on silica (50 g) as above (3.2.1).

(b) Copper oxide/Palladium oxide/Silica PQ ($CuO/PdO/SiO_2$ *a*)

Copper nitrate (27 g) and palladium nitrate (0.03 g) were dissolved in water (75 ml) and impregnated on silica (50 g) as above (3.2.1).

Additional copper oxide/palladium oxide/silica PQ catalyst precursors were then prepared in which the copper nitrate concentration was kept constant and the palladium nitrate concentration increased to give nominal concentrations of 1320, 2640 and 5280 ppm palladium in the calcined precursor. These calcined catalyst precursors were named as $CuO/PdO/SiO_2$ *b*, *c* and *d*.

(c) Copper oxide/Palladium oxide/Silica PQ ($CuO/PdO/SiO_2$ *e*)

Copper nitrate (27 g) and palladium chloride (0.03 g) were dissolved in water (75 ml) and impregnated on silica (50 g) as above (3.2.1).

(d) Copper oxide/Ruthenium oxide/Silica Grace ($CuO/RuO_2/SiO_2$)

Copper nitrate (27 g) and ruthenium chloride (0.18 g) were dissolved in water (75 ml) and impregnated on silica (50 g) as above (3.2.1).

Additional copper oxide/ruthenium oxide/silica catalyst precursors were then prepared in which the copper nitrate concentration was kept constant and the ruthenium chloride concentration was increased to give nominal concentrations of 2640 and 5280 ppm of ruthenium in the calcined precursor.

The catalyst precursors were either calcined in a muffle oven at 723 K or by using the apparatus shown in Figure 3.1. In the latter case the catalyst was calcined by heating at 10 K per minute to 623 or 723 K in flowing air at 40 ml per minute. The catalyst was held at this temperature for 180 minutes.

A full list of all the catalysts used in this study and their nominal metal loadings are given in Table 3.1. The active catalysts were in reduced form but for convenience were referred to as in Table 3.1.

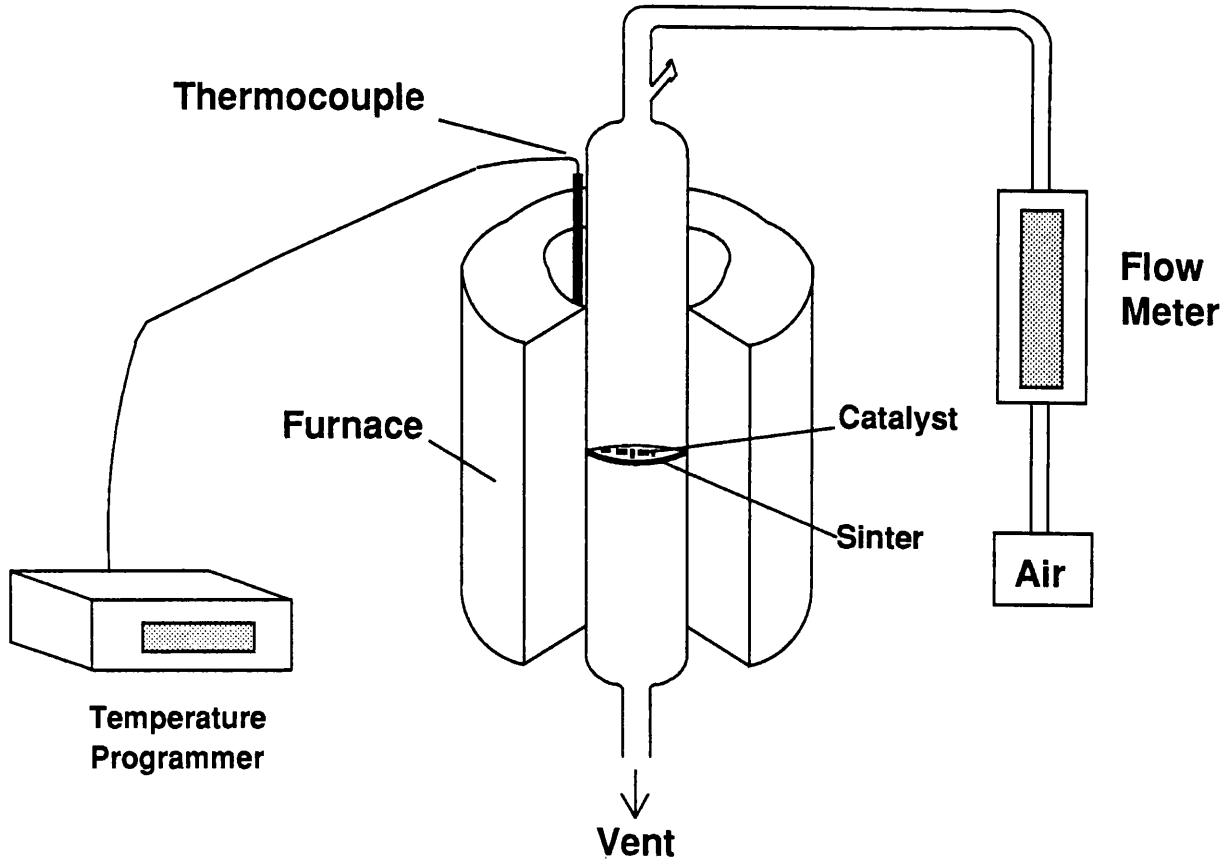

Figure 3.1. Apparatus for Calcination

Table 3.1 The Catalysts.

Industrial Catalysts

Catalyst	Type of Silica	Nominal Metal Loading %		
		Cu	V	Pd
ICI CuO/SiO_2/PQ *a*	PQ	14.46		
ICI CuO/SiO_2/Grace *a*	GRACE	14.46		
ICI CuO/SiO_2/PQ *b*	PQ	7.23		
ICI CuO/SiO_2/Grace *b*	GRACE	7.23		
$CuO/V_2O_5/SiO_2$	PQ	14.46		
$CuO/V_2O_5/PdO/SiO_2$	PQ	14.46		0.03
V_2O_5/SiO_2	PQ			

Glasgow Catalysts

Catalyst	Type of Silica	Nominal Metal Loading %		
		Cu	Pd	Ru
GU CuO/SiO_2	PQ	14.46		
$CuO/PdO/SiO_2$ *a*	PQ	14.46	0.03	
$CuO/PdO/SiO_2$ *b*	PQ	14.46	0.18	
$CuO/PdO/SiO_2$ *c*	PQ	14.46	0.36	
$CuO/PdO/SiO_2$ *d*	PQ	14.46	0.72	
$CuO/PdO/SiO_2$ *e*	PQ	14.46	0.03	
$CuO/RuO_2/SiO_2$ *a*	GRACE	14.46		0.18
$CuO/RuO_2/SiO_2$ *b*	GRACE	14.46		0.36
$CuO/RuO_2/SiO_2$ *c*	GRACE	14.46		0.72

3.3 CHARACTERISATION OF CATALYSTS

3.3.1 Atomic Absorption

The copper metal content of each calcined catalyst precursor was determined by atomic absorption spectrometry using a Perkin Elmer 1100B Spectrophotometer fitted with a Cathodean Ltd. hollow cathode lamp, suitable for detecting copper.

A calibration curve for copper was constructed by preparing standard solutions containing 1, 2, 3, 4 and 5 parts per million (ppm) of the metal being studied from a 1000 ppm standard solution. Sample solutions were then prepared as follows. A known weight (ca. 0.1 g) of catalyst was placed in concentrated nitric acid (5 ml) and left overnight. The resultant solution was then separated from the support using filtration and transferred, with washings, to a 100 ml volumetric flask and water added to make up to a volume of 100.00 ml. This gave a 1000 ppm solution of catalyst and an approximately 100 ppm solution of copper metal, by assuming copper metal loading to be approximately 10% by weight of the catalyst. This solution was further diluted to give a final concentration of approximately 2.5 ppm metal. It was necessary to carry out these dilutions in order for the sample to be on the linear region of the calibration curve.

The copper content of standard solutions were first measured. The copper content of sample solutions were then measured.

Using suitable standard solutions and a cathode lamp suitable for

detecting palladium, the procedure was repeated to determine palladium content of the catalyst precursors containing palladium.

3.3.2 Temperature Programmed Reduction

Temperature programmed reduction (TPR) and chemisorption experiments were performed using the gas apparatus shown schematically in Figure 3.2. The apparatus consisted of mass flow controllers, a thermal conductivity detector (TCD) and a reaction vessel which were all connected using stainless steel tubing.

Gases were all purified before use by passage through a deoxygenating catalyst and then molecular sieves. The deoxygenating catalyst was prepared as follows. A known weight of palladium chloride (0.34 g) was dissolved in water (100 ml) and impregnated on to WO_3 (20 g), the water being removed using a rotary evaporator. The catalyst was then placed in a small glass vessel and activated by passing hydrogen gas over it for 60 minutes. After passage through the deoxygenator the inlet gases were dried using Linde 5a molecular sieves contained in a brass cylinder which was reactivated by heating to 423 K every two weeks.

Mass flow controllers were used to give a desired flow of H_2/N_2. Mass flow control differs from volumetric flow control in that it measures the number of molecules in the process gas rather than the volume of the gas. This produces a more consistent measurement of gas flow since, unlike volumetric flow, the mass of the gas is not affected by environmental factors such as temperature and pressure.

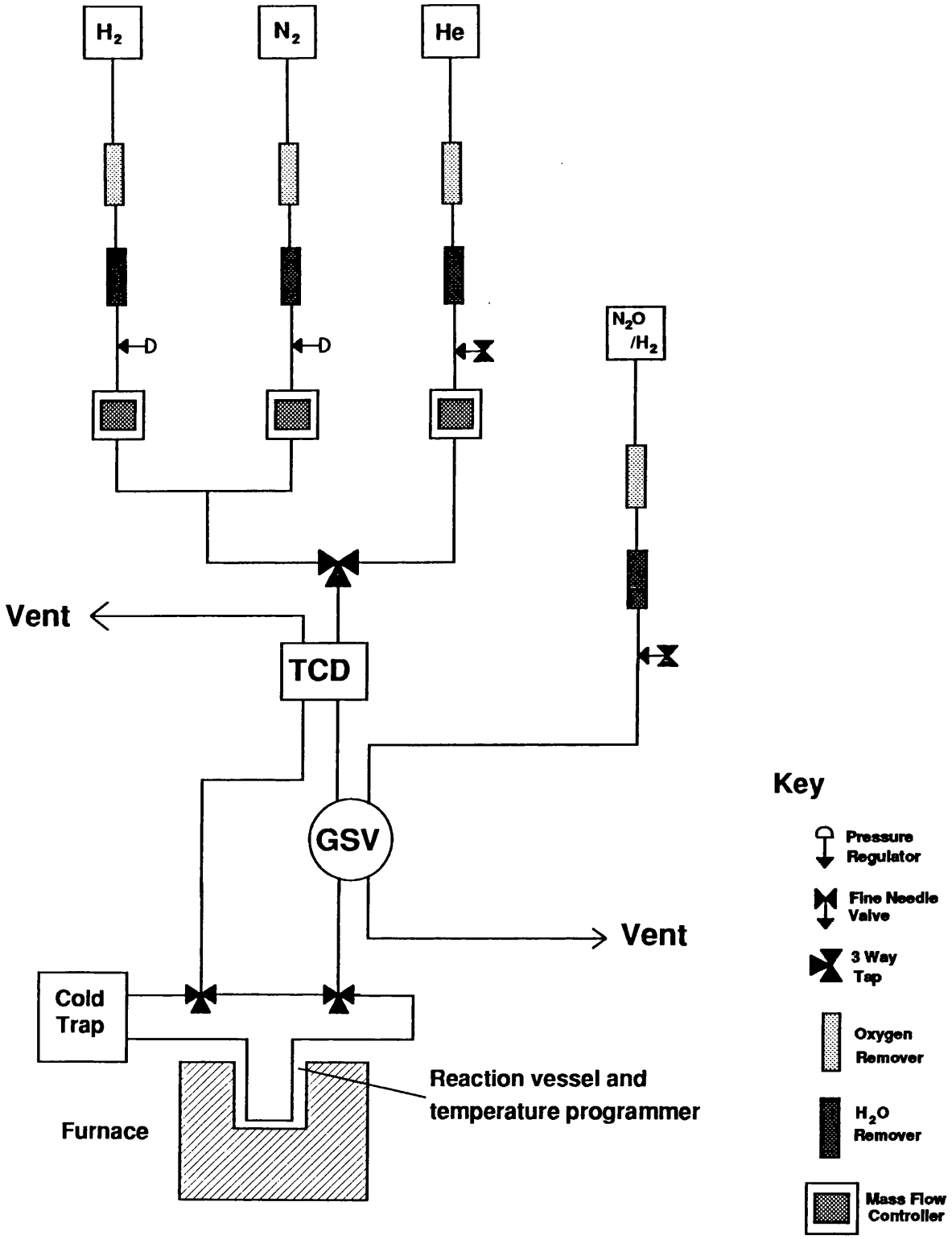

Figure 3.2. Schematic Diagram of the TPR Line

The mass flow controllers consisted of three basic units; a flow sensor, a control valve and an electronic control system. The flow through the sensor was measured thermodynamically. Heat is directed to the midpoint of a flow carrying sensor tube (Figure 3.3). Resistance temperature elements (T_1 and T_2) are placed at equidistant points upstream and downstream of the heat input. The gas stream carries an increasing amount of heat towards the downstream element, T_2, from the upstream element, T_1, during carrier gas flow. A temperature difference, proportional to the amount of gas flow is interpreted by a bridge circuit and an amplifier provides the output to the controller readout. The power supply to each controller could be adjusted between 0 and 100% to produce a range of flows. A bubble flow meter attached to the reactor effluent stream was used to calibrate the hydrogen and nitrogen gas flows (Figures 3.4 and 3.5). In this way a reducing gas of 94% nitrogen and 6% hydrogen was obtained.

The thermal conductivity detector (TCD) consisted of a set of two twin filaments, axially mounted in spaces containing the gas to be analysed. One set of filaments was in contact with a stream of reference gas (unreacted gas) while the second was in contact with the gas to be analysed. Heat was transferred from these hot wires, situated in the gases, at a rate proportional to the thermal conductivity of the gas which was in turn related to its composition. The filaments were connected to a Wheatstone Bridge circuit with a sample arm and a reference arm. The reducing gas was directed through the reference side, then through the

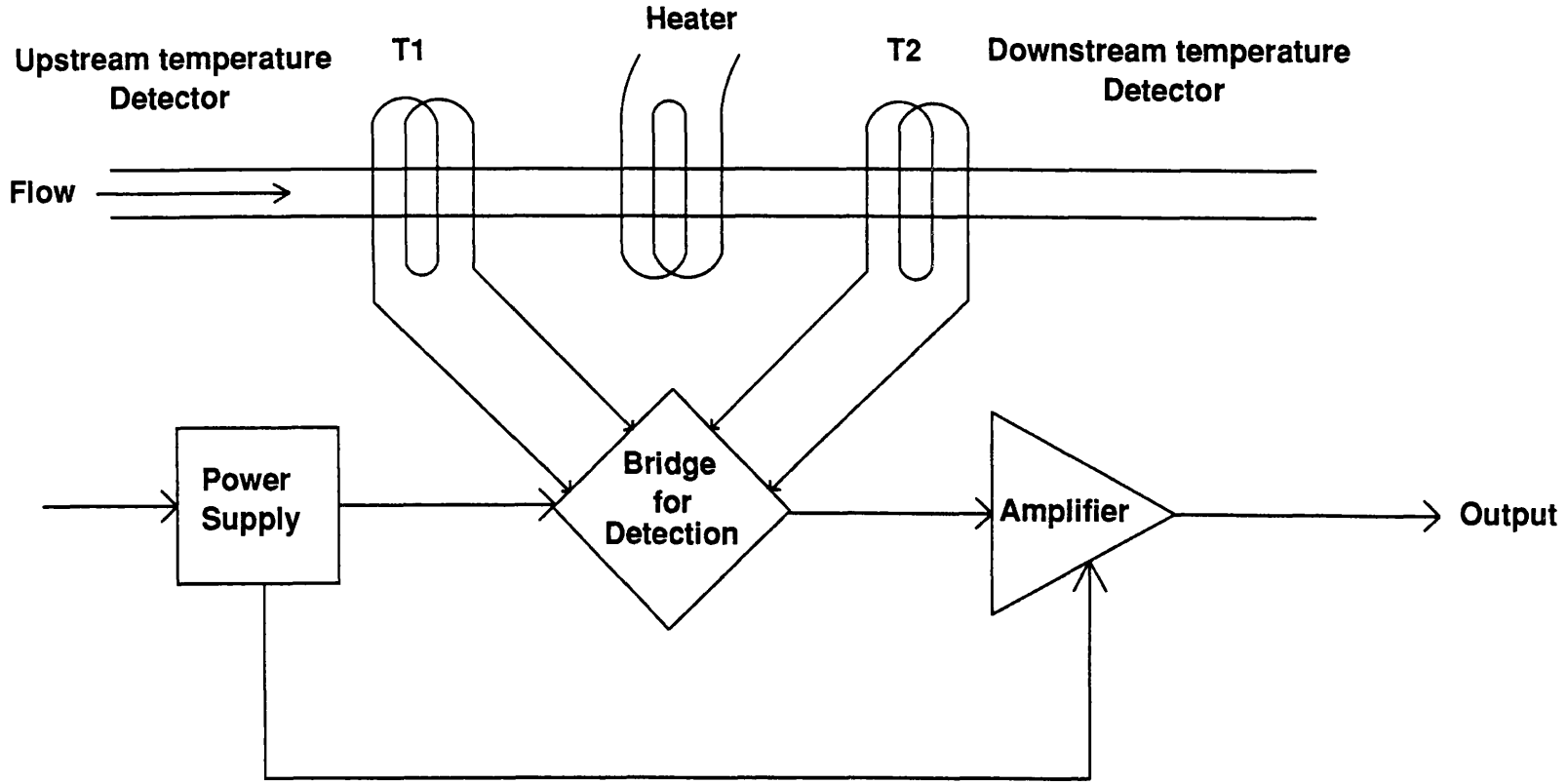

Figure 3.3. Schematic Diagram of a Mass Flow Controller

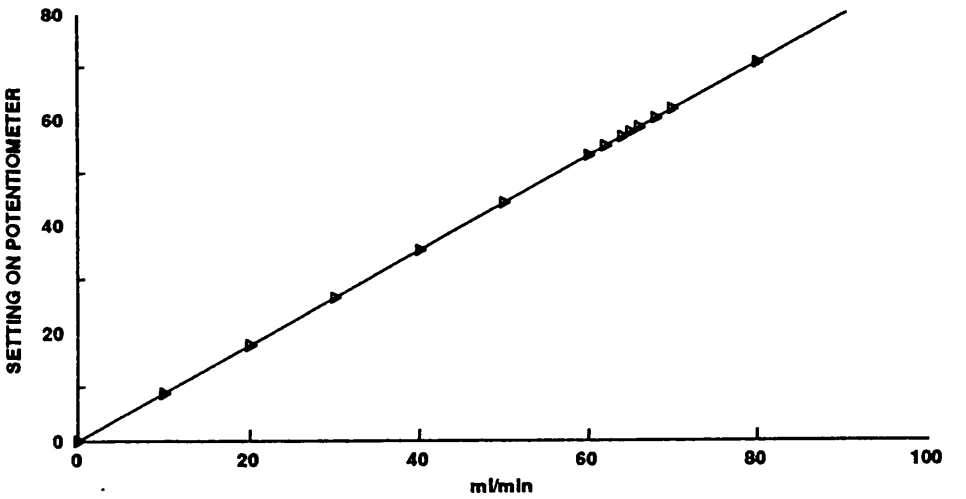

Figure 3.4 Calibration of the Mass Flow Controller for Hydrogen.

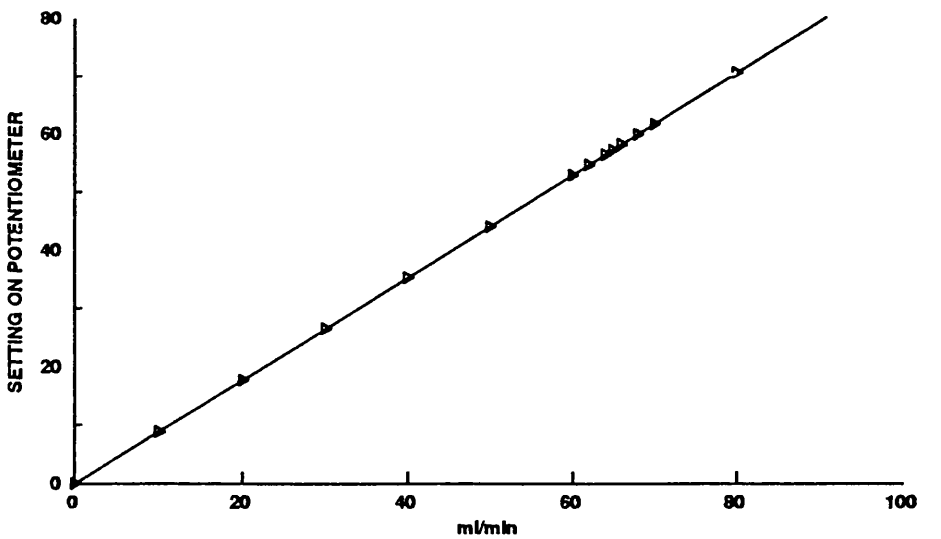

Figure 3.5 Calibration of the Mass Flow Controller for Nitrogen.

reactor vessel containing the catalyst sample and finally, via a cold trap, through the other arm of the TCD. Any differentiation in the gas composition between the arms of the detector resulted in an imbalance in the Wheatstone Bridge which was measured and, after amplification, plotted as a peak on the integrator. The TCD was therefore used to detect any hydrogen taken up by the catalyst. The cold trap consisted of a dewar flask containing dry ice and acetone and was incorporated to remove any reduction products from the gas stream which may have been harmful to the tungsten filaments of the TCD.

The use of the sample valve is explained later in this section. The reactor vessel is shown in Figure 3.6. The reactor was surrounded by a furnace which was connected to a temperature programmer. The temperature in the reactor was measured by a thermocouple.

The furnace and programmer were supplied by Cambridge Process Controls, the amplifier by Gow-Mac Ltd., the integrator by Hewlett Packard Ltd. and the mass flow controllers by Brooks Control Ltd.

A summary of the experimental conditions used in a normal TPR experiment are shown in Table 3.2.

Table 3.2 TPR Experimental Conditions.

6% H_2/N_2 gas flow rate	40 ml min^{-1}
He gas flow rate	50 ml min^{-1}
Ramp rate	10 K min^{-1}

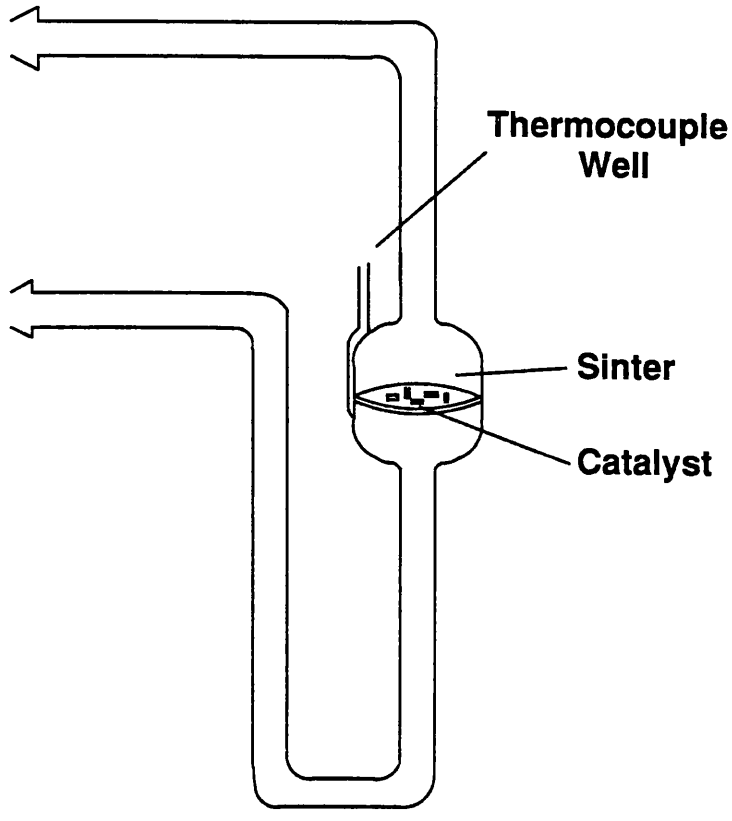

Figure 3.6. Schematic Diagram of the TPR Vessel

The experimental procedure was as follows. A known weight (ca. 0.2 g) of catalyst sample was placed in the reactor vessel and purged with helium until a steady base line was obtained on the integrator. The reducing gas was then brought on line at ambient temperature and the base line again allowed to settle. Once a steady, level plot was obtained the temperature was ramped steadily at a linear rate of 10 K min^{-1}. As the reduction temperature of a specific species in the catalyst was reached, consumption of hydrogen occurred and the corresponding change in the composition of the effluent gas was monitored by the TCD, resulting in a peak on the integrator. The temperature was recorded at this point. In this way a TPR profile was obtained for each of the catalysts. TPR profiles with a starting temperature of 193 K were obtained by placing a vessel containing dry ice and acetone around the reactor before heating.

The number of moles of hydrogen consumed by a catalyst during reduction can be measured using the apparatus shown in Figure 3.2. Initially the apparatus was calibrated using a pulse flow technique. A reactor, containing no catalyst, was attached to the line and the system was purged with nitrogen. The gas sample valve (Figure 3.7) was used to inject fixed volumes of hydrogen into the nitrogen carrier gas stream, which were recorded as a peak on the integrator as explained earlier. By varying the sample loop size a calibration curve of volume of hydrogen versus area under the peak on the integrator could be constructed. This was used to calculate the hydrogen consumption for each catalyst being studied.

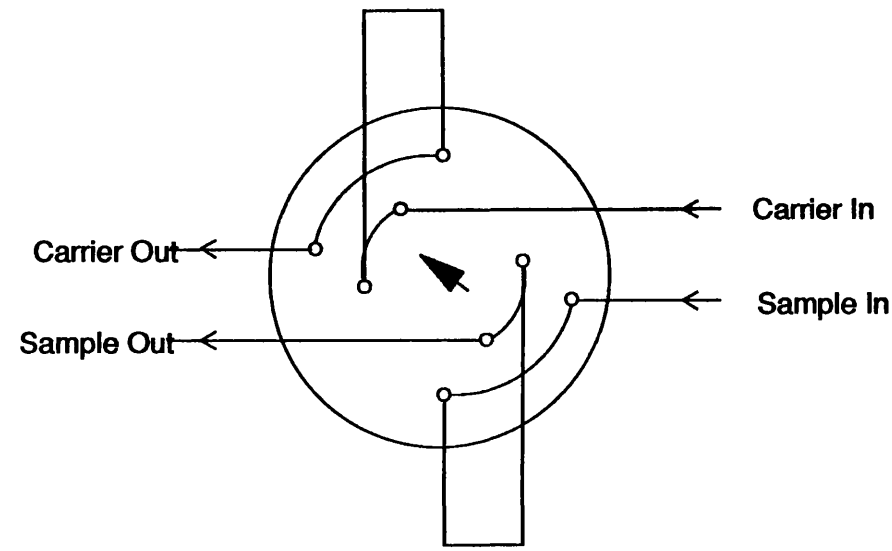

Position A

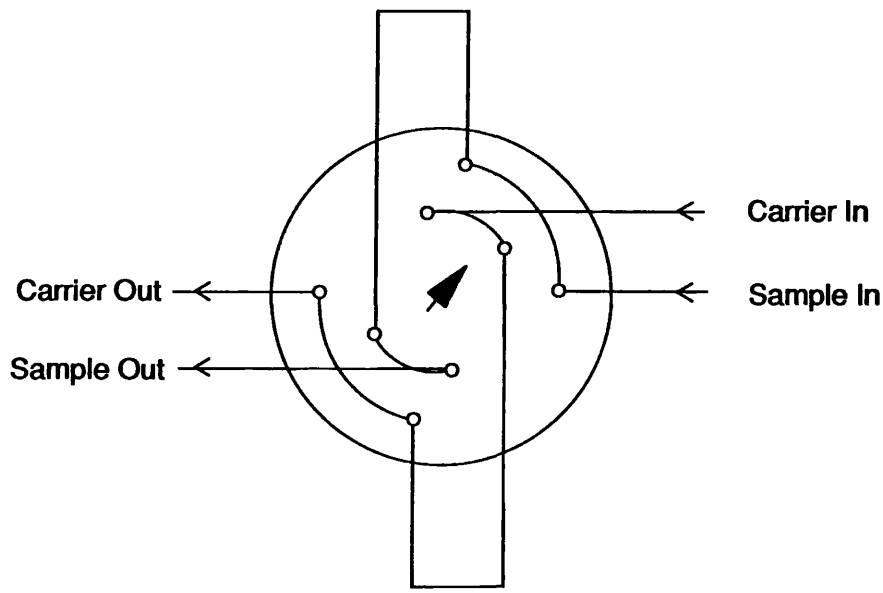

Position B

Figure 3.7. Schematic diagram of the gas sampling valve.

3.3.3 Nitrous Oxide Decomposition

A pulse chromatographic method was used to determine the copper metal surface areas. Pulses of nitrous oxide (N_2O) were passed over the reduced catalyst. The nitrous oxide undergoes decomposition on the copper surface (115)

$$2\ Cu + N_2O \rightarrow N_2 + Cu_2O$$

and hence the number of moles of nitrogen formed can be used as a measure of the copper surface area. The gas line shown in Figure 3.2 was used, but a chromatography column was placed before the sample side of the TCD. The column was packed with Poropak N which separated the nitrogen gas, formed during the decomposition, and nitrous oxide. The catalysts were reduced as before (Section 3.3.2), held at 673 K for 30 minutes and cooled to 333 K in helium gas prior to pulsing with nitrous oxide. A gas sample valve (Figure 3.7) was used to inject fixed volumes of nitrous oxide into the helium carrier gas stream. A sample chromatograph is shown in Figure 3.8. The system was calibrated for nitrogen by pulsing known volumes of nitrogen gas into the helium gas stream.

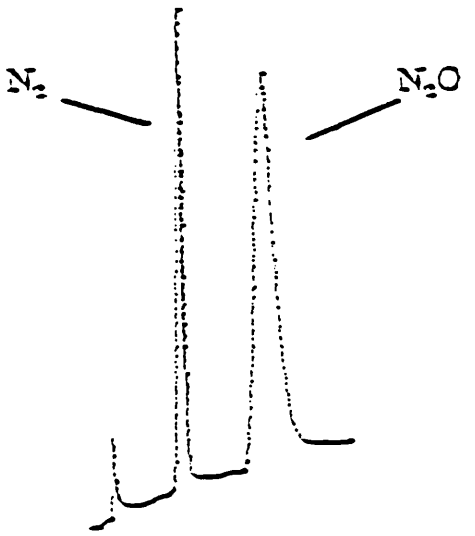

Figure 3.8 Sample Chromatograph of Nitrous Oxide Decomposition.

3.3.4 Transmission Electron Microscopy

Selected catalyst samples were studied by transmission electron microscopy (TEM) using a JEOL, 1200EX transmission electron microscope. Specimens were prepared by suspending the catalyst samples in water and then mounting them on carbon covered copper grids.

3.3.5 Characterisation Experiments at ICI

3.3.5a Determination of the Surface Areas and Pore Size Distributions of the Catalyst Precursors

BET surface areas (N_2, 77 K) were obtained from five-point adsorption isotherms using a Fluorosorb 2300 Micromeritics instrument. The pore size distribution of each of the supports and the catalyst precursors were determined by mercury porosimetry using an Autoport 9200.

3.3.5b Study of the Phase Changes Occurring on Reduction Using Hot Stage X-ray Diffraction

Hot stage X-ray diffraction studies of the calcined catalyst precursors were carried out using a Siemens Kristalloflen D500 diffractometer and iron filtered cobalt radiation ($\lambda(K_\alpha)$ = 0.179 nm). Catalysts were heated in 1.5% hydrogen in nitrogen from 303 K to 423 K and then in 50 K steps up to 573 K. A diffraction trace (counts per second against 2Θ) was collected at each temperature step.

3.4 HYDROGENATION REACTIONS

The selective hydrogenation of cinnamaldehyde (3-phenyl prop-2-enone) was carried out in the liquid phase at atmospheric pressure and at 408 K. Decalin (decahydronapthalene) was used as the solvent for the reaction.

3.4.1 Materials

Decalin (99%) was supplied by Aldrich in 500 ml sureseal bottles, stored under nitrogen. Cinnamaldehyde (3-phenyl prop-2-enone) (99%) and the hydrogenation products, hydrocinnamaldehyde (3-phenyl propionaldehyde) (95%), phenyl propanol (98%) and cinnamyl alcohol (3-phenyl prop-2-enol) (98%) were supplied by Aldrich. Cinnamaldehyde, hydrocinnamaldehyde and phenyl propanol were further purified by distillation and degassed in flowing helium before use. Cinnamyl alcohol, being a high melting point solid, was used as obtained from Aldrich.

3.4.2 The Reactor System

Liquid phase hydrogenations of cinnamaldehyde were carried out using the apparatus shown in Figure 3.9. Helium and a 6% H_2/N_2 reducing gas mixture were supplied to the reaction vessel using the system shown in Figure 3.10. Hydrogen gas was supplied separately to the system using a bubbler inserted into one of the arms on the reaction vessel. Gas flow rates were measured with a bubble flow meter attached to the exit side of the reaction vessel and are listed in Table 3.3.

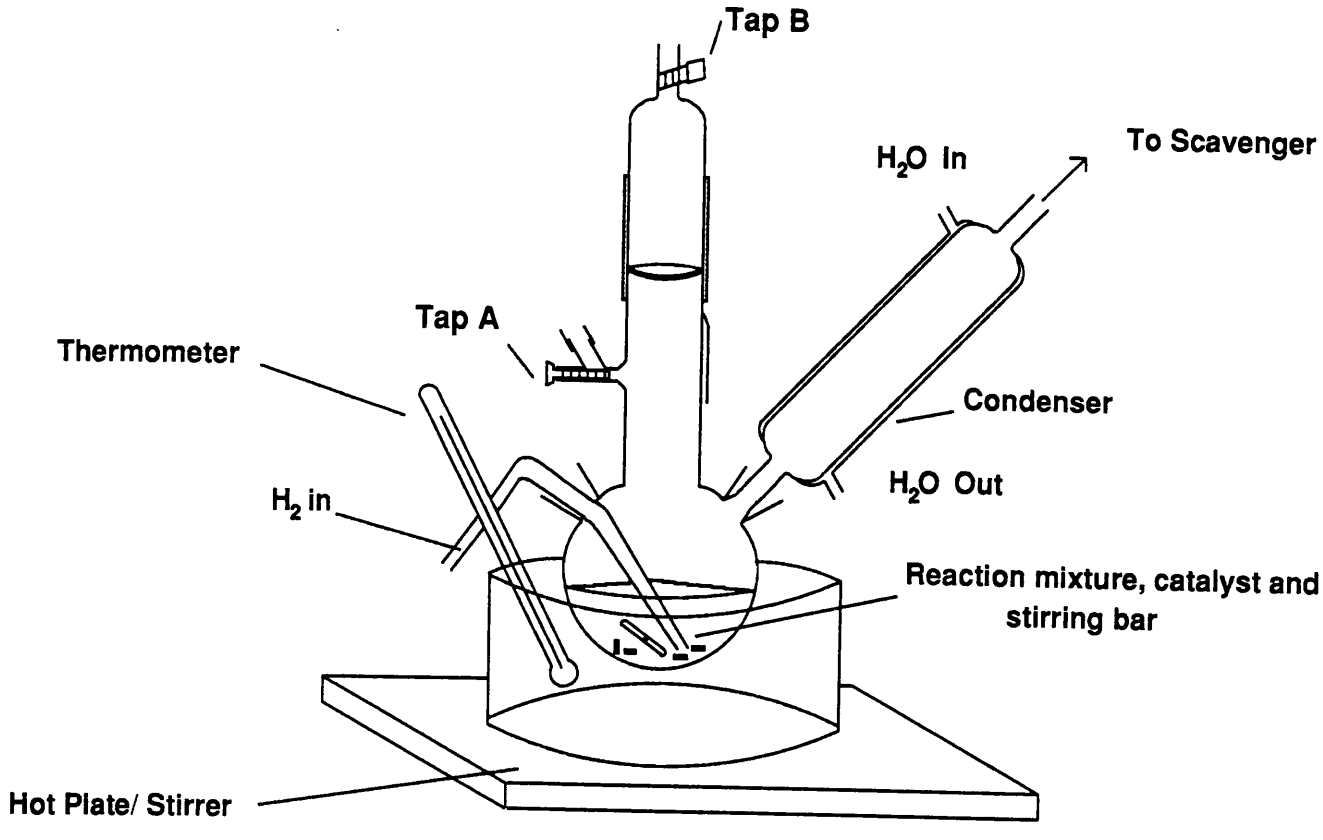

Figure 3.9. Schematic Diagram of the Hydrogenation Apparatus

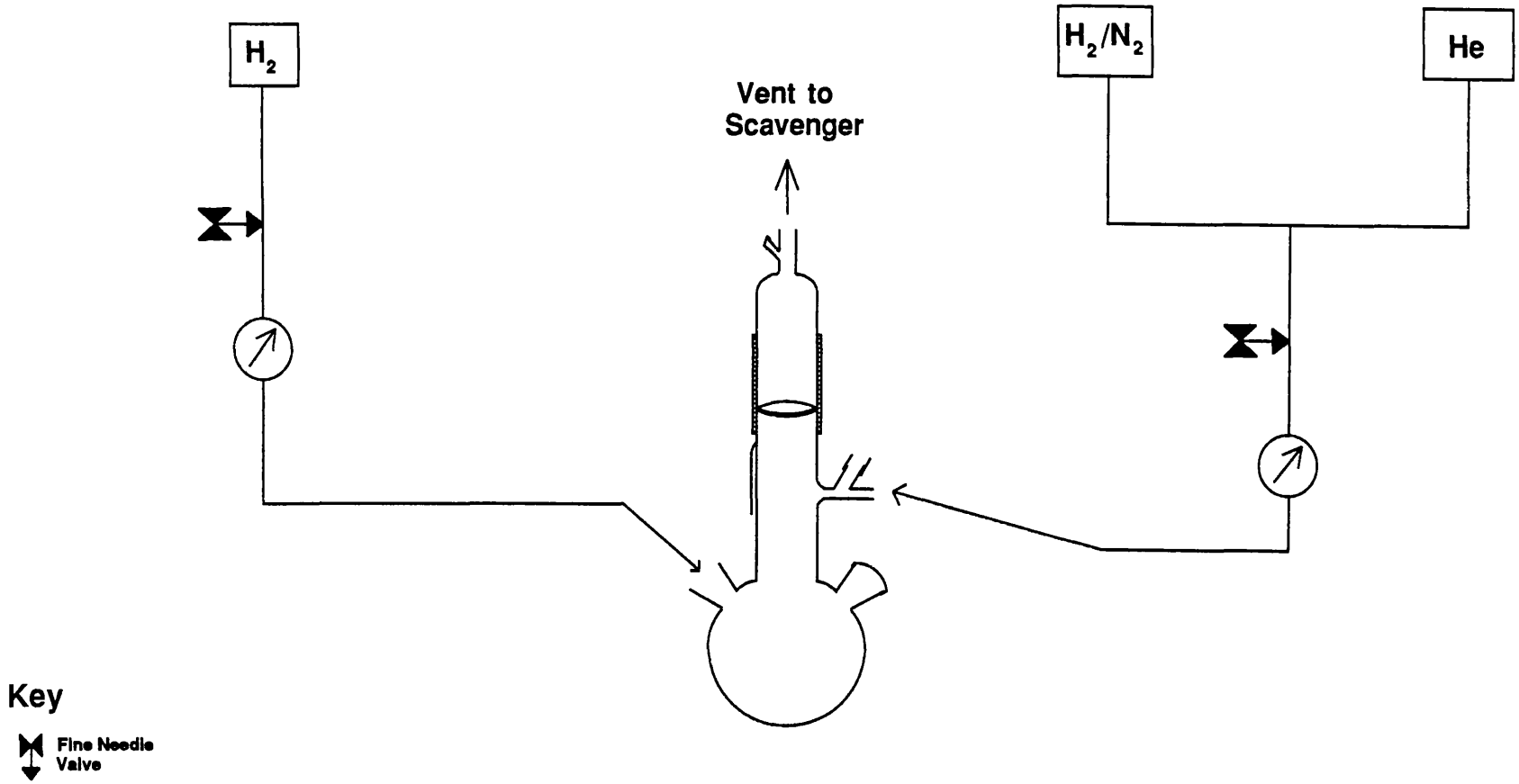

Figure 3.10. Schematic Diagram of the Gas Supply tp the Reactor

Table 3.3 Gas Flow Rates for Hydrogenation Reaction.

Gas	Flow Rate (ml min^{-1})
6% H_2/N_2	20
He	50
H_2	35

The reaction vessel was surrounded by an electric furnace the current to which was controlled using a Variac transformer. The temperature at the sinter was measured by an electronic thermocouple placed into a well at the side of the reaction vessel.

3.4.3 Experimental Conditions

Each calcined precursor was reduced in the reaction vessel prior to its use for the hydrogenation reaction. To facilitate this the reaction vessel was turned upside down as in Figure 3.11, clamped and connected to the gas supply, at tap A, and to the gas scavenger system, at tap B. A known weight of catalyst was placed on the sinter and the two arms of the reaction vessel were sealed off with B14 septum caps. Taps A and B were then opened and the system purged in helium for five minutes. The gas supply was then switched to the 6% hydrogen/nitrogen gas mixture and the catalyst reduced overnight. Unless stated otherwise, the catalysts were heated at 10 K per minute to 673 K and held at this temperature overnight.

After reduction the catalyst was purged with helium at the reduction temperature and then allowed to cool to room temperature in a

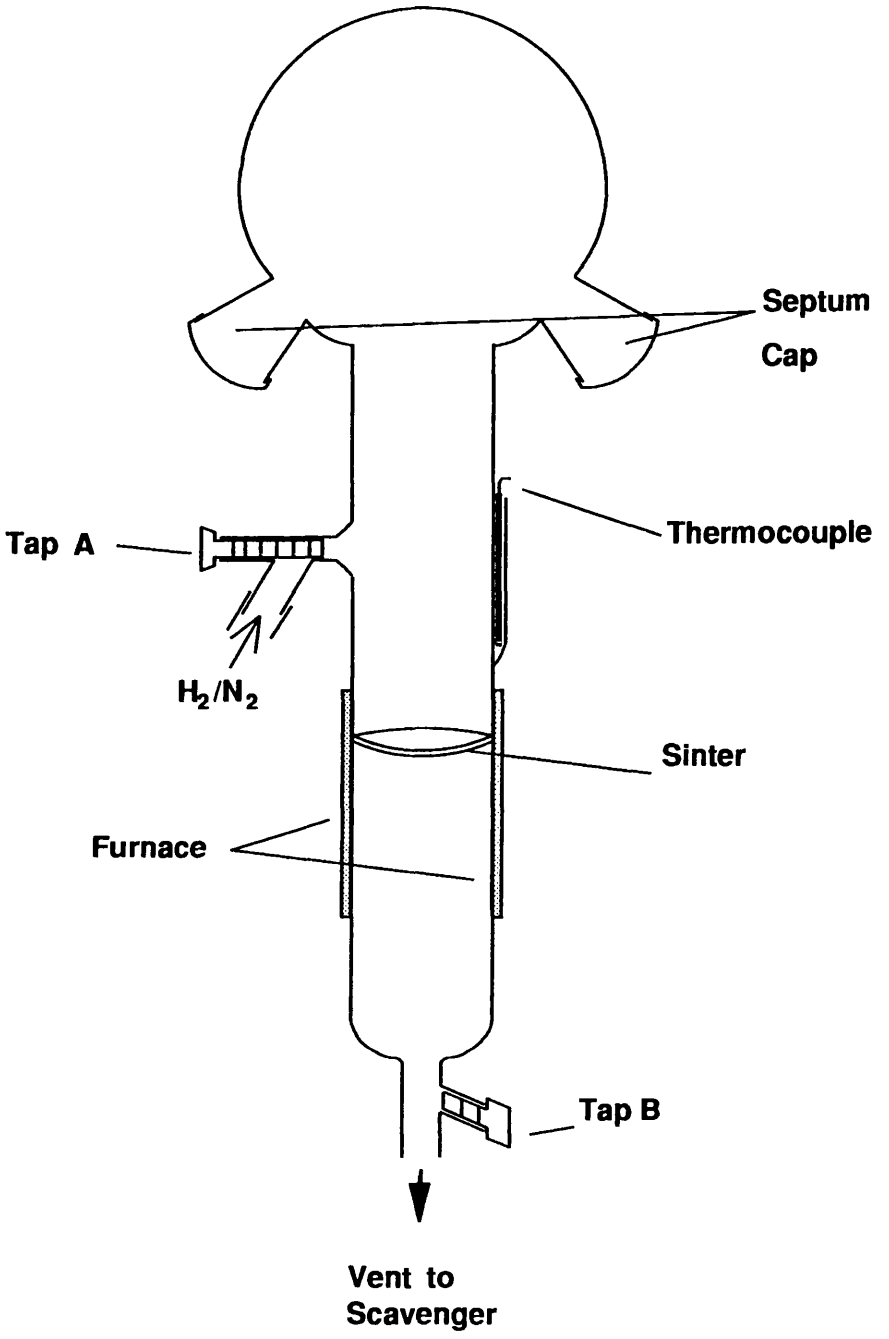

Figure 3.11. Apparatus for Reduction

steady flow of helium. The reaction vessel was then inverted and placed in a heated oil bath on a magnetic stirrer as in Figure 3.9. Tap B was then closed resulting in a positive pressure of helium within the reaction vessel. Decalin (25 ml) was then injected into the reaction vessel through a septum. The catalyst was less susceptible to oxidation once covered in solvent and the two septa on the reaction vessel outlet could be removed at this stage to permit a condenser to be attached to one arm and a hydrogen bubbler to the other arm of the reaction vessel. Hydrogen gas was bubbled through the solvent for five minutes. The hydrogen bubbler contained a porous sinter to disperse the hydrogen and enhance its solubility in the solvent thus increasing the amount of hydrogen available at the catalyst surface. Reactant was then added to the solvent using a syringe. The helium flow was then switched off and the reaction mixture was stirred using a magnetic stirrer. Hydrogen gas was bubbled through the reaction mixture for varying lengths of time. With a positive pressure of helium in the reaction vessel samples of the reaction mixture were withdrawn at regular intervals and analysed to follow the reaction.

3.4.4 Analysis of the Reaction Mixture

A Phillips PU4500 Gas Chromatograph fitted with a flame ionisation detector (FID) was used to analyse both the reactant and hydrogenation reaction products. The FID was attached to an electronic integrator. Samples were injected on to a glass column (length 2 metres, internal diameter 4 mm) using a 10 µl syringe. The injection port was

held at a temperature of 493 K. The column was packed with 5% (w/w) Carbowax 20M on Chromosorb WAW (mesh size 80 - 100). The column and the packing were supplied by Phase-Sep. The column was conditioned by heating, in flowing nitrogen (20 ml min^{-1}), from room temperature to 453 K at a ramp rate of 0.5 K min^{-1}. The column was then held at 453 K overnight. The column separated out the solvent, reactant and products. They were eluted in the order

Decalin < Hydrocinnamaldehyde < Cinnamaldehyde

< Phenyl propanol < Cinnamyl alcohol

During the analysis the nitrogen carrier gas flow rate was set at 40 ml min^{-1}. The column was held at 403 K for ten minutes then ramped to 433 K at 1 K min^{-1}. The sample constituents were detected using an FID. The FID was attached to an electronic integrator.

When a sample was injected into the G.C. it was immediately vapourised. The vapourised sample was then separated on the column. When one of the constituents of the sample passed through the FID the change in the composition of the nitrogen carrier gas was detected by the FID and this appeared as a peak on the electronic integrator. A typical printout from the electronic integrator is shown in Figure 3.12. Peak areas were calculated by the integrator.

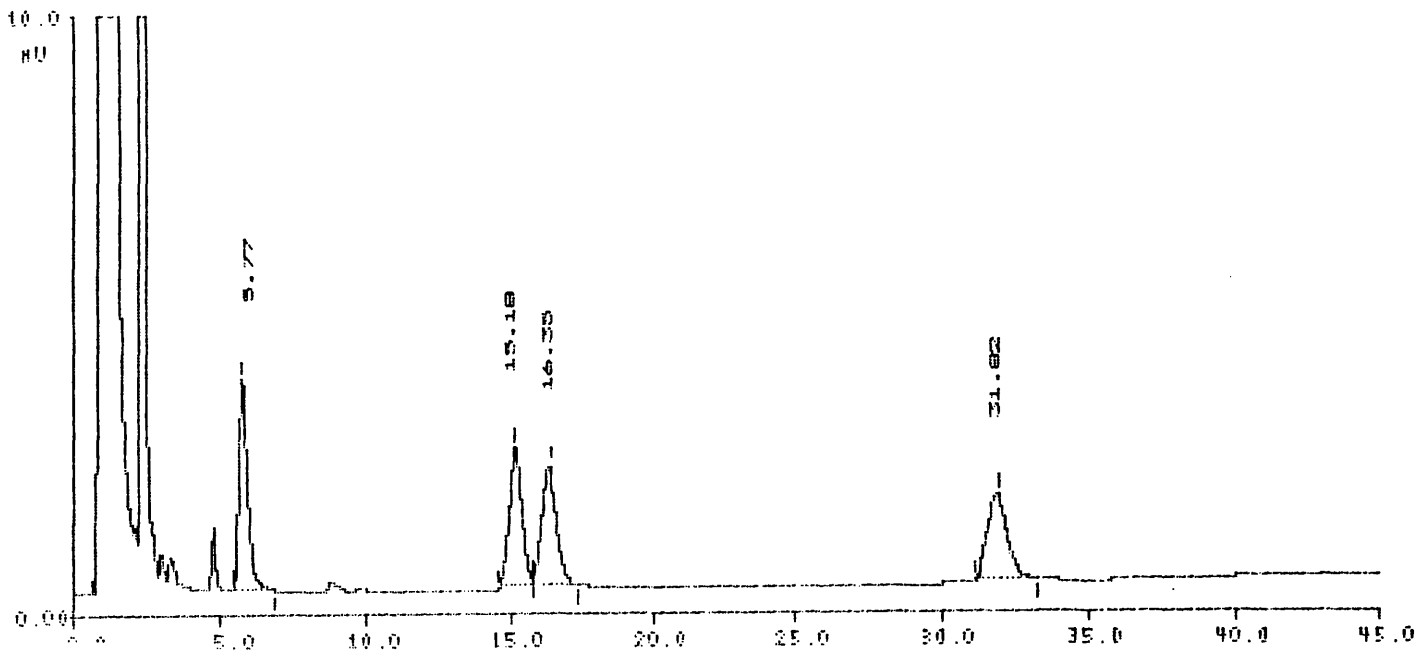

Figure 3.12 Sample Chromatograph for Hydrogenation Reaction.

3.4.5 Deuteration of Cinnamaldehyde

The mechanism of the hydrogenation of cinnamaldehyde was followed by employing deuterium as a tracer atom. In those experiments in which deuterium was used instead of hydrogen, the catalyst, (1.80 g G.U. CuO/SiO_2), was reduced as before. Decalin (15 ml) was then sprayed over the catalyst and deuterium was bubbled through the solvent at 2 ml min^{-1}. Cinnamaldehyde (2 ml) was then added to the reaction mixture and the reaction carried out at 408 K. The constituents of the reaction mixture were measured at set time intervals by G.C. The reaction mixture was also analysed by proton and deuterium NMR using a Brooker AM 200MHz spectrometer. Chloroform ($CHCl_3$) was used as the solvent.

Chapter 4

TREATMENT OF RESULTS

4.1 ATOMIC ABSORPTION

Metal loadings were determined for copper and palladium containing catalysts by atomic absorption as outlined in the experimental section (Section 3.3.1). Calibration curves were constructed for each metal using appropriate standards. A typical calibration curve is shown in Figure 4.1 where absorption (arbitrary units) is plotted against ppm copper.

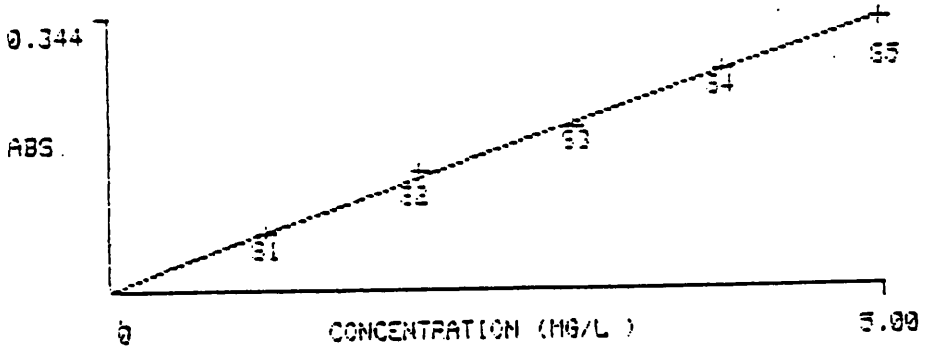

Figure 4.1 Calibration curve for atomic absorption.

A sample was then tested and a reading of the amount of metal present was given. This reading was given in micrograms per ml. This value was then converted to the amount of metal present in the sample of catalyst used and then to a percentage metal present in the catalyst.

4.2 TEMPERATURE PROGRAMMED REDUCTION

Temperature programmed reduction experiments were carried out in the pulse-flow system described in Section 3.3.2. Hydrogen consumptions by the catalysts during reduction were measured by this system. As described earlier fixed volumes of hydrogen gas were injected into a nitrogen carrier gas stream using the sample valve. These fixed volumes were recorded as peaks on the electronic integrator.

The number of moles of hydrogen gas injected into the nitrogen carrier stream per pulse was calculated by substitution into the gas equation

$$n = \frac{PV}{RT}$$

where n = number of moles of H_2

P = pressure of H_2 (atmospheric pressure)

T = temperature

V = volume of sample loop.

The number of hydrogen molecules injected per pulse was calculated by multiplying the number of moles of hydrogen by Avogadro's number.

A hydrogen calibration curve of number of molecules H_2 against integrator area was constructed by varying the size of the H_2 pulse injected into the carrier stream of the detector (Table 4.1, Figure 4.2).

Table 4.1 Values for H_2 Calibration.

Sample Loop Size µl	No. Of Molecules H_2 x 10^{17}	Average Area
10	2.46	28195
20	4.92	56398
50	12.30	141142
100	24.61	282205

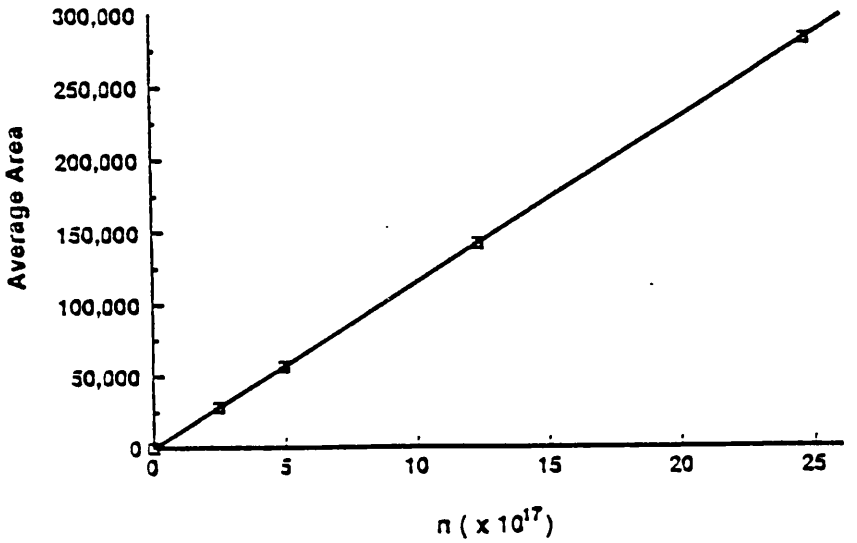

Figure 4.2 Calibration curve for H_2.

The plot of area against molecules H_2 (Figure 4.2) showed that the number of molecules of hydrogen pulsed was directly proportional to the area on the integrator.

The number of molecules of hydrogen consumed during an experiment could be calculated by comparing the area under the peak, or peaks, after a T.P.R. experiment to that for a fixed volume of hydrogen pulsed earlier. Standard deviations were calculated as follows:-

$$\sigma = \sqrt{\frac{\Sigma(\overline{X} - X)^2}{N}}$$

$\overline{X}$ = mean hydrogen consumption of T.P.R. experiments

X = hydrogen consumption for T.P.R. experiment

N = the number of T.P.R. experiments.

4.3 NITROUS OXIDE DECOMPOSITION

Nitrous oxide decomposition experiments were carried out in the pulse-flow system described in Section 3.3.2 in order to measure the copper surface areas of the reduced catalysts. Initially fixed volumes of nitrogen were injected into a helium carrier gas stream and a calibration curve of the integrated area against the number of molecules of nitrogen was plotted.

Table 4.2 Values for N_2 Calibration.

Volume N_2 µl	No. Of Molecules N_2 x 10^{17}	Average Area
10	2.46	38006
20	4.92	75634
50	12.30	189518
100	24.61	379162

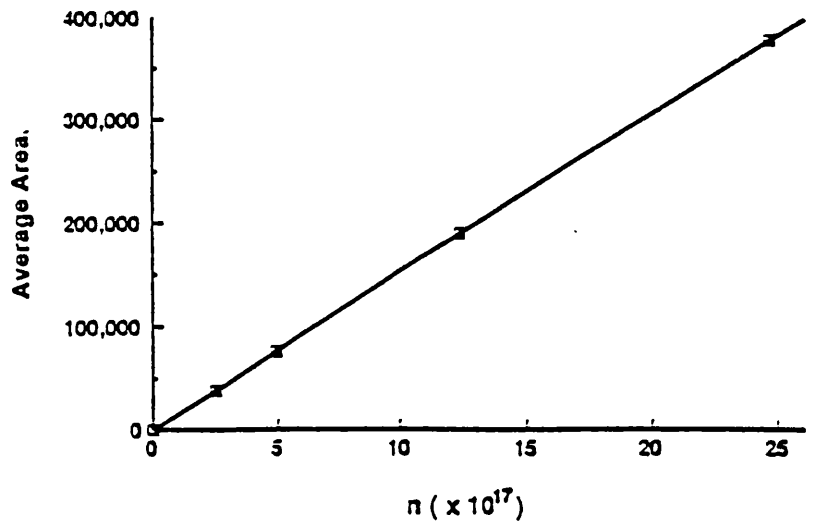

Figure 4.3 Calibration Curve for N_2 Formation.

Nitrous oxide gas was pulsed over the reduced catalyst as described in Section 3.3.3. Nitrous oxide undergoes decomposition at surface copper sites to give nitrogen gas and a surface species, Cu_2O. Nitrogen gas evolved was measured chromatographically. Pulsing was continued until no more nitrogen was detected on the chromatogram. At this point it was assumed the catalyst was completely saturated. The number of molecules of nitrogen formed was then calculated from the calibration curve (Figure 4.3).

The copper metal dispersion (d) can be calculated from the volume of nitrogen evolved. The reaction of nitrous oxide with copper has been shown to take the form (115):-

$$N_2O(g) + 2\ Cu(s) \rightarrow N_2(g) + Cu_2O(s)$$

where $Cu_2O(s)$ is a surface species.

A bridged copper species is formed on the catalyst and the number of surface copper atoms is equal to twice the number of oxygen molecules chemisorbed or nitrogen molecules formed. Therefore the number of surface copper atoms can be determined from the number of nitrogen molecules formed. The dispersion d of a catalyst is then defined as

$$d = \frac{\text{number of surface metal atoms}}{\text{total number of metal atoms}} \times 100\ \%$$

The copper metal surface area can be calculated if the number of metal atoms per unit area of surface is known. If it is assumed that a surface consists of equal proportions of main low index crystal planes then for a polycrystalline surface of copper the number of metal atoms per unit area of surface is defined as being equal to $1.47 \times 10^{19}\ m^{-2}$ (73). The copper

metal surface area A is then defined as

$$A = \frac{\text{number of surface metal atoms}}{\text{number of surface atoms per unit of polycrystalline surface.}}$$

4.4 HYDROGENATION REACTIONS

4.4.1 Calibration of the G.C.

The hydrogenation reactions were carried out in the reactor system described in Section 3.4. Gas chromatography was used to analyse the reaction products. The G.C. was calibrated by making several standard mixtures of all of the reaction products with known mole fractions of each reaction product in each mixture. For example, 5 microlitres of cinnamaldehyde, hydrocinnamaldehyde and phenyl propanol were added to a vessel containing 5 ml of decalin solvent. Cinnamyl alcohol is a solid at room temperature so a standard solution was prepared by dissolving 0.4321 g of cinnamyl alcohol in 100 ml of decalin. The molarity of the standard solution was 0.0315 M. The number of moles of cinnamaldehyde added was 3.965×10^{-5} moles. Therefore 1.26 ml of the standard cinnamyl alcohol solution were added in order to add a similar number of moles of cinnamyl alcohol to the standard mixture. This gave a standard solution with known mole fractions of the reactant products.

A microsample of this standard was then analysed by the G.C. The results are shown in Table 4.3.

Table 4.3

Product	Mole Fraction	% Area
Cinnamaldehyde	0.257	24.79
Hydrocinnamaldehyde	0.246	25.20
Cinnamyl alcohol	0.257	25.42
Phenyl propanol	0.240	24.59

The procedure was repeated for standard solutions with mole fractions in the range 0.05 - 0.95 for each product. A graph of percentage area against mole fraction was then plotted for cinnamaldehyde, hydrocinnamaldehyde, cinnamyl alcohol and phenyl propanol (Figures 4.4 - 4.7). The composition of any reaction could then be determined using the calibration graphs.

4.4.2 Conversion Levels

The mole fraction of reaction which has undergone hydrogenation is denoted as A. When cinnamaldehyde is the reactant

A = 1 - mole fraction cinnamaldehyde.

The percentage conversion is then given by

% Conversion = (A x 100) %.

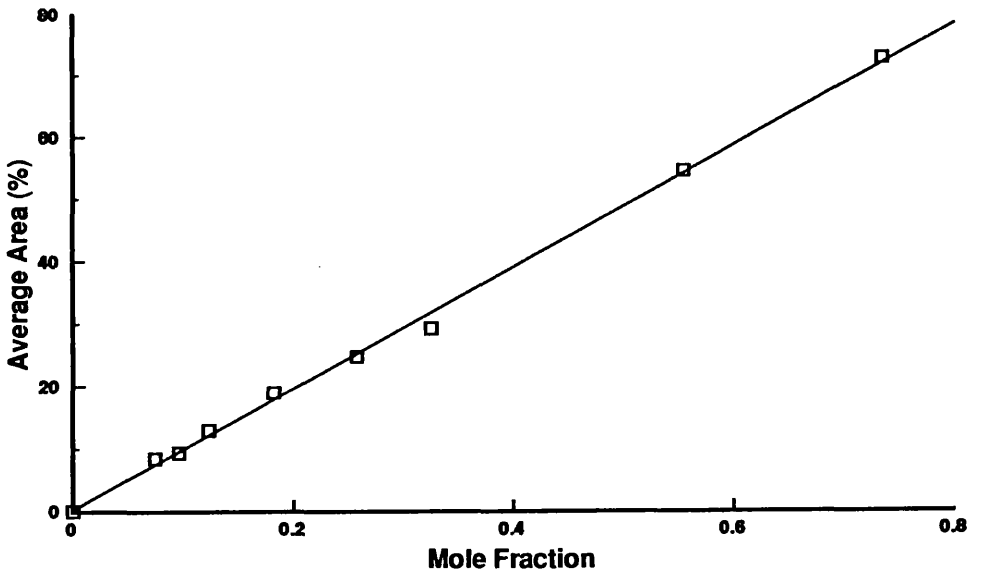

Figure 4.4. Calibration graph for cinnamaldehyde

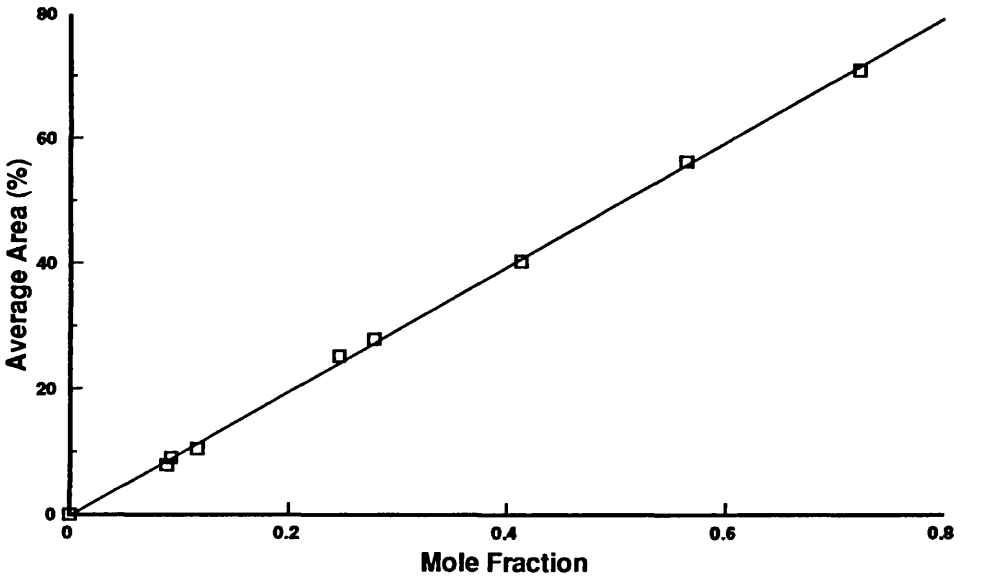

Figure 4.5. Calibration graph for hydrocinnamaldehyde

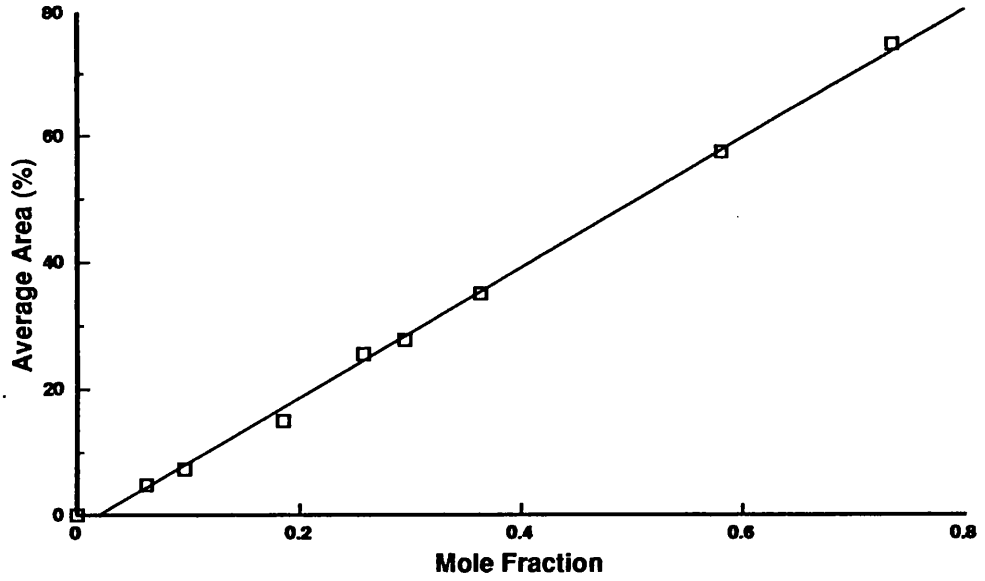

Figure 4.6. Calibration graph for cinnamyl alcohol

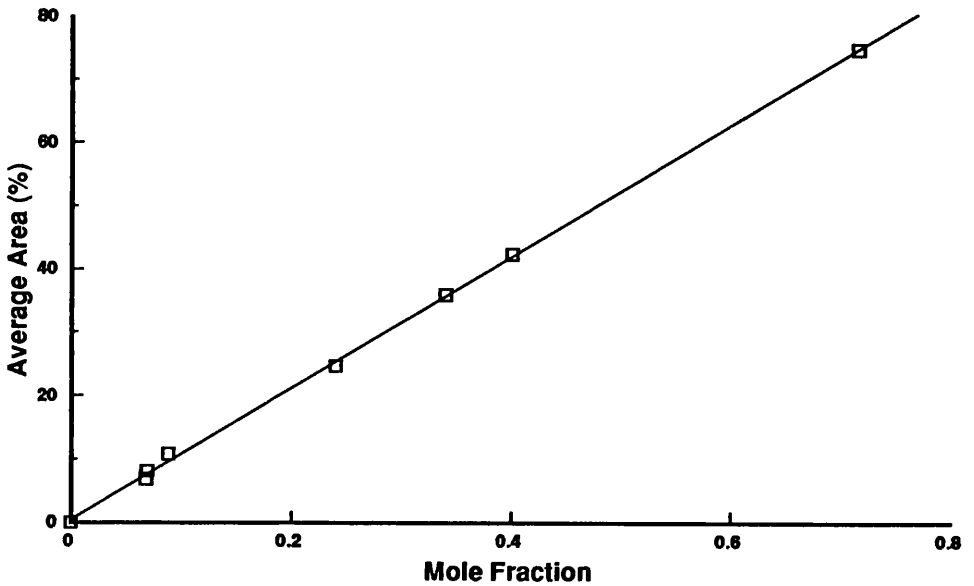

Figure 4.7. Calibration graph for phenyl propanol

4.4.3 Selectivity (S)

Percentage selectivities have been calculated from the following equations.

(1) Selectivity to cinnamyl alcohol.

$$S_{CAL} = 100 \times \frac{\text{mole fraction cinnamyl alcohol } (M_{CALC})}{\text{mole fraction of reactant which has been hydrogenated}}$$

$$i.e. \quad S_{CAL} = \frac{M_{CALC}}{A} \times 100 \qquad (i)$$

(2) Selectivity to hydrocinnamaldehyde.

$$S_{HCA} = 100 \times \frac{\text{mole fraction hydrocinnamaldehyde } (M_{HCA})}{A}$$

$$i.e. \quad S_{HCA} = \frac{M_{HCA}}{A} \times 100 \qquad (ii)$$

(3) Selectivity of CAL over HCA.

$$S_{CAL\text{-}HCA} = \frac{\text{mole fraction CAL}}{\text{mole fraction HCA}}$$

$$i.e. \quad S_{CAL\text{-}HCA} = \frac{M_{CAL}}{M_{HCA}}$$

4.4.4 Reaction Rates

Reaction rates were calculated by comparing the disappearance of reactant with time. Graphs of percentage conversion versus time were constructed for each catalyst. The reaction rate at any time is given by the slope of the tangent to the curve at that time. The gradients of the linear regions of the plots of conversion against time were used to determine rate constants for each of the catalysts.

Chapter 5

RESULTS

5.1 ATOMIC ABSORPTION

Copper, vanadium and palladium loadings were determined by atomic absorption as outlined in Section 3.3.1. The ruthenium content of the catalysts had to be estimated as a cathode lamp for the spectrophotometer, suitable for detecting ruthenium, was not available. A full list of the calcined catalyst precursors and their metal loadings, as calculated by atomic absorption, is shown in Table 5.1.

Table 5.1

Industrial Catalysts	Metal loadings as calculated by atomic absorption			Estimated Ru Content
	Cu	V	Pd	
ICI CuO/SiO_2/PQ *a*	12.4			
ICI CuO/SiO_2/Grace *a*	12.4			
ICI CuO/SiO_2/PQ *b*	6.1			
ICI CuO/SiO_2/Grace *b*	5.6			
$CuO/V_2O_5/SiO_2$	12.1	4.5		
$CuO/V_2O_5/PdO/SiO_2$	12.6	4.4	0.022	
V_2O_5/SiO_2		5.2		
Glasgow Catalysts				
G.U. CuO/SiO_2	13.7			
$CuO/PdO/SiO_2$ *a*	13.2		0.01	
$CuO/PdO/SiO_2$ *b*	14.5		0.027	
$CuO/PdO/SiO_2$ *c*	13.7		0.079	
$CuO/PdO/SiO_2$ *d*	17.0		0.15	
$CuO/PdO/SiO_2$ *e*	13.4		0.01	
$CuO/RuO_2/SiO_2$ *a*	10.9			0.027
$CuO/RuO_2/SiO_2$ *b*	10.7			0.079
$CuO/RuO_2/SiO_2$ *c*	14.1			0.15

5.2 TEMPERATURE PROGRAMMED REDUCTION

Temperature programmed reduction (TPR) experiments were performed using the pulse flow reactor system described in Section 3.3.2. The TPR profiles of the catalysts described in Table 5.1. are shown in Figures 5.3 - 5.18. Figures 5.1 and 5.2 show the profiles for analar grade copper oxide and copper oxide prepared from the calcination of copper nitrate respectively. The TPR profile for pure copper oxide consisted of a single reduction peak with a maximum at 533 K. The peak maximum was shifted to 653 K for calcined copper nitrate.

The temperature at each peak maximum, the number of molecules of hydrogen consumed per gram of catalyst and the theoretical hydrogen consumption for each calcined catalyst precursor are given in Tables 5.2 - 5.5. Results for the copper oxide dispersed on silica catalysts are presented in Table 5.2 and results for vanadium containing catalysts are listed in Table 5.3. The supported oxides described in Tables 5.2 and 5.3 were prepared by calcination of the supported precursor salts at 723 K in a muffle oven. The results for CuO/SiO_2 doped with palladium or ruthenium are shown in Tables 5.4 and 5.5 respectively. The impregnated precursors to these catalysts (Tables 5.4 and 5.5) were calcined at 723 K using the apparatus shown in Figure 3.1.

The TPR profiles of the calcined catalyst precursors containing palladium all gave a small broad peak at 263 K after starting the reduction at 193 K instead of 298 K in addition to the peaks shown in Figures 5.10 - 5.15.

Table 5.2

Catalysts	Experimental H_2 consumption (No. of molecules x 10^{21} g^{-1})	Theoretical H_2 consumption (No. of molecules x 10^{21} g^{-1})	$T_{MAX(S)}$ (K)
ICI CuO/SiO_2/ PQ *a*	1.03 ± 9 %	1.18	603
ICI CuO/SiO_2/ Grace *a*	1.12 ± 3 %	1.18	563
ICI CuO/SiO_2/ PQ *b*	0.53 ± 11 %	0.58	559
ICI CuO/SiO_2/ Grace *b*	0.41 ± 3 %	0.42	546
G.U CuO/SiO_2	1.10 ± 6 %	1.30	608, 628

Table 5.3.

Catalysts	Experimental H_2 consumption (No. of molecules x 10^{21} g^{-1})	Theoretical H_2 consumption (No. of molecules x 10^{21} g^{-1})	$T_{MAX(S)}$ (K)
V_2O_5/SiO_2	0.19 ± 16 %	0.30 ($V^{(V)} \rightarrow V^{(IV)}$)	613, 808, 893
$CuO/V_2O_5/SiO_2$	1.32 ± 10 %	1.40	603
$CuO/V_2O_5/PdO/SiO_2$	1.44 ± 11 %	1.44	263, 613

Table 5.4

Catalysts	Experimental H_2 consumption (No. of molecules x 10^{21} g^{-1})	Theoretical H_2 consumption (No. of molecules x 10^{21} g^{-1})	$T_{MAX(S)}$ (K)
$CuO/PdO/SiO_2$ *a*	1.20 ± 6 %	1.25	263, 599
$CuO/PdO/SiO_2$ *b*	1.11 ± 5 %	1.37	263, 553
$CuO/PdO/SiO_2$ *c*	1.11 ± 5 %	1.30	263, 532
$CuO/PdO/SiO_2$ *d*	1.15 ± 5 %	1.61	263, 455, 543
$CuO/PdO/SiO_2$ *e*	1.24 ± 12 %	1.27	263, 697, 729

Table 5.5.

Catalysts	Experimental H_2 consumption (No. of molecules x 10^{21} g^{-1})	Theoretical H_2 consumption (No. of molecules x 10^{21} g^{-1})	$T_{MAX(S)}$ (K)
$CuO/RuO_2/SiO_2$ *a*	0.92 ± 5 %	1.03	530, 567
$CuO/RuO_2/SiO_2$ *b*	1.03 ± 3 %	1.01	534, 569
$CuO/RuO_2/SiO_2$ *c*	1.11 ± 4 %	1.34	536, 581

The TPR profile for G.U. CuO/SiO_2, calcined in flowing air at 723 K using the apparatus shown in Figure 3.1, is shown in Figure 5.19. Lowering the calcination temperature to 623 K resulted in the profile shown in Figure 5.20. The experimental and theoretical hydrogen consumption for each of these calcined catalyst precursors and the temperature at each peak maximum is given in Table 5.6.

Table 5.6.

Catalysts	Calcination Method	Experimental H_2 consumption (No. of molecules x 10^{21} g^{-1})	Theoretical H_2 consumption (No. of molecules x 10^{21} g^{-1})	$T_{MAX(S)}$ (K)
G.U. CuO/ SiO_2 CIA	Flowing air at 723 K	1.18 ± 5 %	1.30	568 603
G.U. CuO/ SiO_2 CIA 623 K	Flowing air at 623 K	1.21 ± 7 %	1.30	525 578 598

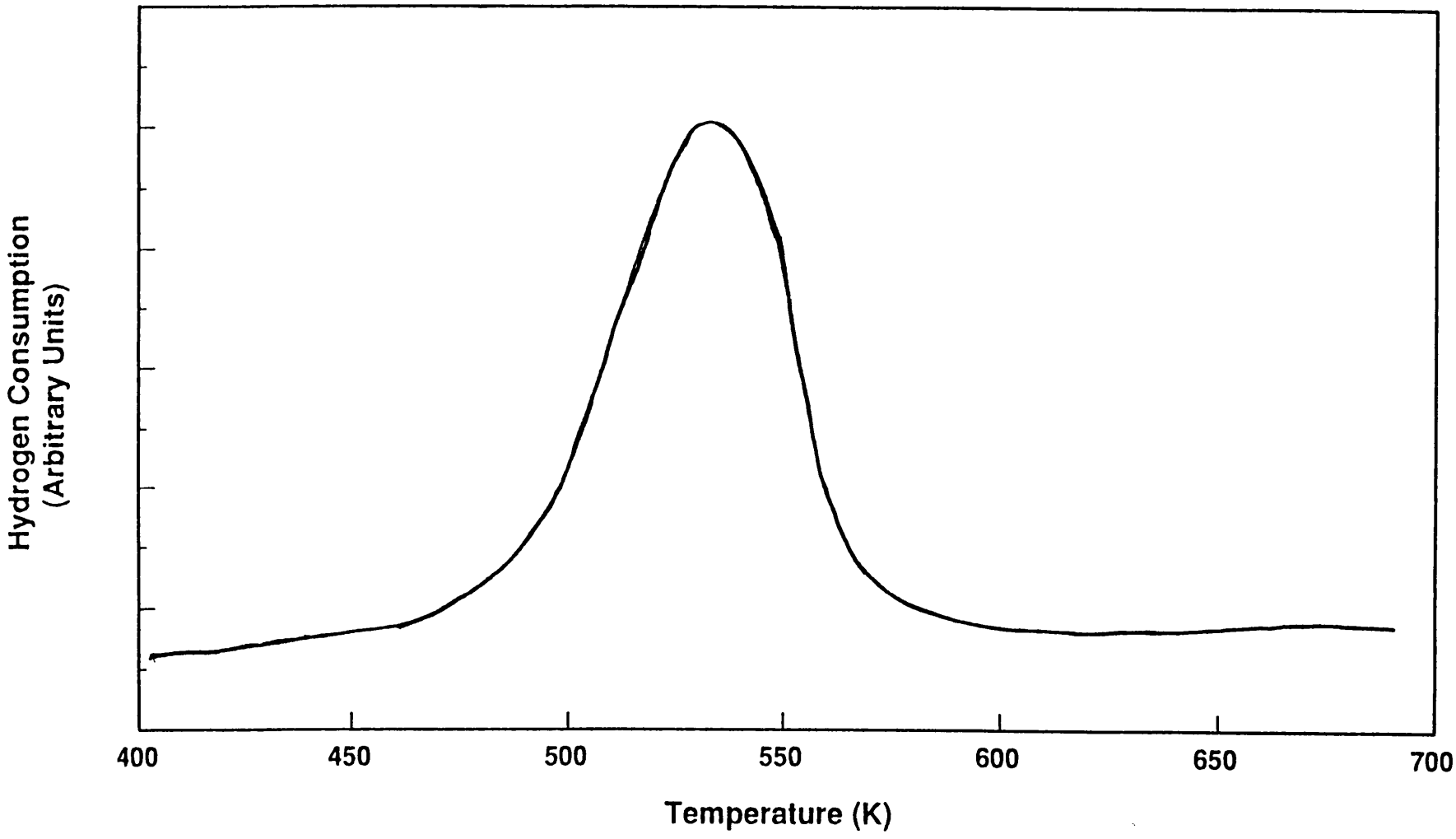

Figure 5.1 TPR Profile of Pure CuO.

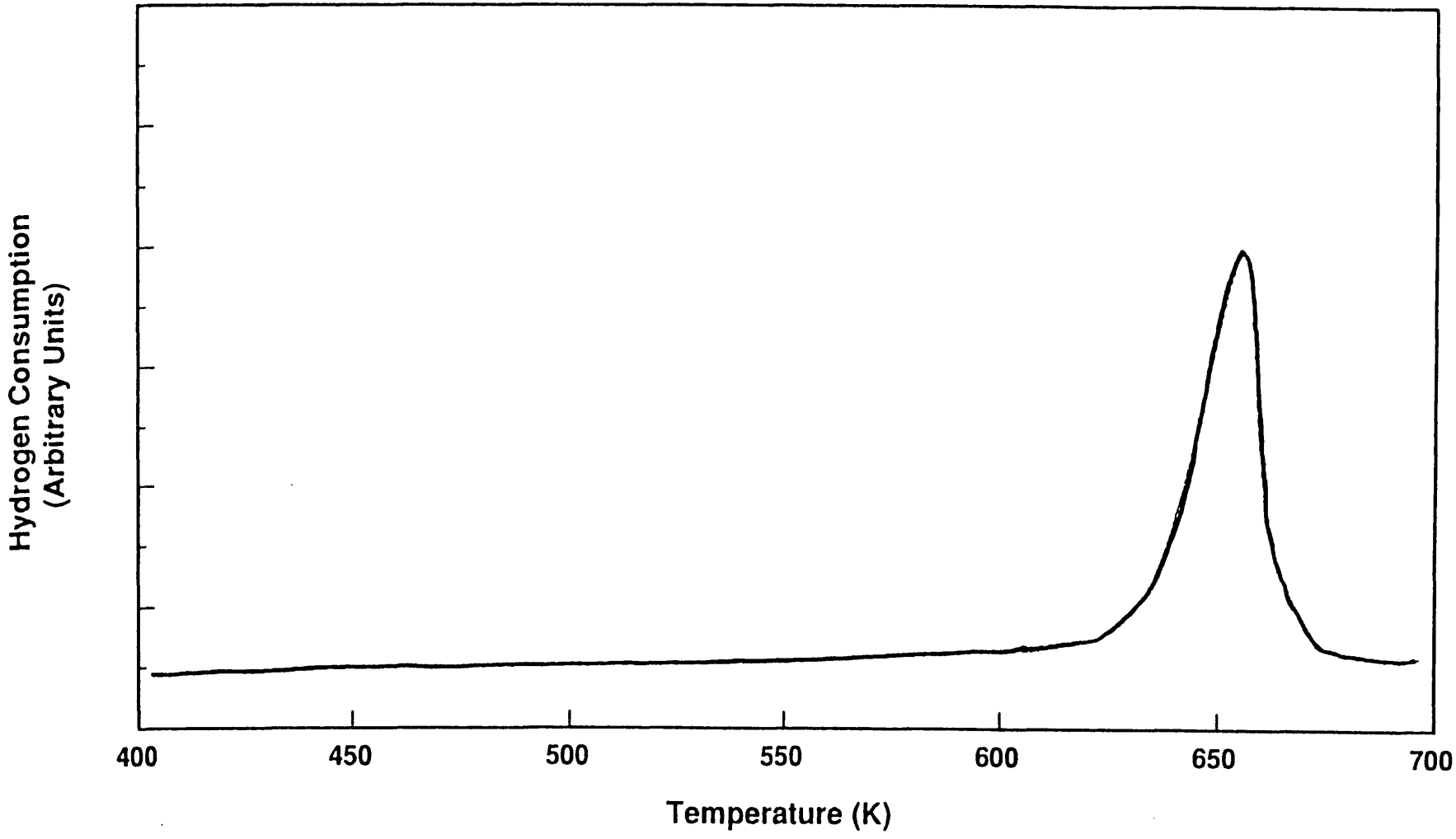

Figure 5.2 TPR Profile of CuO Prepared from the Calcination of $Cu(NO_3)_2.3H_2O$.

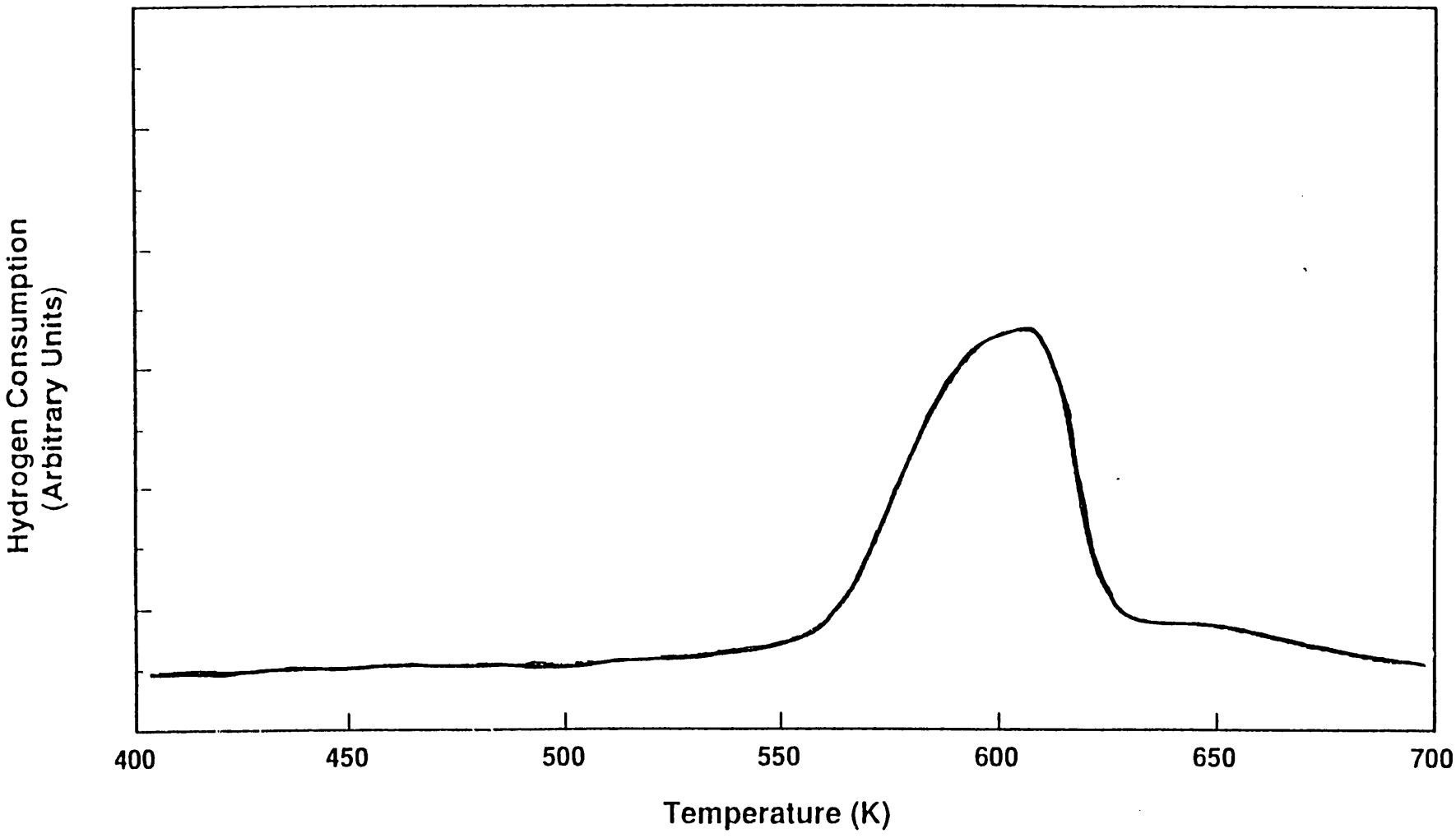

Figure 5.3 TPR Profile of ICI CuO/SiO_2/PQ *a*.

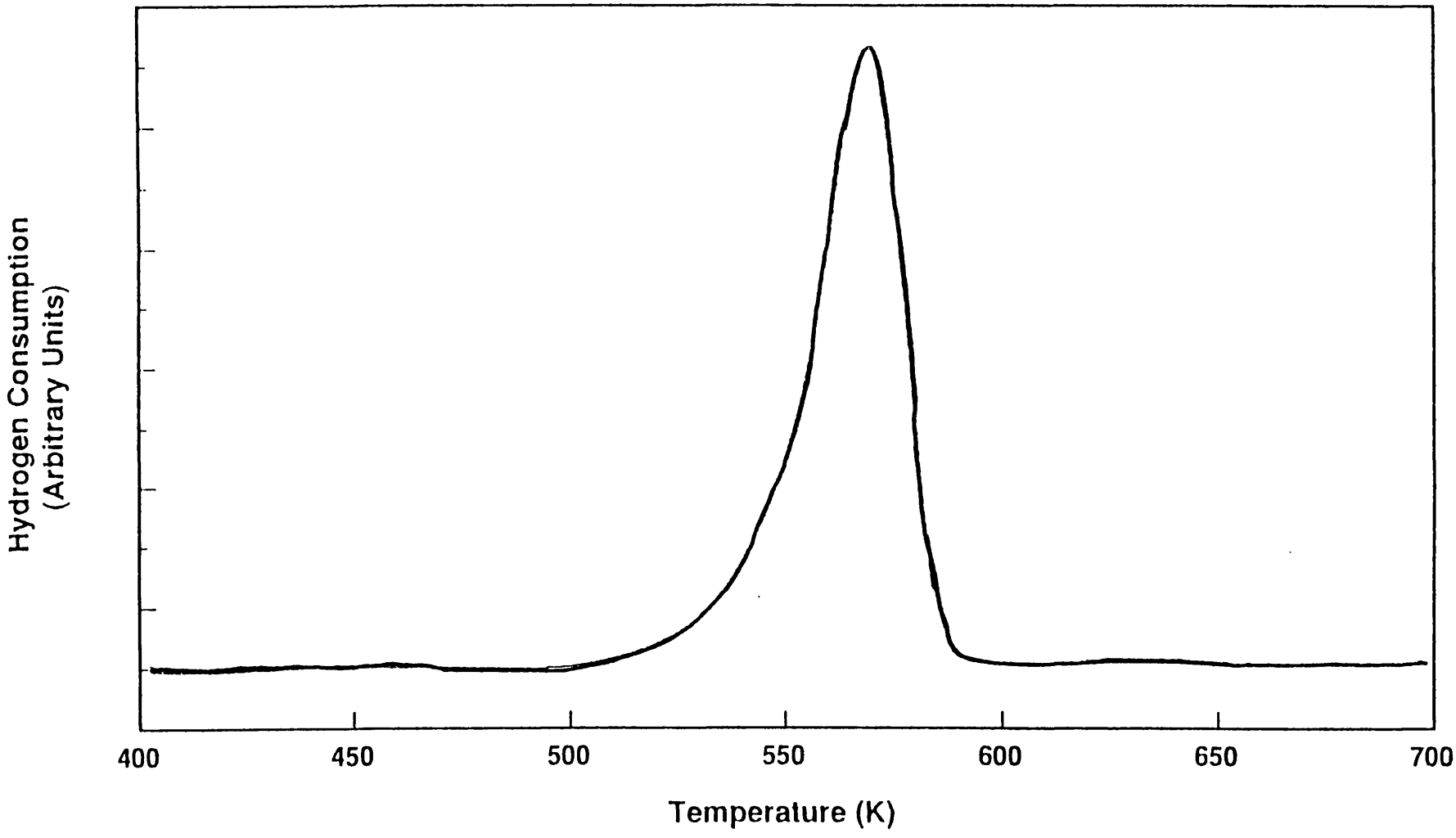

Figure 5.4 TPR Profile of ICI CuO/SiO_2/Grace *a*.

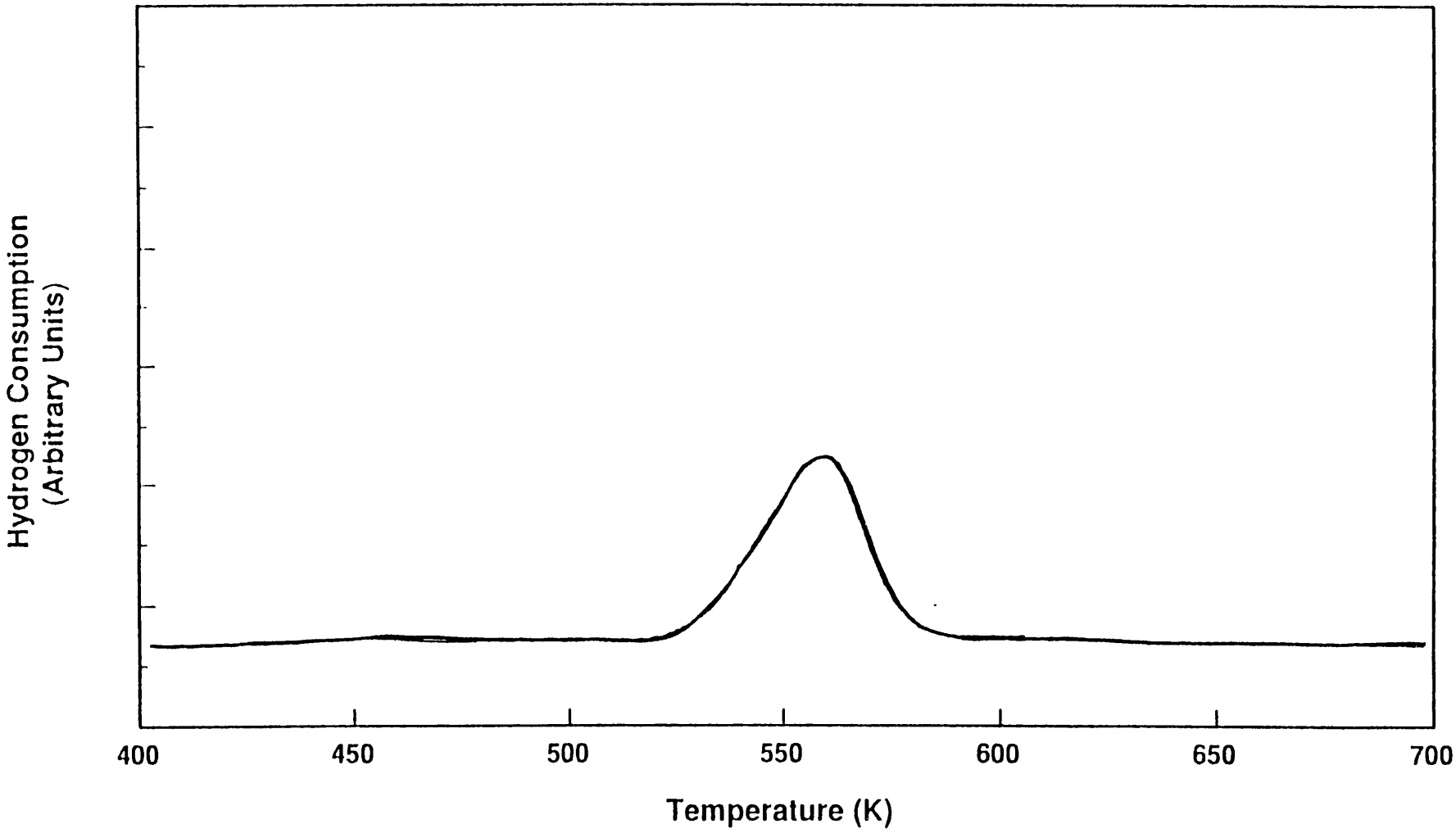

Figure 5.5 TPR Profile of ICI CuO/SiO_2/PQ *b*.

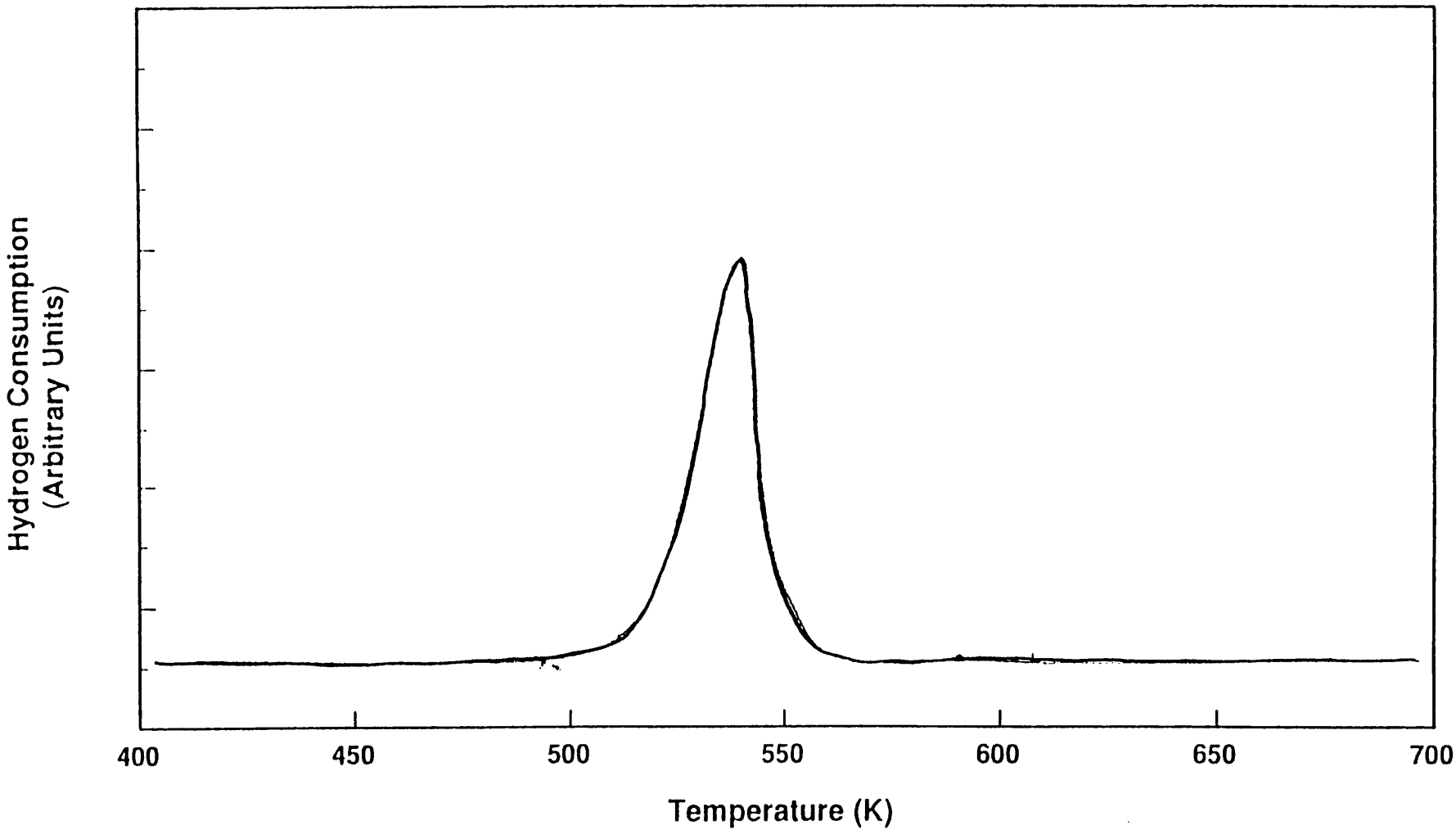

Figure 5.6 TPR Profile of ICI CuO/SiO_2/Grace *b*.

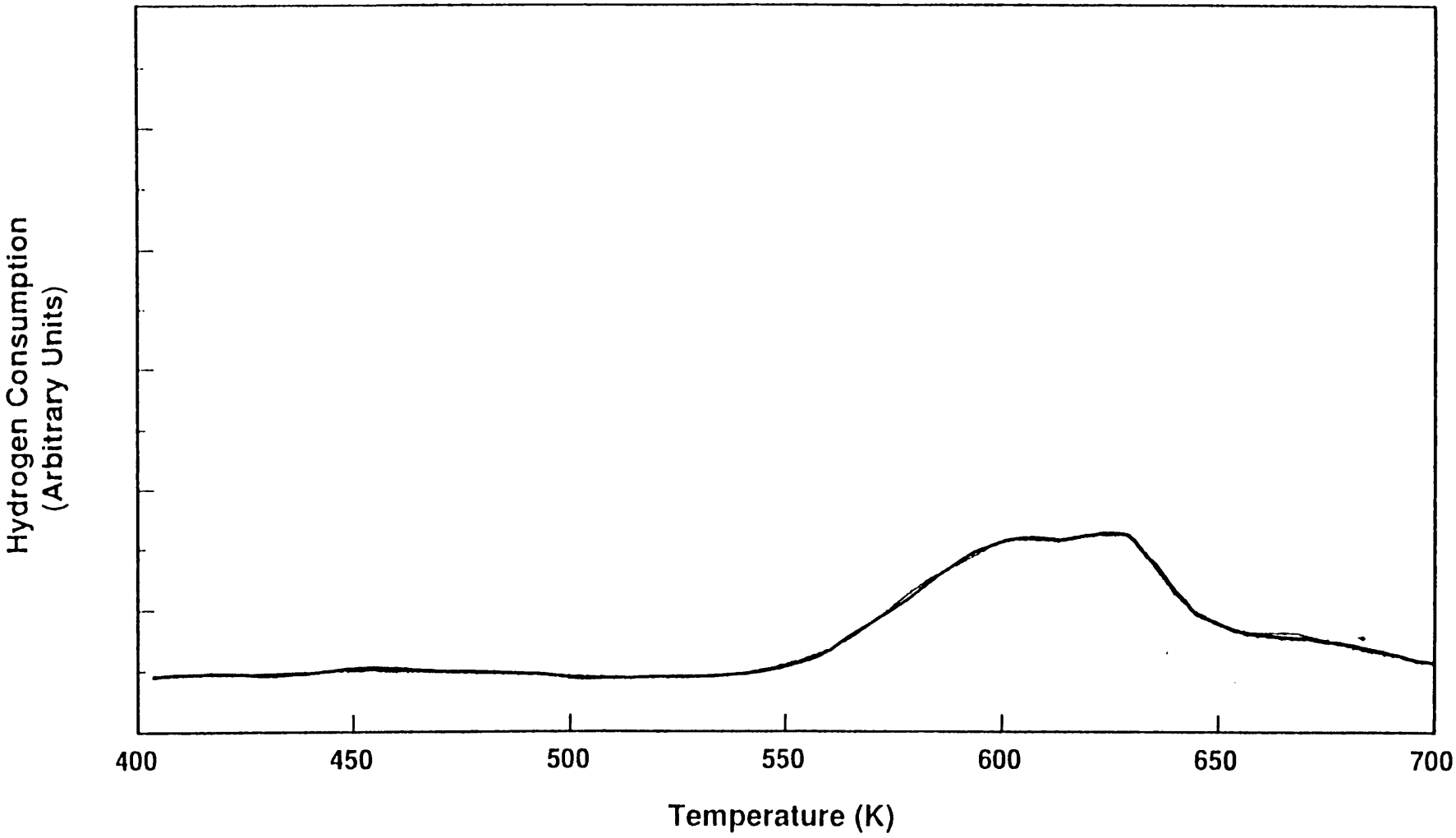

Figure 5.7 TPR Profile of G.U. CuO/SiO_2.

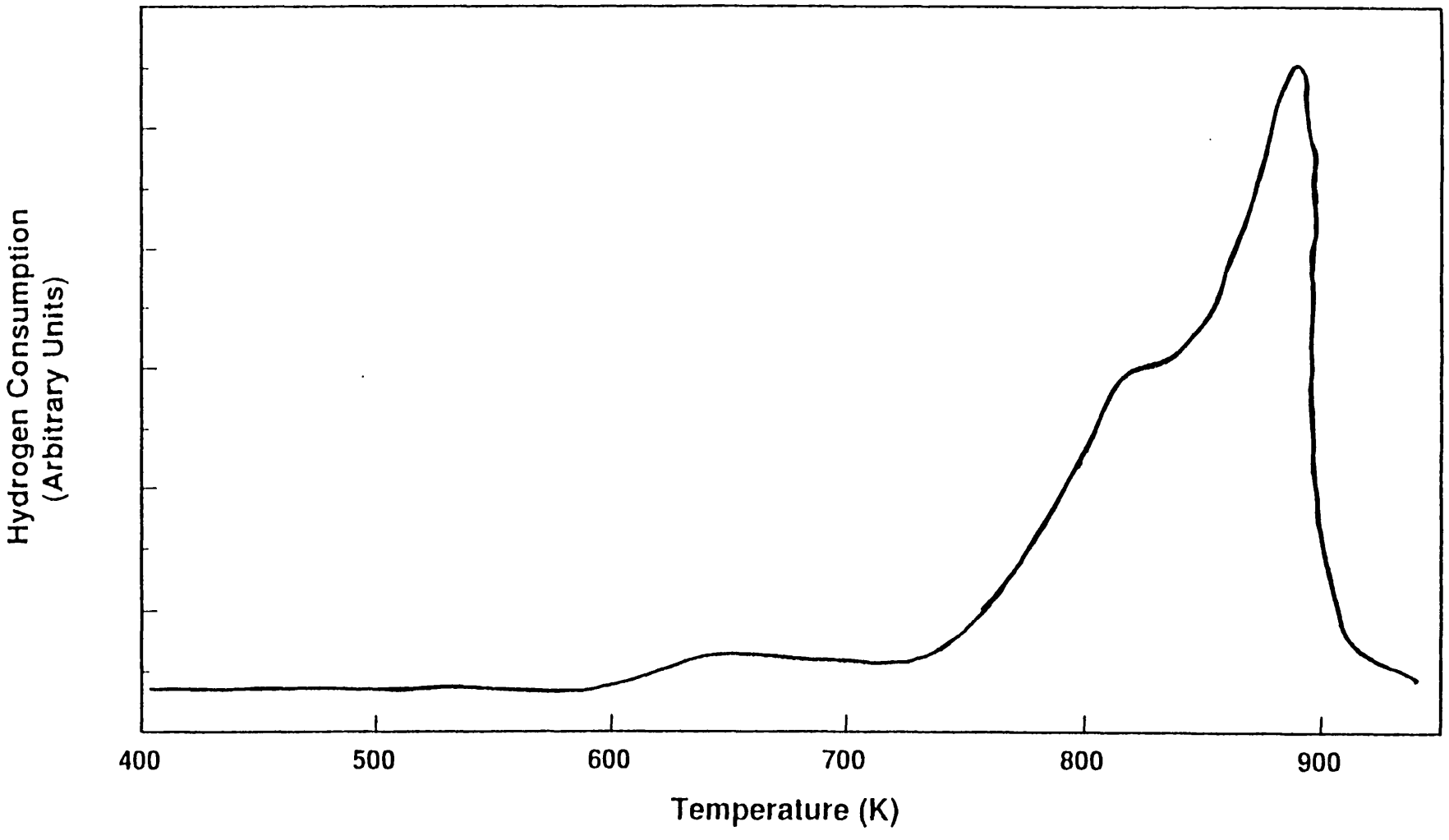

Figure 5.8 TPR Profile of V_2O_5/SiO_2.

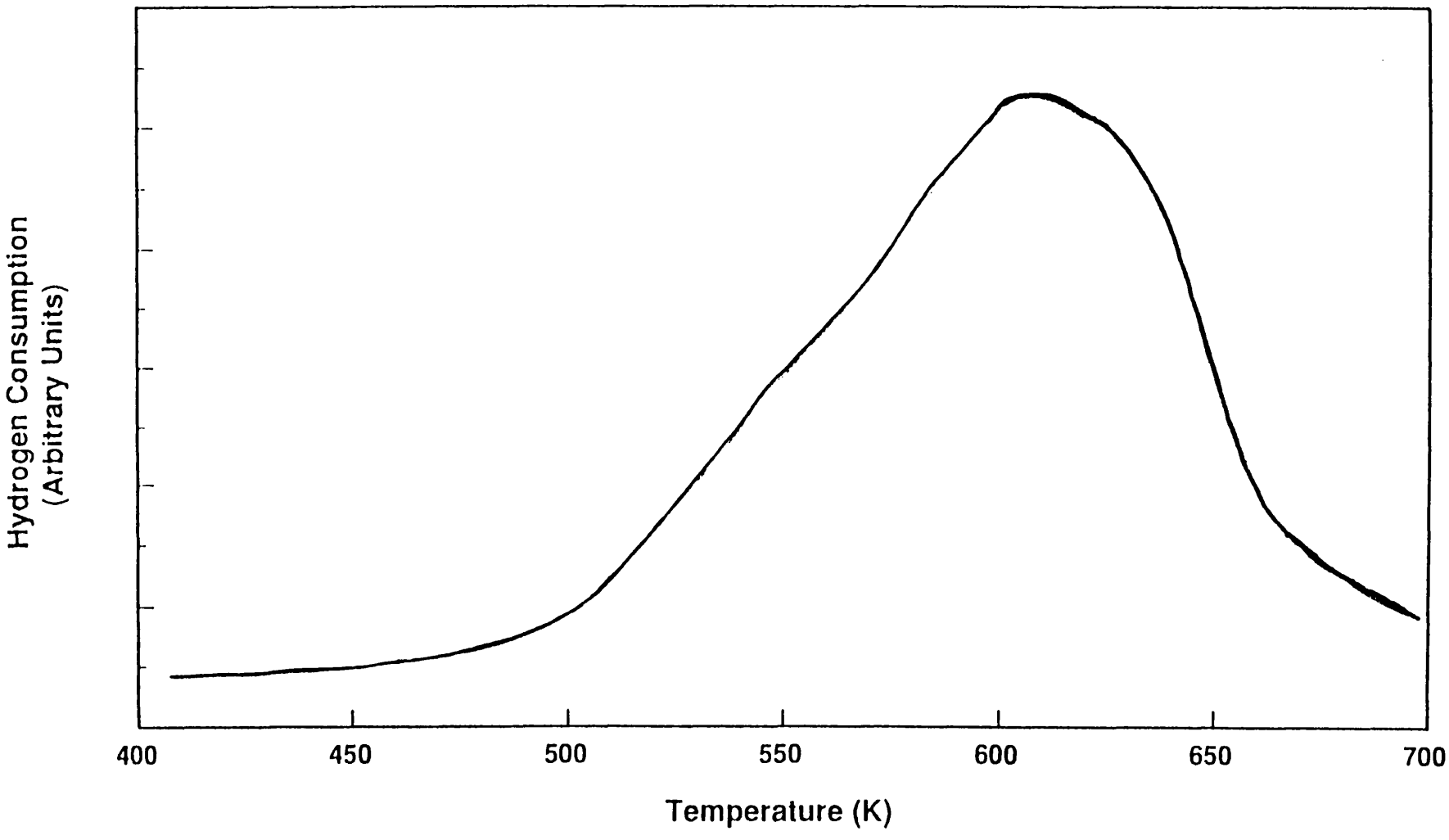

Figure 5.9 TPR Profile of $CuO/V_2O_5/SiO_2$.

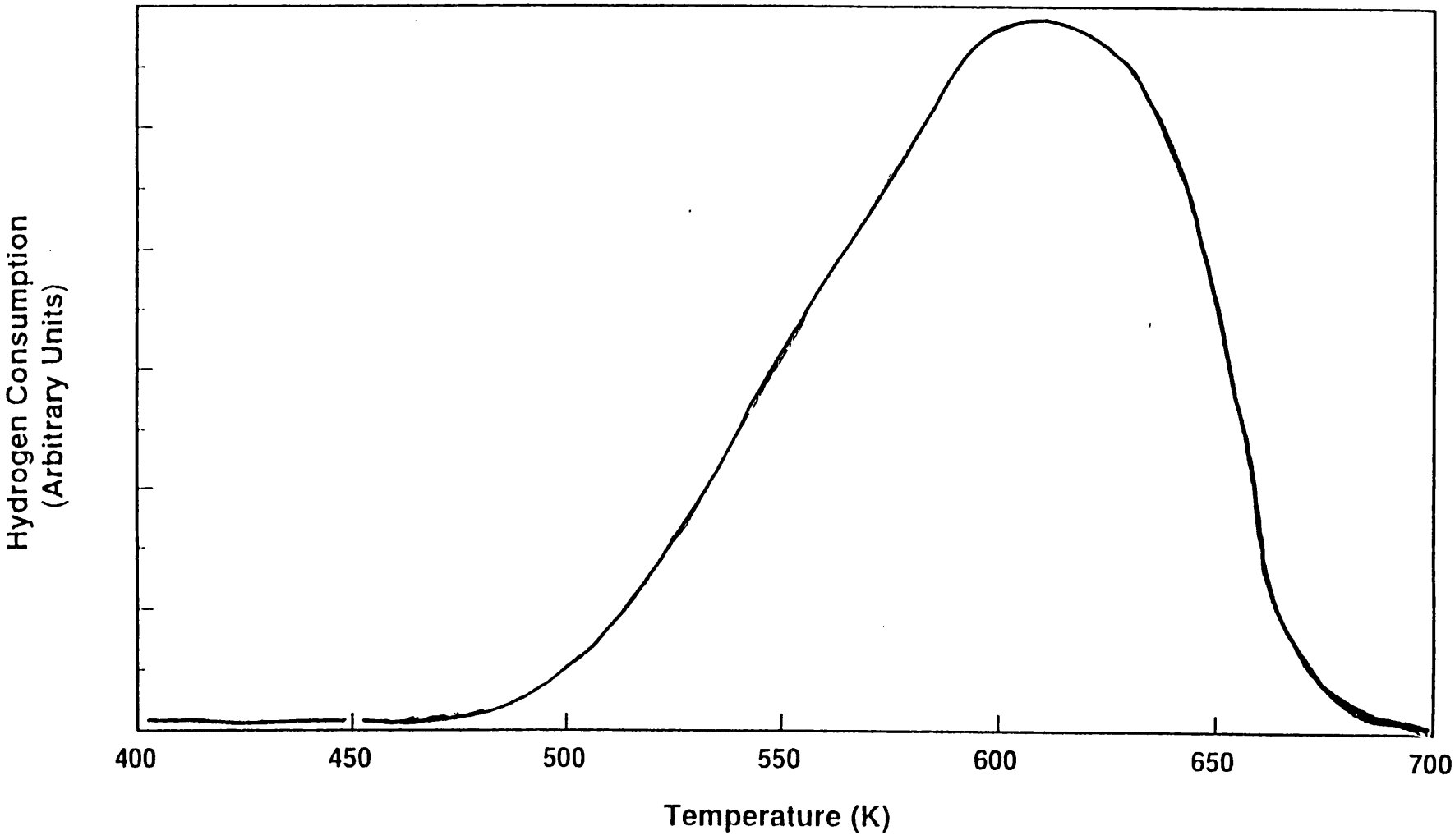

Figure 5.10 TPR Profile of $CuO/V_2O_5/PdO/SiO_2$.

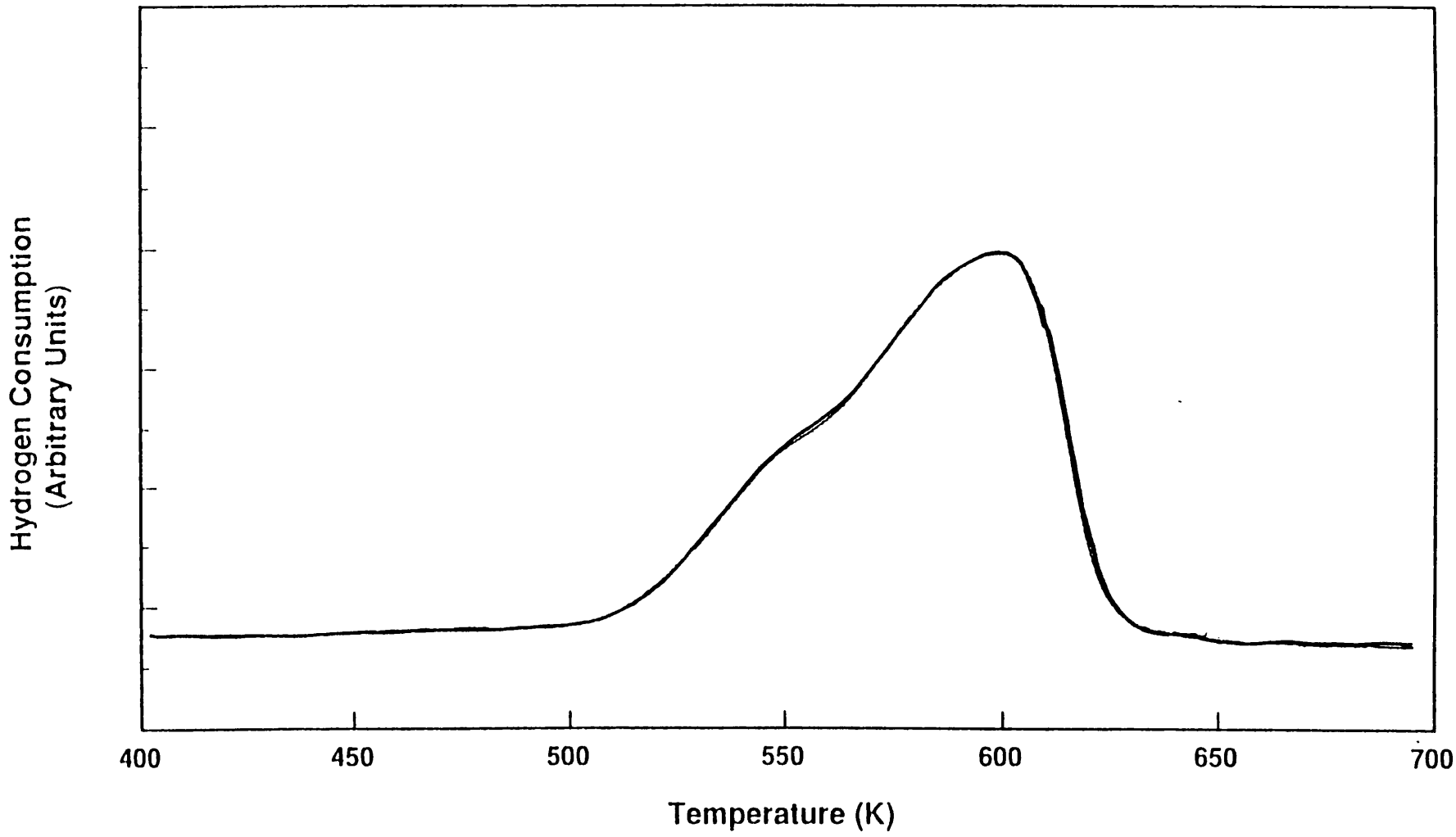

Figure 5.11 TPR Profile of $CuO/PdO/SiO_2$ *a*.

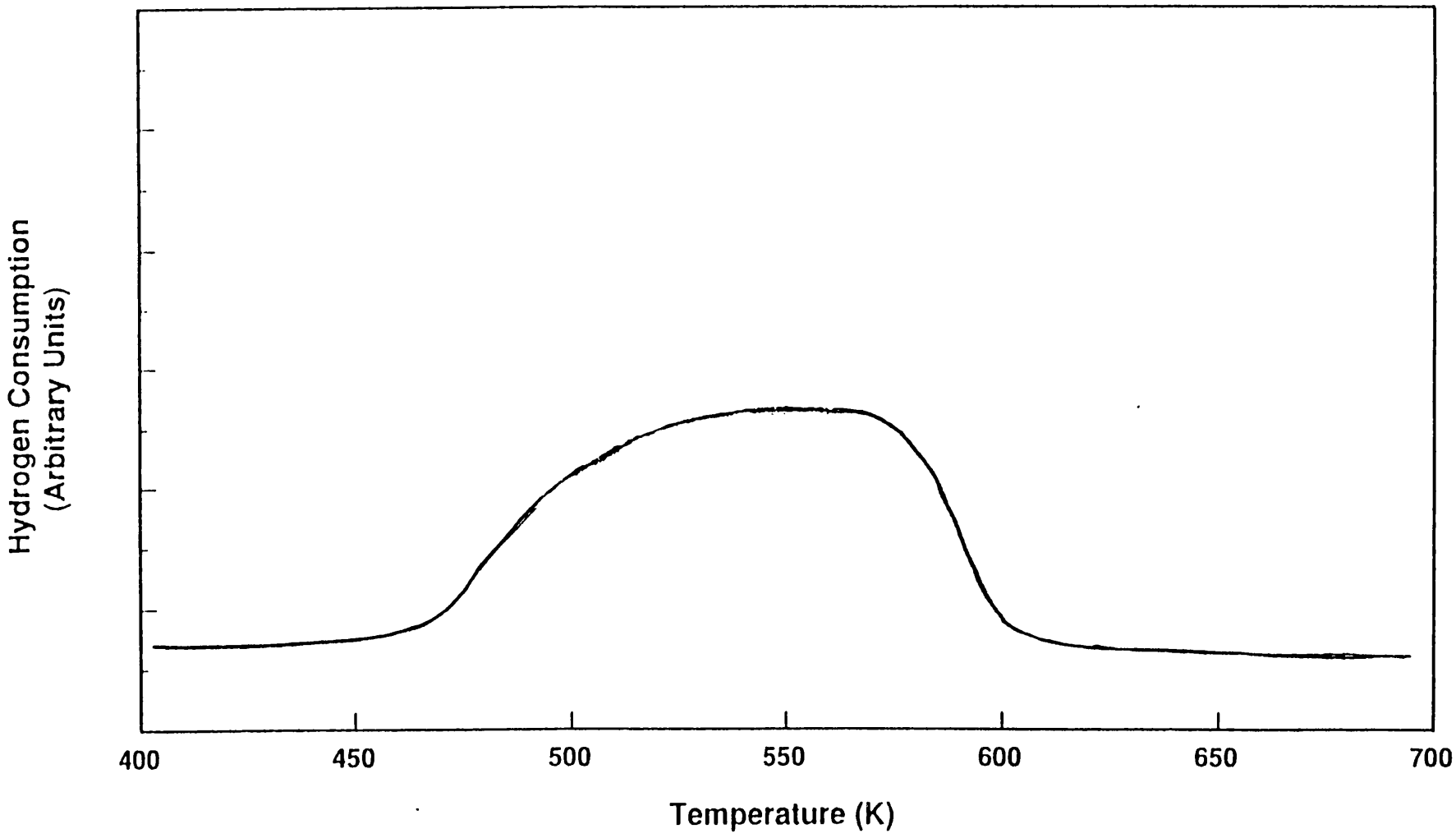

Figure 5.12 TPR Profile of $CuO/PdO/SiO_2$ *b*.

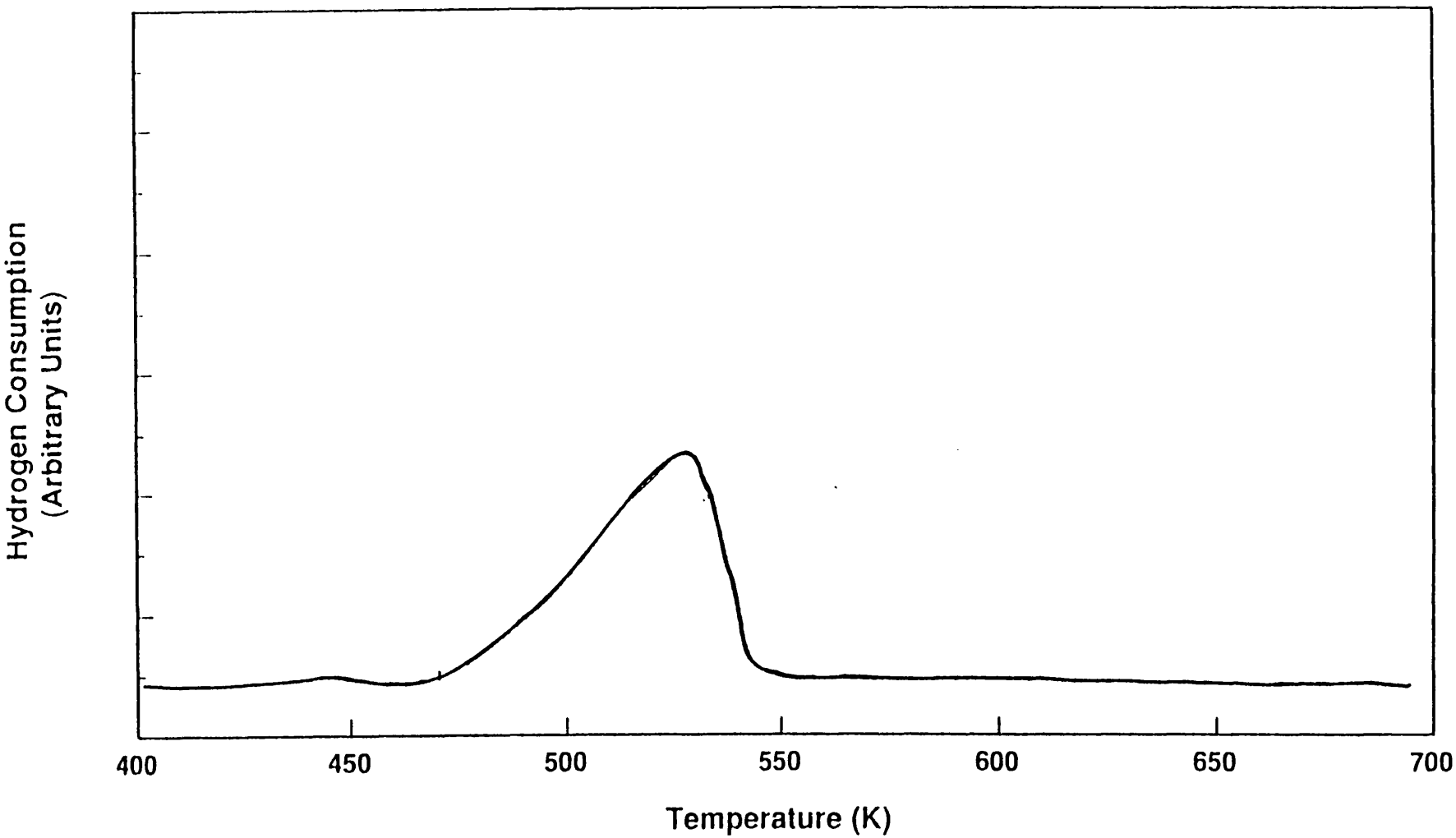

Figure 5.13 TPR Profile of $CuO/PdO/SiO_2$ *c*.

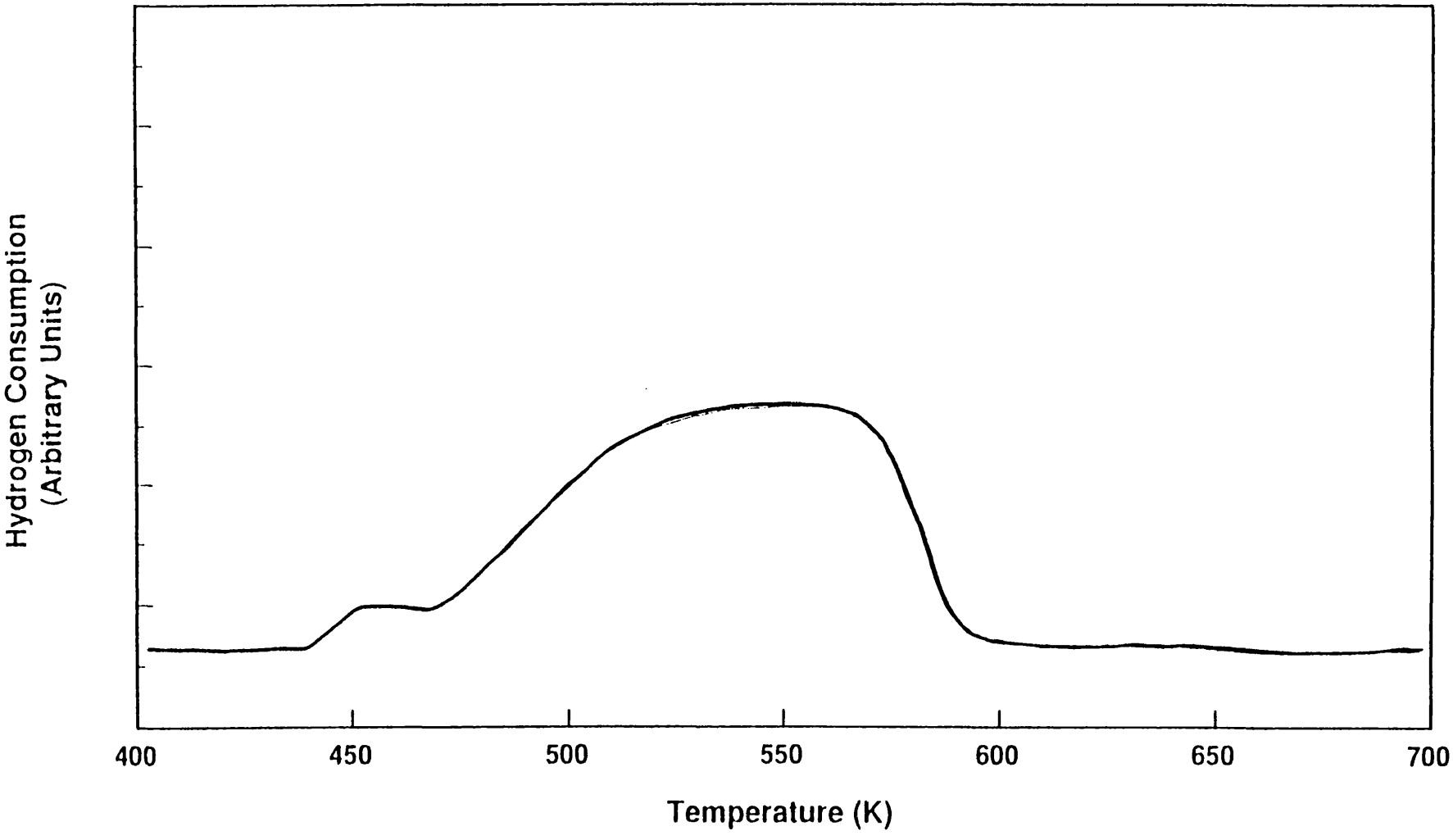

Figure 5.14 TPR Profile of $CuO/PdO/SiO_2$ *d*.

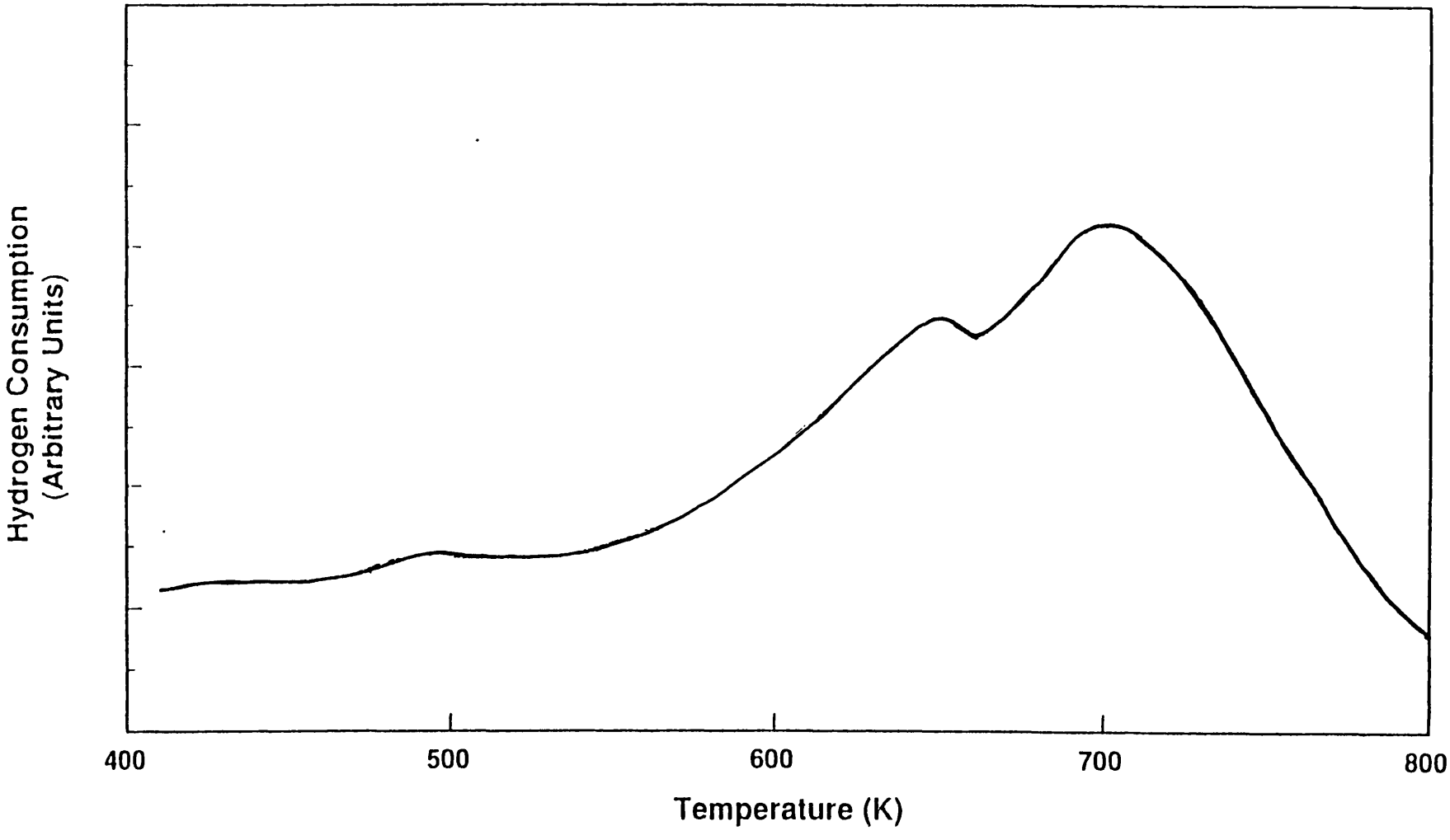

Figure 5.15 TPR Profile of $CuO/PdO/SiO_2$ *e*.

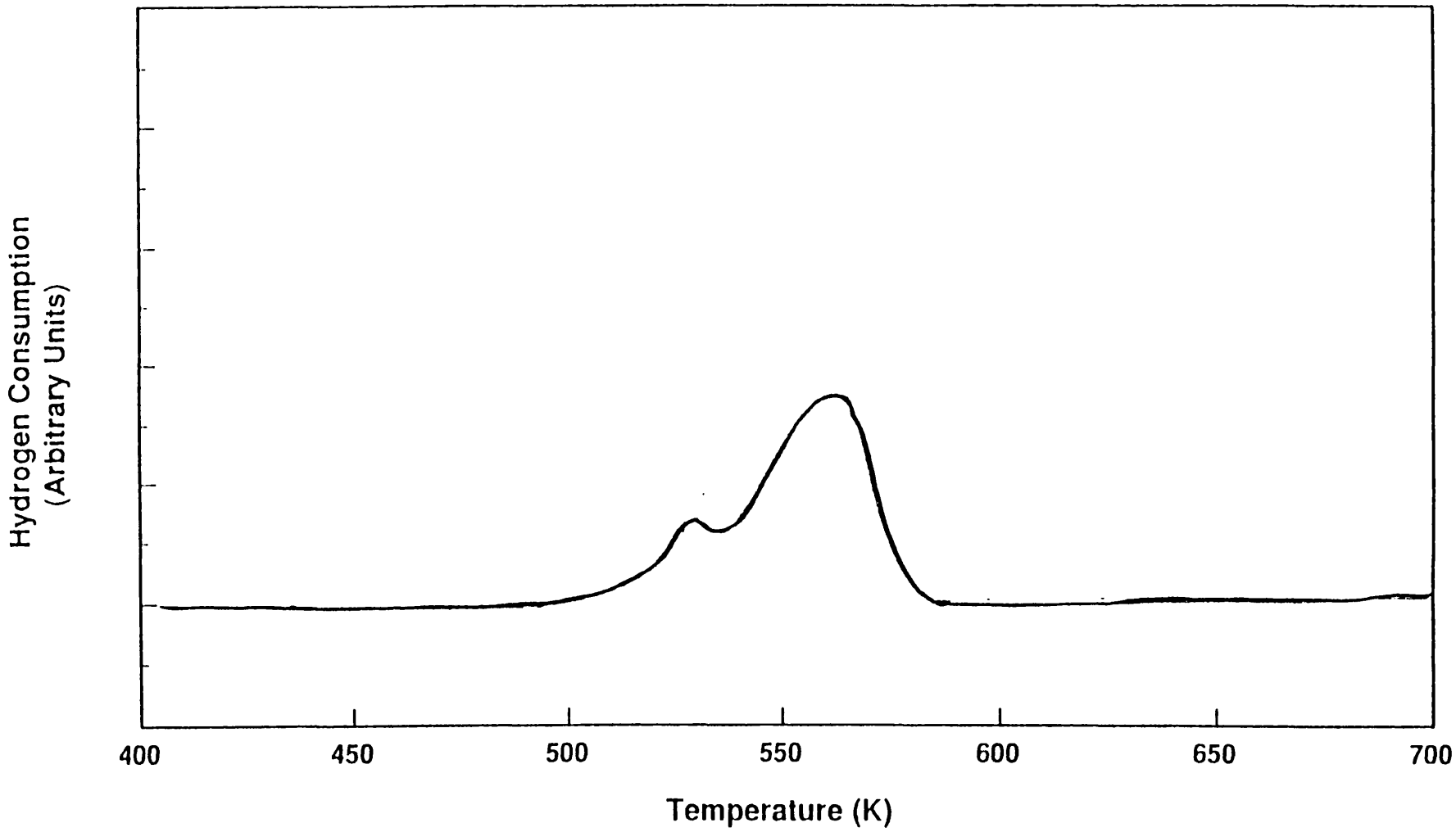

Figure 5.16 TPR Profile of $CuO/RuO_2/SiO_2$ *a*.

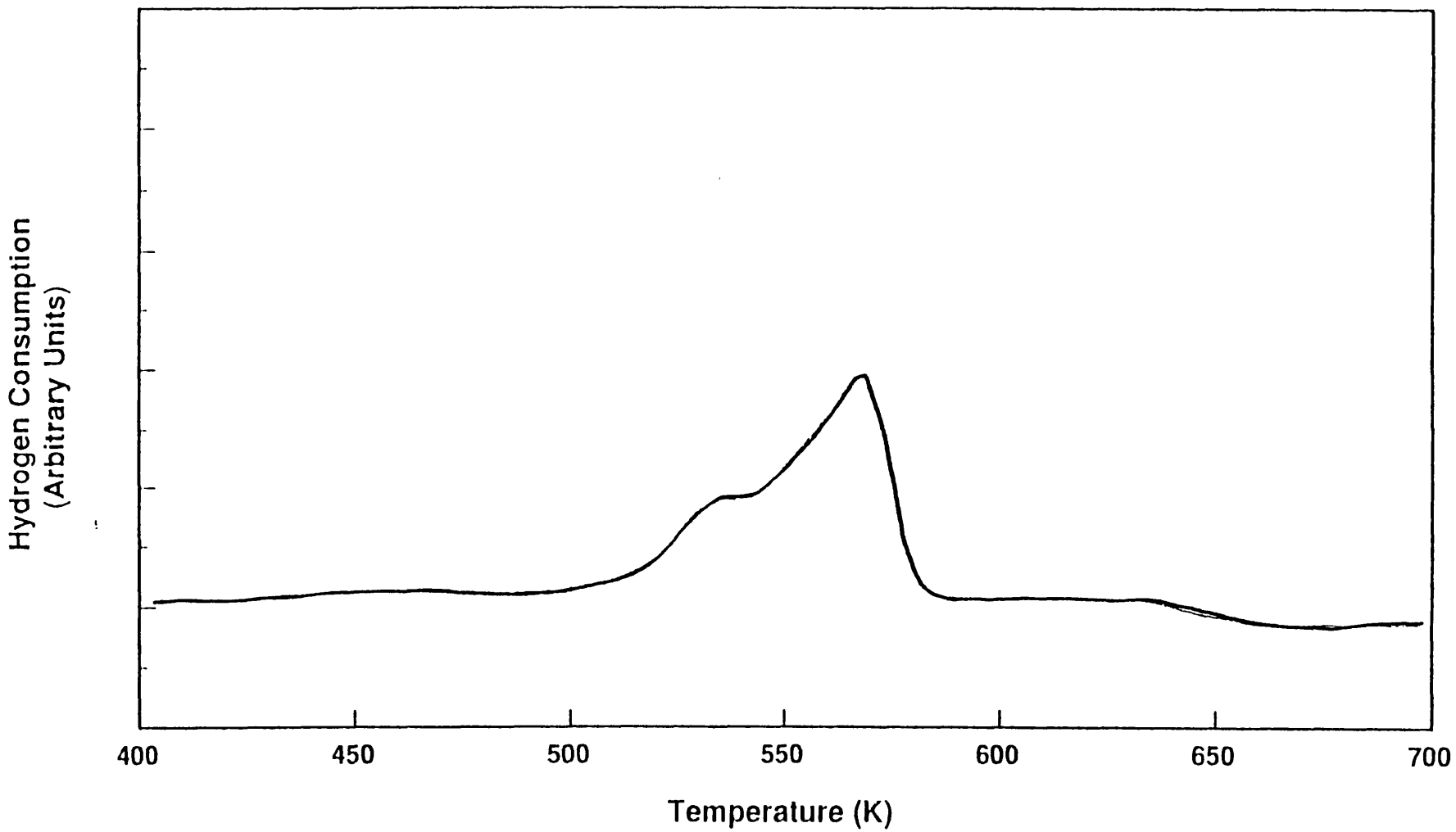

Figure 5.17 TPR Profile of $CuO/RuO_2/SiO_2$ *b*.

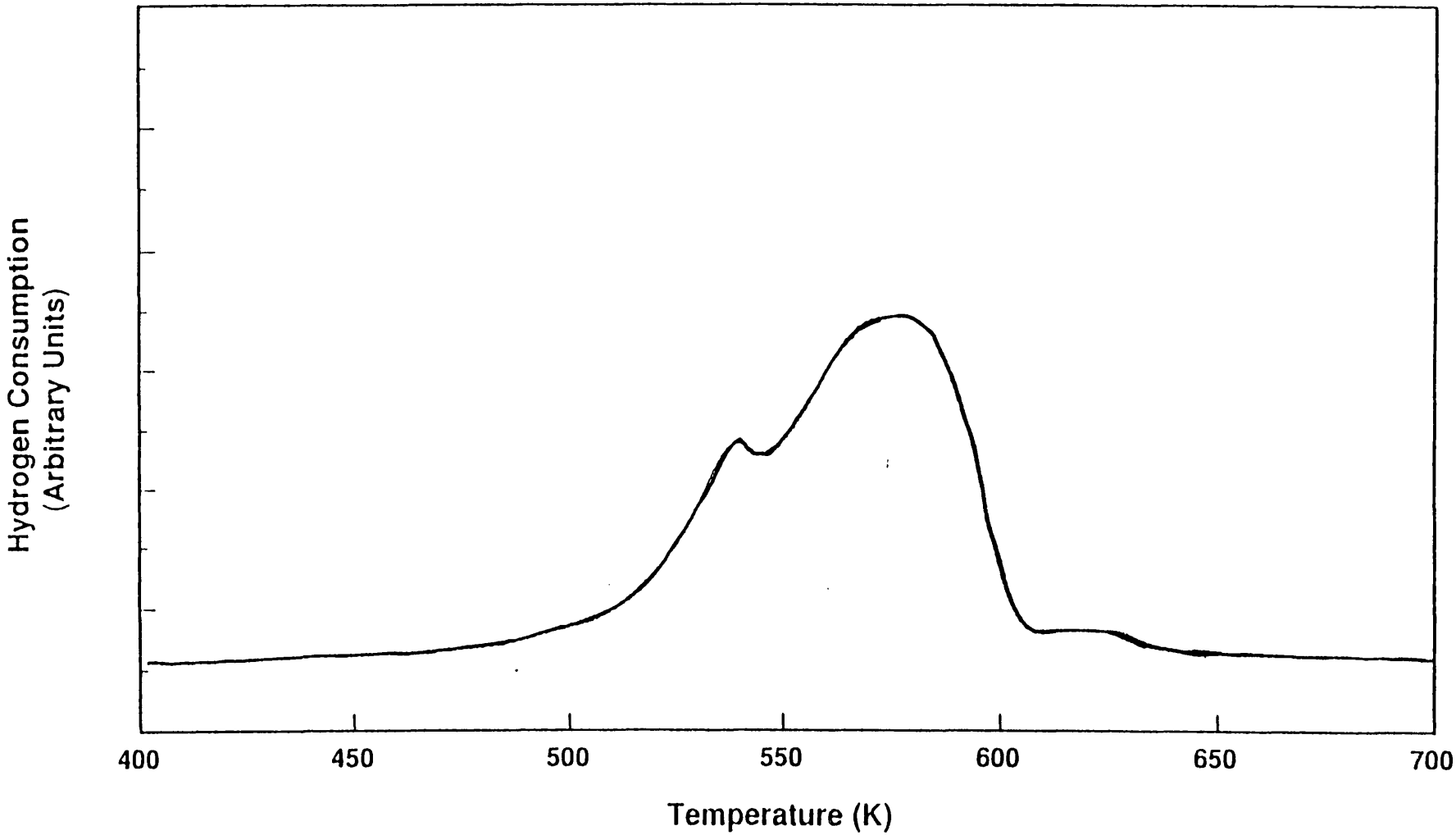

Figure 5.18 TPR Profile of $CuO/RuO_2/SiO_2$ *c*.

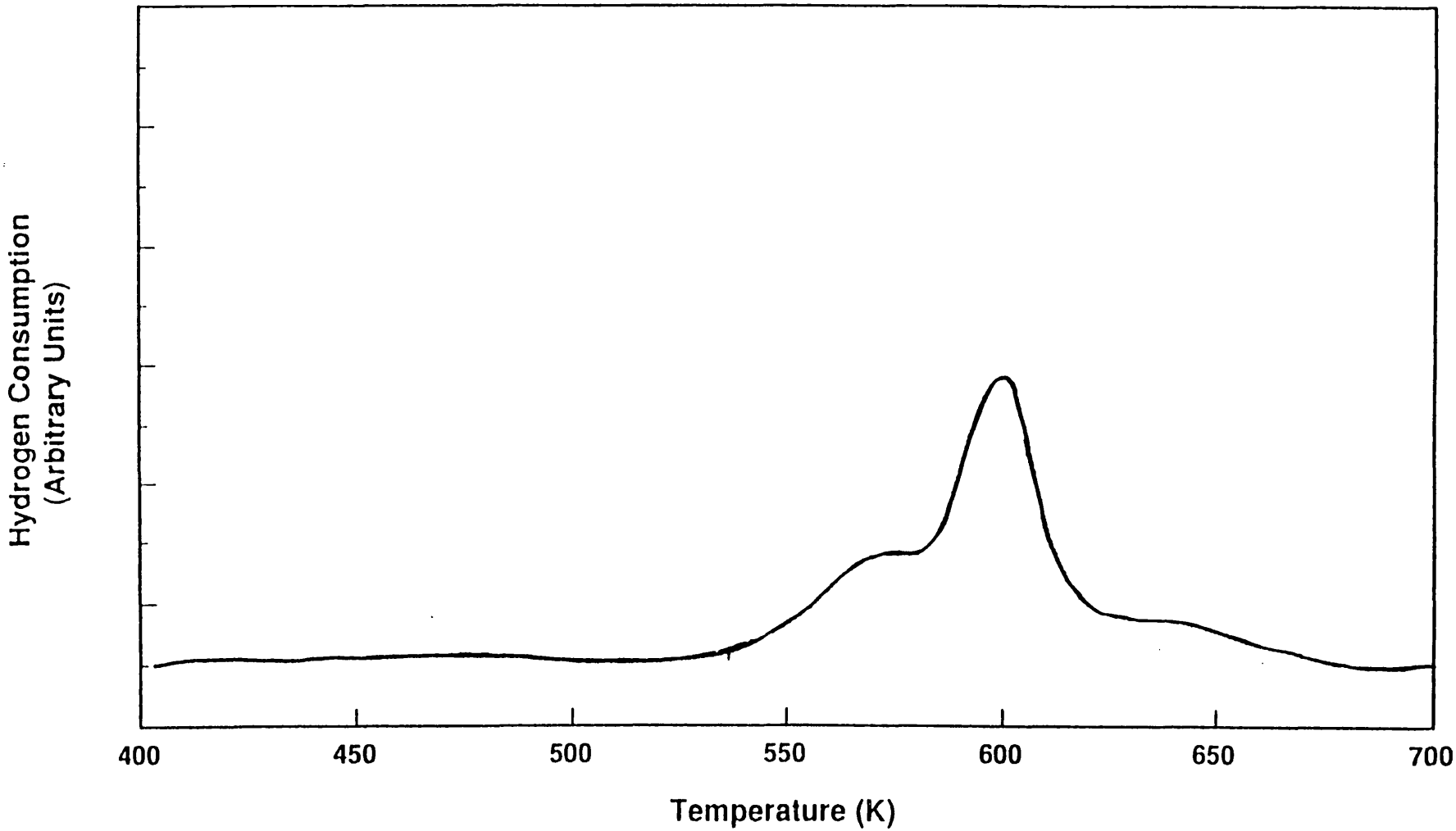

Figure 5.19 TPR Profile of G.U. CuO/SiO_2 CIA.

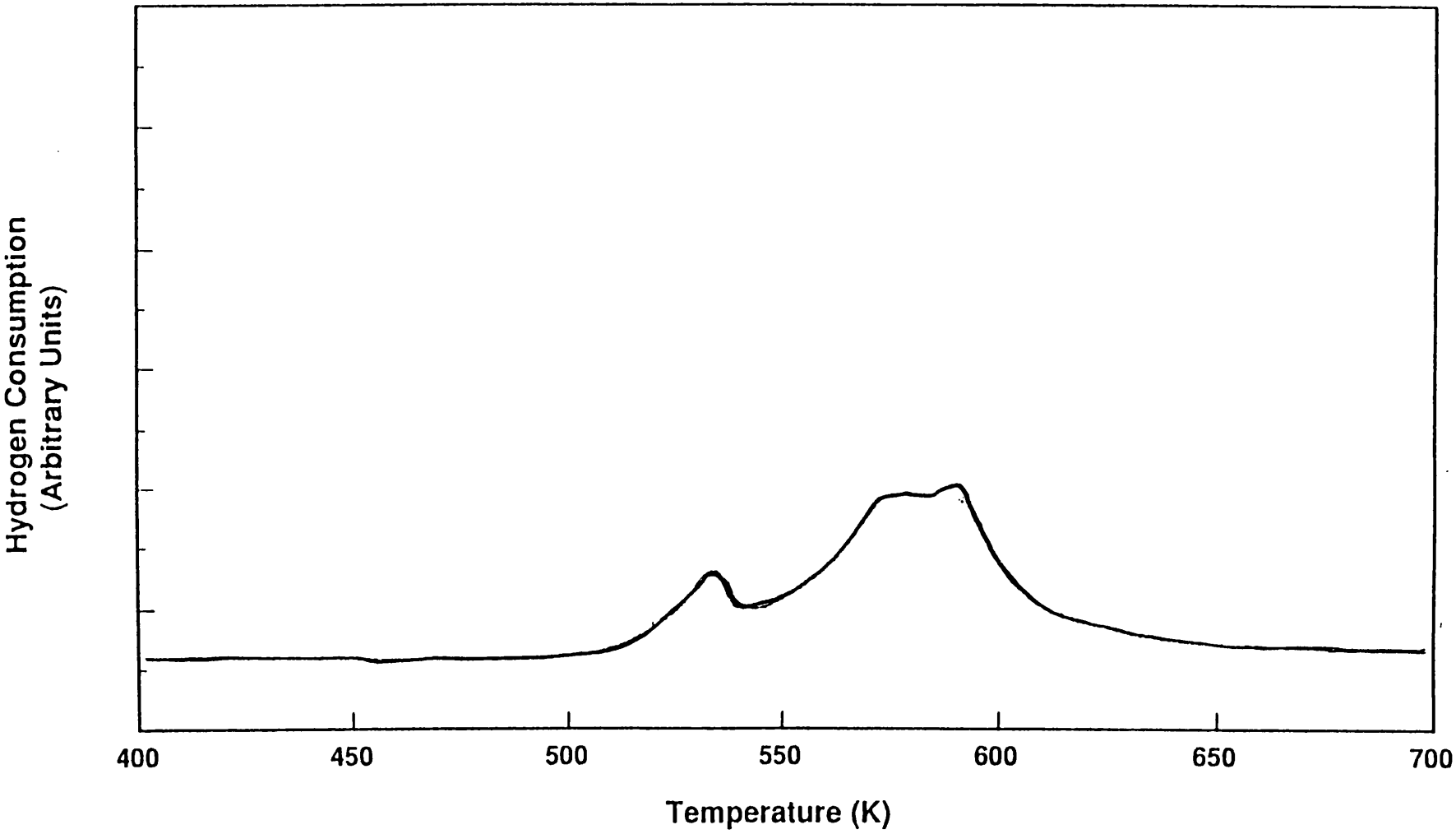

Figure 5.20 TPR Profile of G.U. CuO/SiO_2 CIA 623 K.

5.3 NITROUS OXIDE DECOMPOSITION

The dispersion (d) and the copper metal surface area (A) of the catalysts used in this study were determined by following the decomposition of nitrous oxide over the reduced catalysts (Section 4.3.). The results of these experiments are shown in Table 5.7.

Table 5.7.

Catalysts	Dispersion (d) %	Copper Metal Surface Area A ($m^2 g^{-1}$)
ICI CuO/SiO_2/PQ a	0.52	0.40
ICI CuO/SiO_2/Grace a	2.85	2.18
ICI CuO/SiO_2/PQ b	-	-
ICI CuO/SiO_2/Grace b	1.00	0.53
G.U. CuO/SiO_2	0.10	0.08
$CuO/V_2O_5/SiO_2$	0.55	0.42
$CuO/V_2O_5/PdO/SiO_2$	0.71	0.57
$CuO/PdO/SiO_2$ a	1.04	0.71
$CuO/PdO/SiO_2$ b	0.90	0.81
$CuO/PdO/SiO_2$ c	0.62	0.55
$CuO/PdO/SiO_2$ d	0.64	0.67
$CuO/PdO/SiO_2$ e	0.58	0.45
$CuO/RuO_2/SiO_2$ a	0.70	0.51
$CuO/RuO_2/SiO_2$ b	0.33	0.24
$CuO/RuO_2/SiO_2$ c	0.11	0.10
G.U. CuO/SiO_2/CIA	0.20	0.15
G.U. CuO/SiO_2/CIA 623 K	0.50	0.40

5.4 CATALYST MORPHOLOGY

The BET surface areas and porosities for the silicas and the calcined industrial catalyst precursors are given in Table 5.8. The lower surface area silica, PQ, had a bimodal pore size distribution with the majority of the pores ≈ 20 nm, and approximately 10% of the pores ≈ 100 nm. All the pores in the Grace silica were concentrated in a narrow band ≈ 10 nm in diameter. The results show that impregnating either PQ or Grace with either copper nitrate or ammonium metavanadate and decomposition to the supported oxides resulted in a similar loss in surface area and a corresponding decrease in the mean pore diameter. A further loss in area occurred on impregnating and calcining PQ silica with both salts. No further loss in surface area occurred on adding palladium nitrate to PQ silica.

Table 5.8.

Sample	N_2 Surface Area ($m^2\ g^{-1}$)	Average Pore Diameter (nm)	Total Intrusion Volume ($cm^3\ g^{-1}$)	Total Pore Area ($m^2\ g^{-1}$)
PQ Silica	200	20		
ICI CuO/SiO_2/PQ a	165	19	1.03	216
V_2O_5/SiO_2	169	18	0.97	215
$CuO/V_2O_5/SiO_2$	135	17	0.83	187
$CuO/V_2O_5/PdO/SiO_2$	138	17	0.80	190
Grace Silica	280	10		
ICI CuO/SiO_2/ Grace a	243	10	0.84	234

5.5 HOT STAGE XRD

The calcined catalyst precursors ICI CuO/SiO_2 PQ *a* and ICI CuO/SiO_2 Grace *a* were studied by XRD. The diffraction patterns corresponded to amorphous silica, which showed only a broad peak at ≈ 0.41 nm and crystalline copper oxide. The copper oxide was more crystalline and gave a more intense signal for the sample supported on the PQ silica than for the Grace silica. After an initial examination in the diffractometer the samples were heated from 303 K to 423 K in 1.5% H_2/N_2 and then in 50 K steps up to 573 K, collecting a diffraction trace at each step. The diffraction patterns are shown in Figures 5.21 and 5.22. No significant change in the diffraction pattern was observed for the PQ sample until 573 K when d spacings for copper were detected with copper oxide as a minor phase. A second diffraction trace taken after maintaining the sample at 573 K in H_2/N_2 for twenty minutes showed that the copper signal had increased, but a significant amount of copper oxide still remained. The first change in the diffraction trace for the Grace silica was detected at 473 K when a decrease in the intensity of the diffraction pattern for copper oxide was observed although no crystalline copper was detected. However by 523 K copper oxide was present as only a minor component with copper being the major crystalline phase. No copper oxide remained after the temperature programming to 573 K. The copper crystallites formed after temperature programming to 573 K in H_2/N_2 had a mean size of ≈ 20 nm in the case of the PQ sample and ≈ 10 nm for the Grace sample. The copper crystallites in the PQ sample were observed to

increase in size from 20 to 30 nm after maintaining the sample in H_2/N_2 at 573 K for 20 minutes.

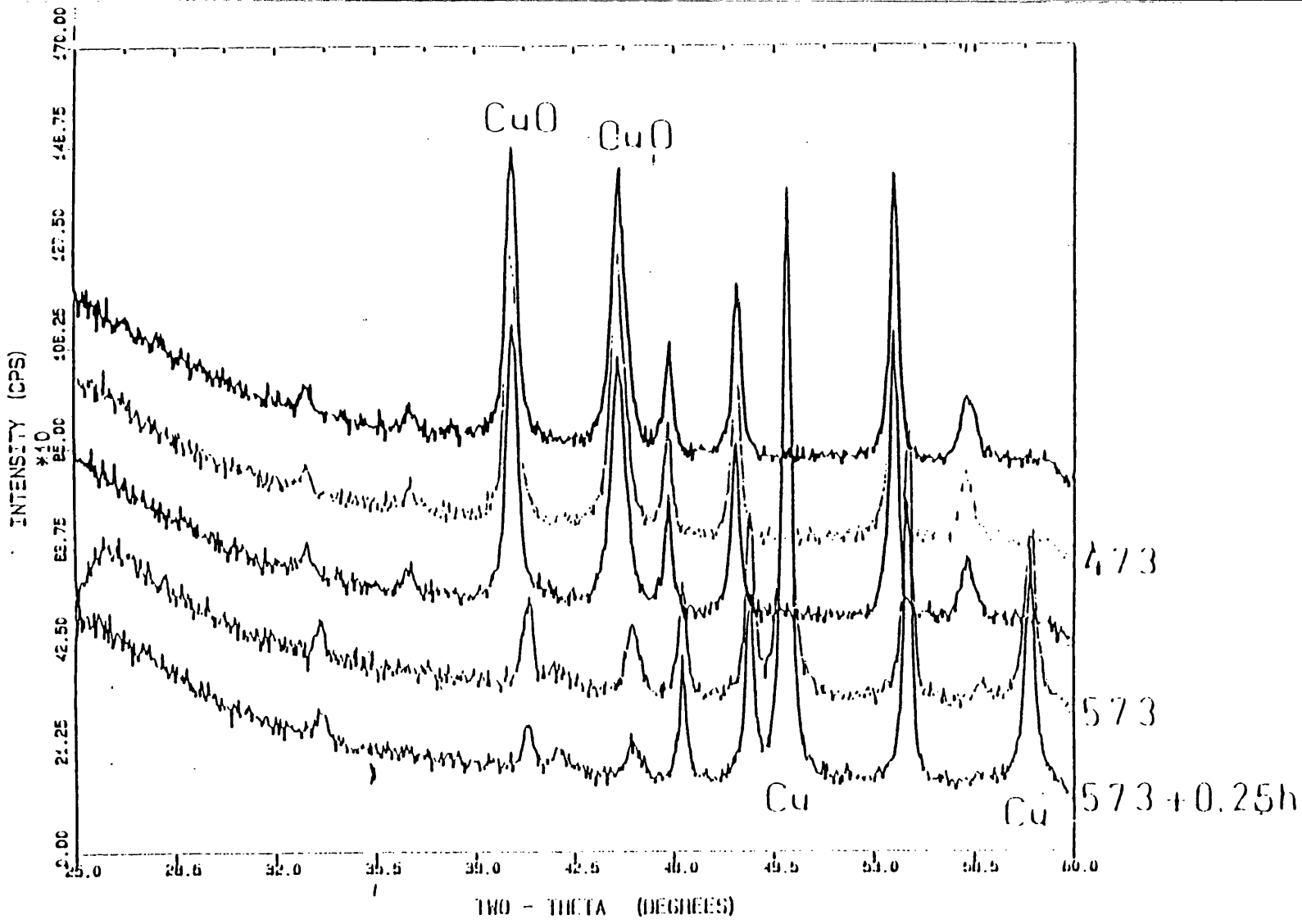

Figure 5.21 Diffraction Pattern for ICI CuO/SiO_2/PQ *a*.

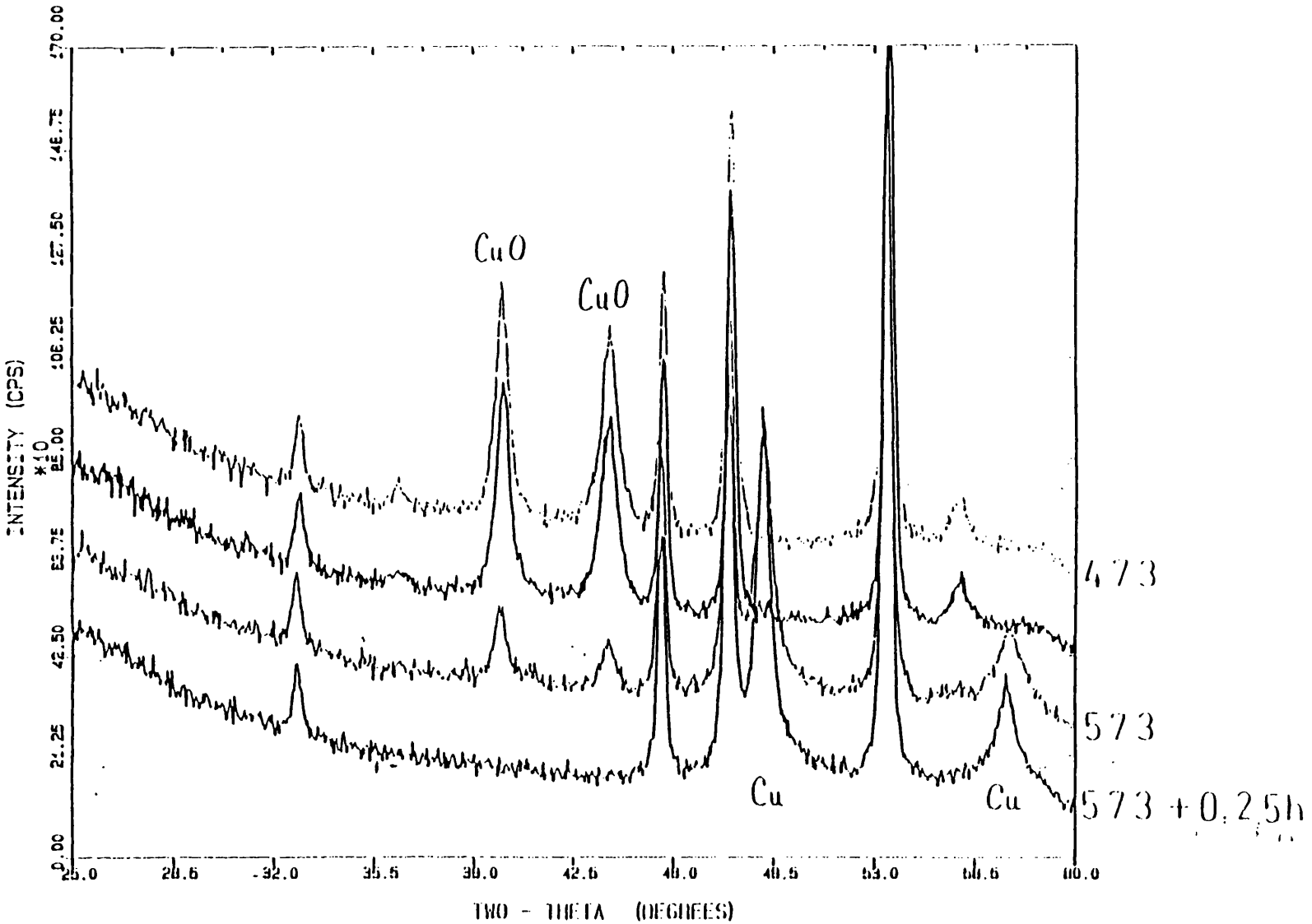

Figure 5.22 Diffraction Pattern for ICI CuO/SiO_2/Grace *a*.

5.6 THE HYDROGENATION REACTION

The hydrogenation of cinnamaldehyde was studied using the apparatus and conditions described in Section 3.4. Initially two control experiments were performed with no catalyst and an unreduced catalyst present. After 48 hours the cinnamaldehyde was still present at its initial concentration and it could therefore be assumed that no reaction had occurred.

Preliminary studies were carried out using the calcined catalyst precursor ICI CuO/SiO_2/PQ *a*. Generally 0.34 g of the calcined catalyst precursor was used in catalytic testing. Initially, however, catalyst weights ranging from 0.3 - 0.7 g were used to check that the reaction was not diffusion limited under the experimental conditions used. The calcined catalysts were reduced and the reactions carried out as described in Section 3.4. In every case the cinnamaldehyde concentration decreased linearly with respect to time except at very high conversions (80 to 90%). Figure 5.23 shows a plot of conversion versus time for ICI CuO/SiO_2/PQ *a*. This indicates that the reaction is overall zero order at low and intermediate conversions. Reaction rates were calculated as described in Section 4.4.4. The rate constant was found to increase linearly with the amount of reduced ICI CuO/SiO_2/PQ *a* catalyst used (Table 5.9) indicating that the reaction was not subject to intraparticle diffusion control.

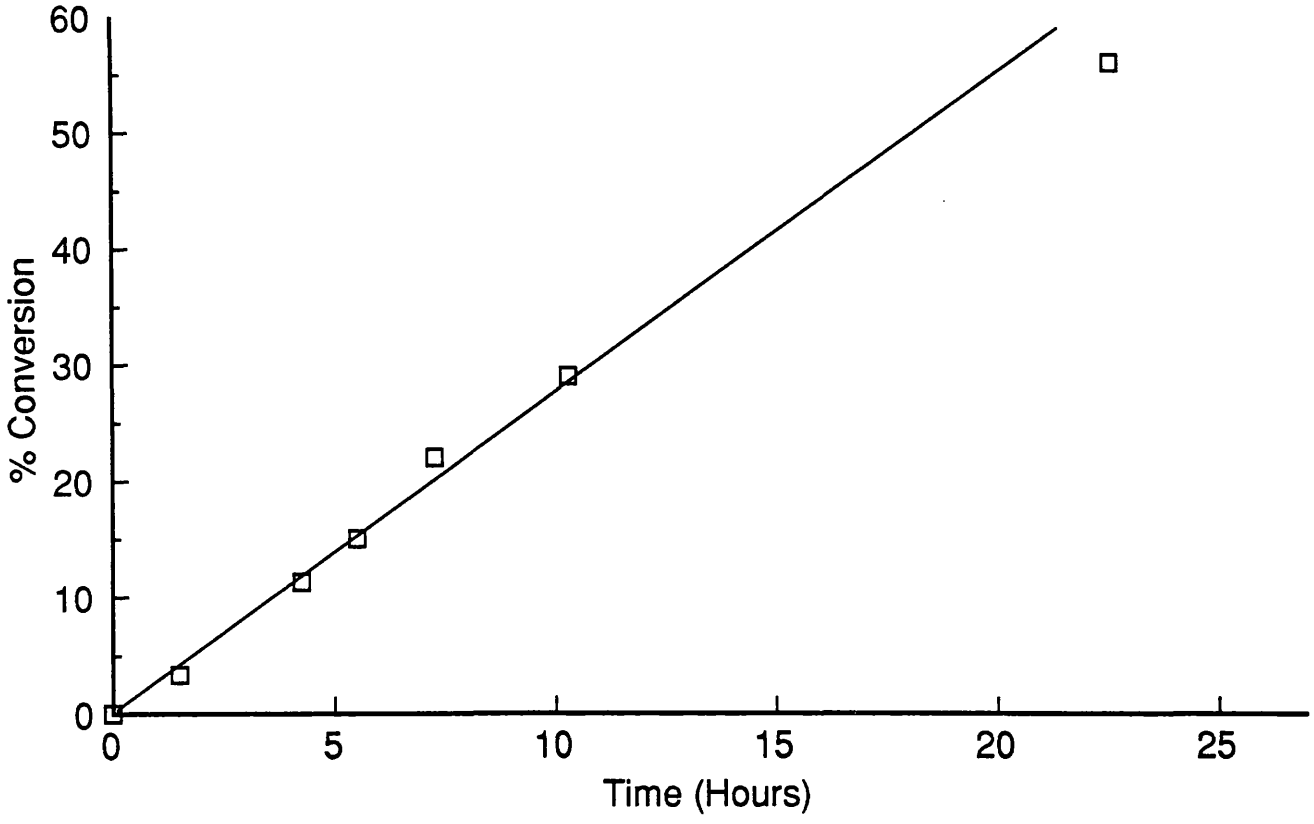

Figure 5.23. % Conversion of cinnamaldehyde versus time for (ICI CuO/SiO_2/PQ a)

Table 5.9

Wt. of Unreduced Catalyst (g) ICI CuO/SiO_2/PQ *a*	Rate Constant for cinnamaldehyde hydrogenation (moles l^{-1} hr^{-1})
0.34	2.9
0.51	4.5
0.68	6.0

The distribution of products (mole fractions) as a function of conversion is plotted for each catalyst in Figures 5.24 - 5.37. The corresponding results are shown in Tables 5.10 - 5.24. Selectivities, as described in Section 4.4.3, are given in Tables 5.10a - 5.24a.

The results for the supported copper catalysts prepared by calcination in flowing air at 723 K and 623 K prior to reduction (G.U. CuO/SiO_2 CIA and G.U. CuO/SiO_2 CIA 623 K) are shown in Figures 5.38 and 5.39 and Tables 5.25, 5.25a, 5.26 and 5.26a. Reaction rate constants are shown in Table 5.27.

The effect of variation in the reduction temperature was studied using G.U. CuO/SiO_2. The catalyst was reduced at 623, 673 and 723 K prior to the catalytic run. The activity and selectivity of the catalyst was found to be independent of the reduction temperature and results were as in Table 5.14.

In a bid to help elucidate the reaction mechanism the hydrogenation of hydrocinnamaldehyde and cinnamyl alcohol were studied using identical conditions to those used for cinnamaldehyde and reduced G.U. CuO/SiO_2

as a catalyst. The results are shown in Figures 5.40 - 5.41 and Tables 5.28 and 5.29. Reaction rate constants relative to the hydrogenation of 2.98×10^{-6} moles of cinnamaldehyde are shown in Table 5.30.

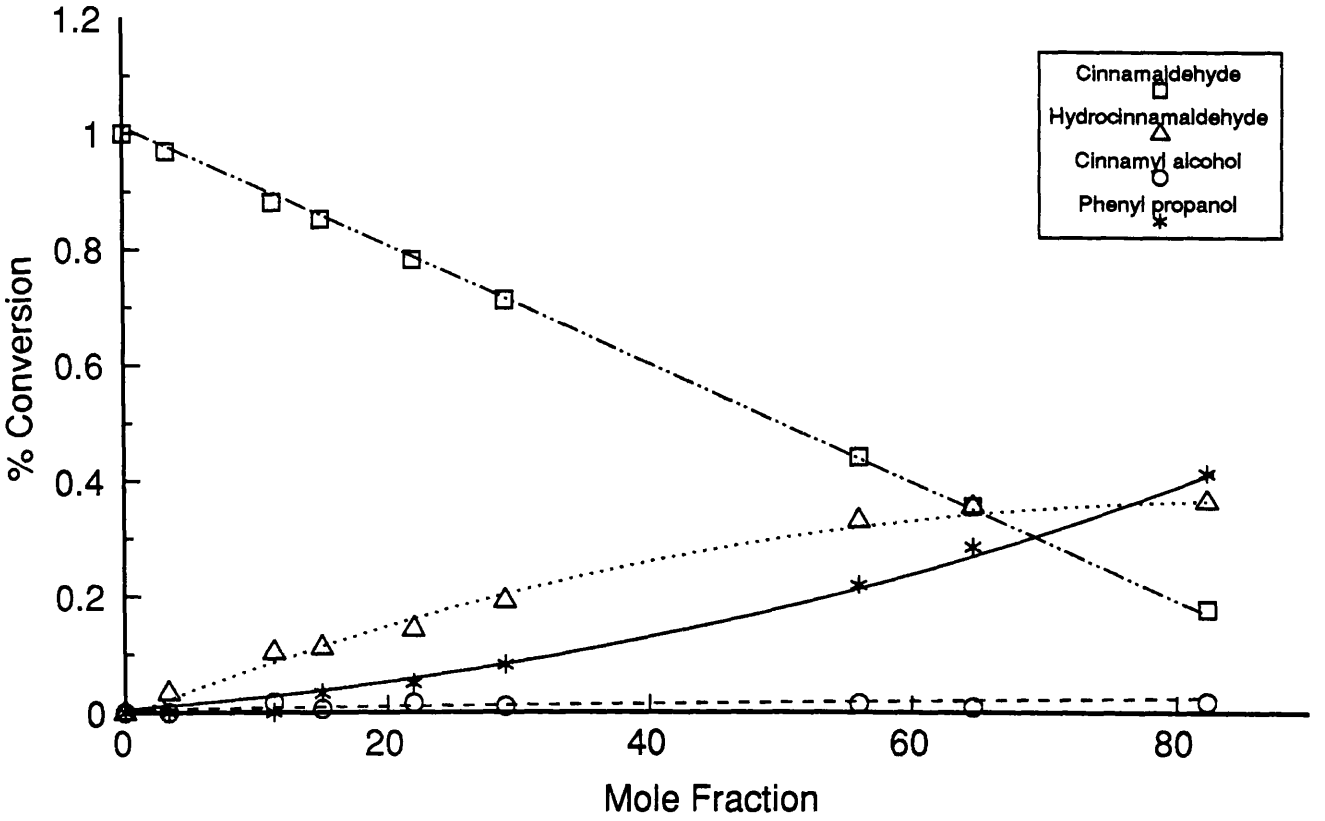

Figure 5.24. % Conversion versus the distribution of products for (ICI CuO/SiO_2/PQ a)

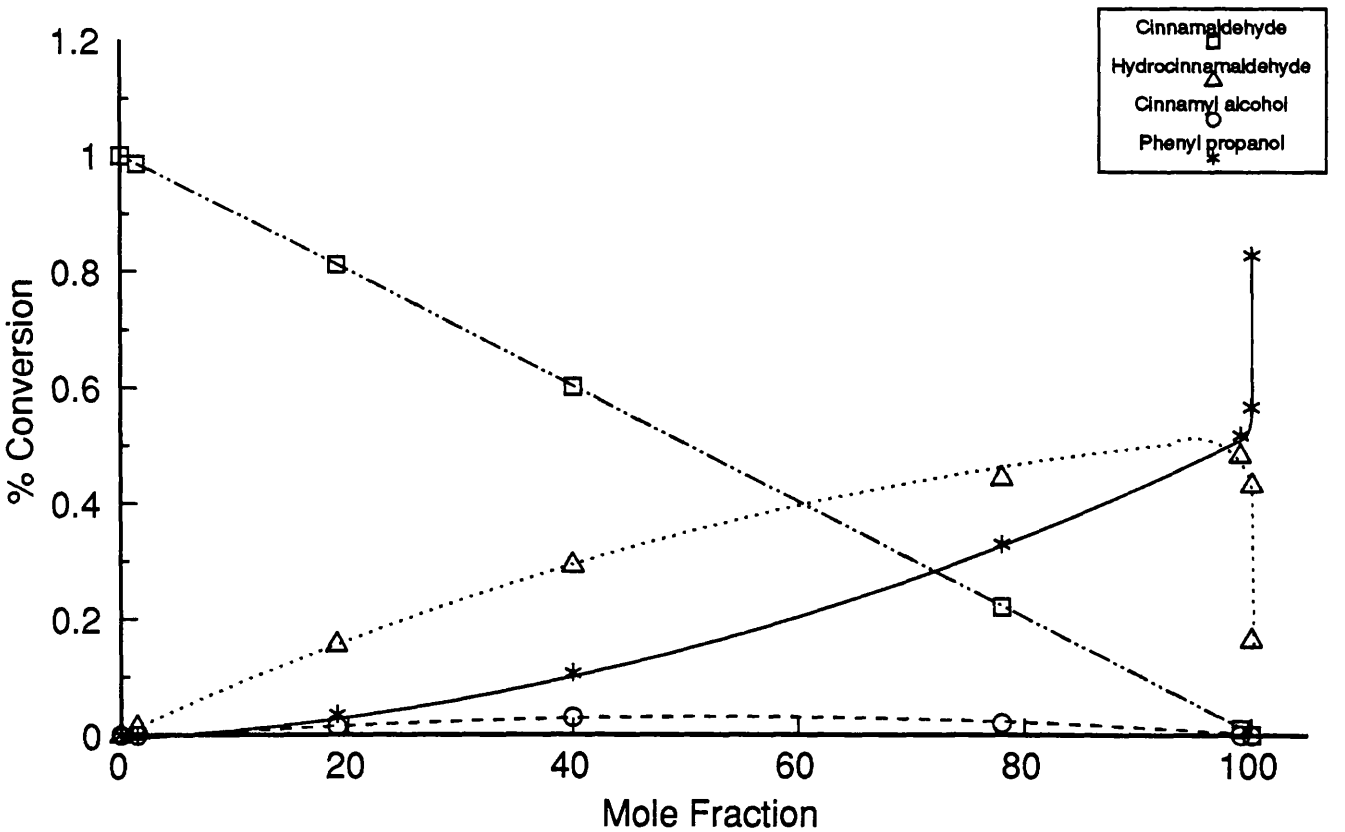

Figure 5.25. % Conversion versus the distribution of products for (ICI CuO/SiO_2/Grace a)

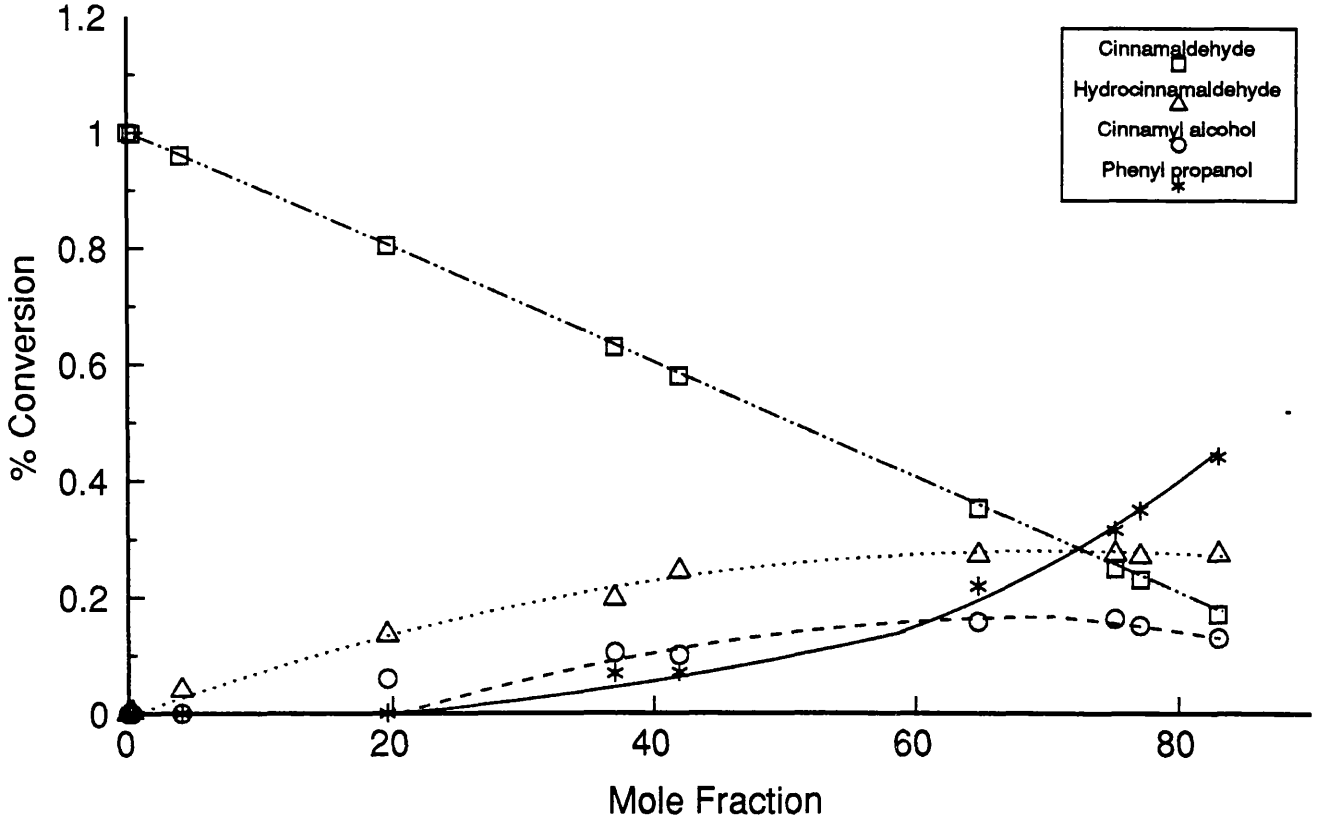

Figure 5.26. % Conversion versus the distribution of products for (ICI CuO/SiO_2/PQ b)

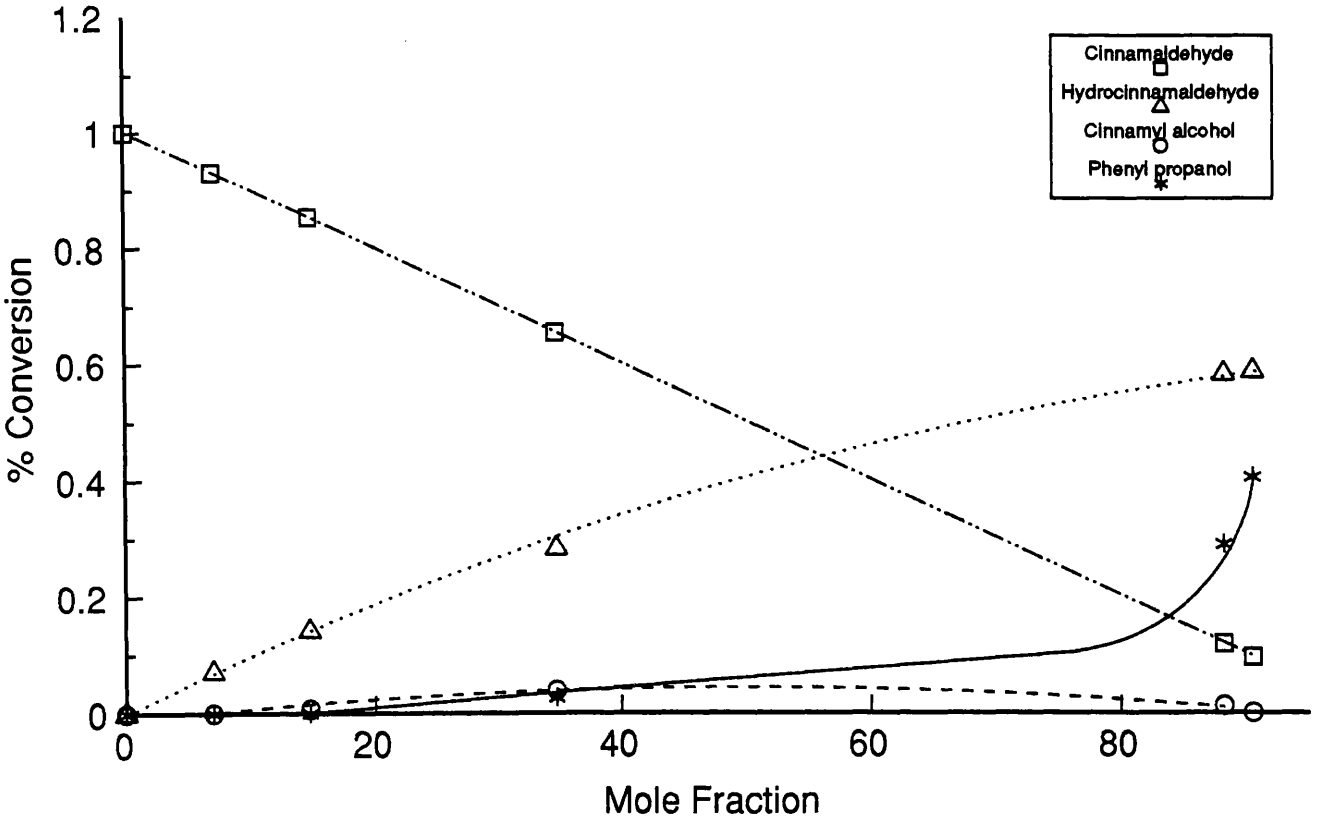

Figure 5.27. % Conversion versus the distribution of products for (ICI CuO/SiO_2/Grace b)

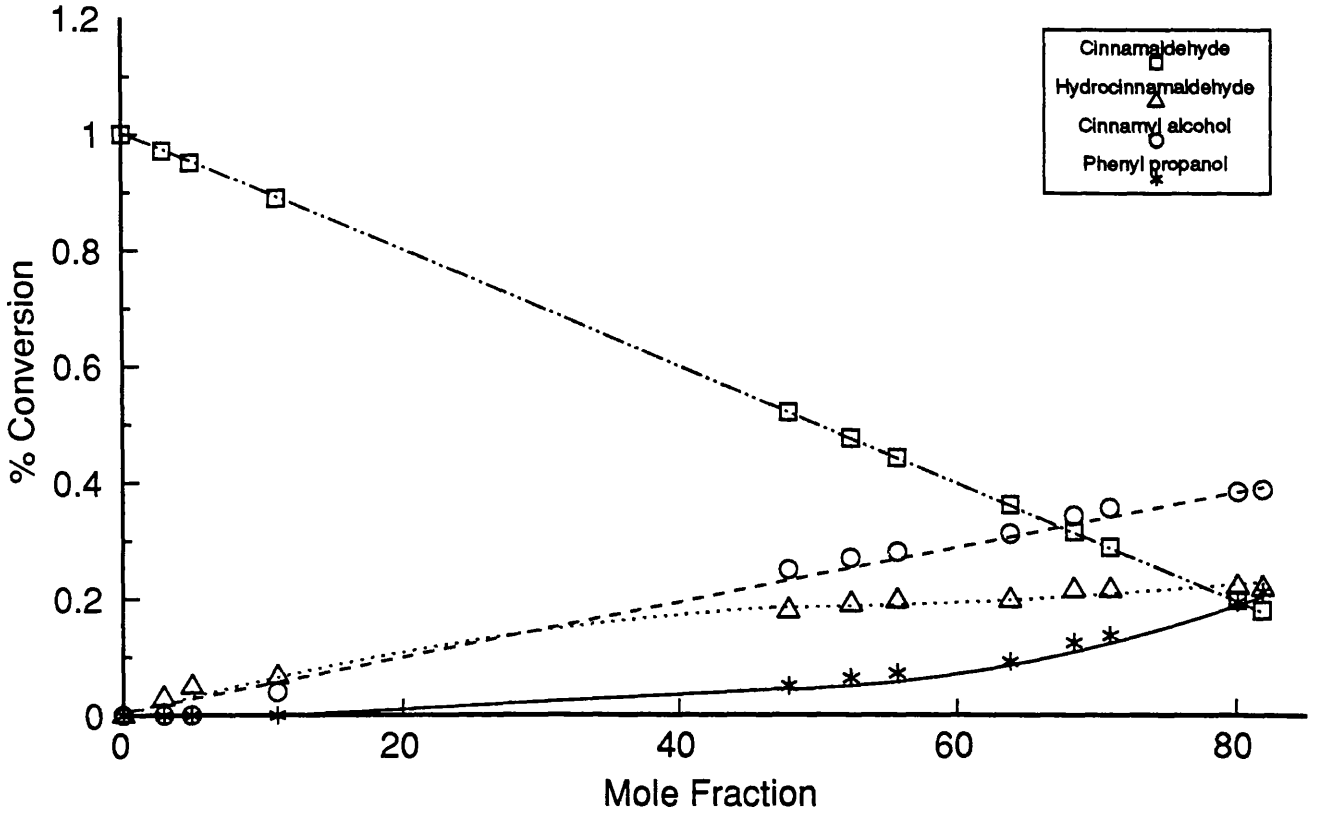

Figure 5.28. % Conversion versus the distribution of products for (G.U. CuO/SiO_2)

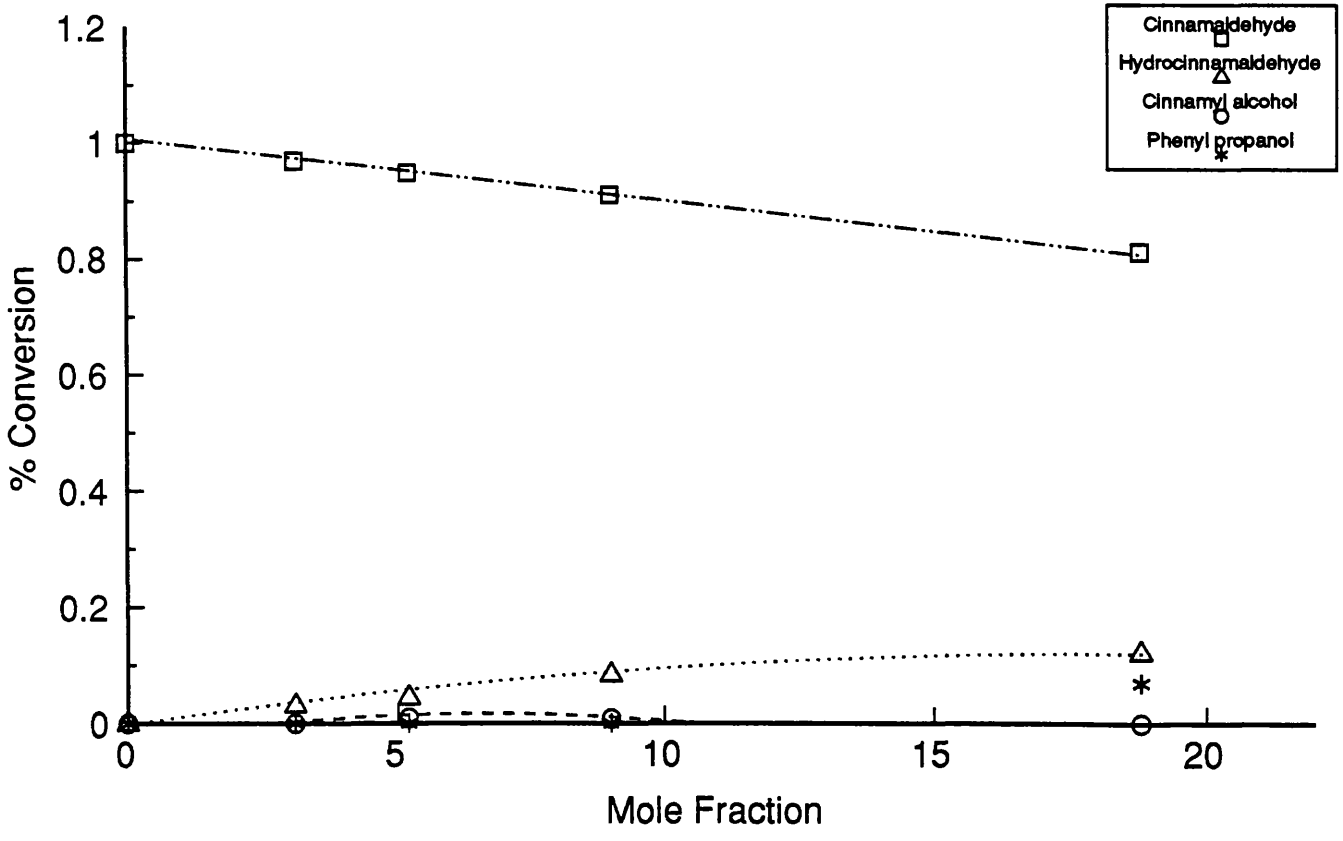

Figure 5.29. % Conversion versus the distribution of products for ($CuO/V_2O_5/SiO_2$)

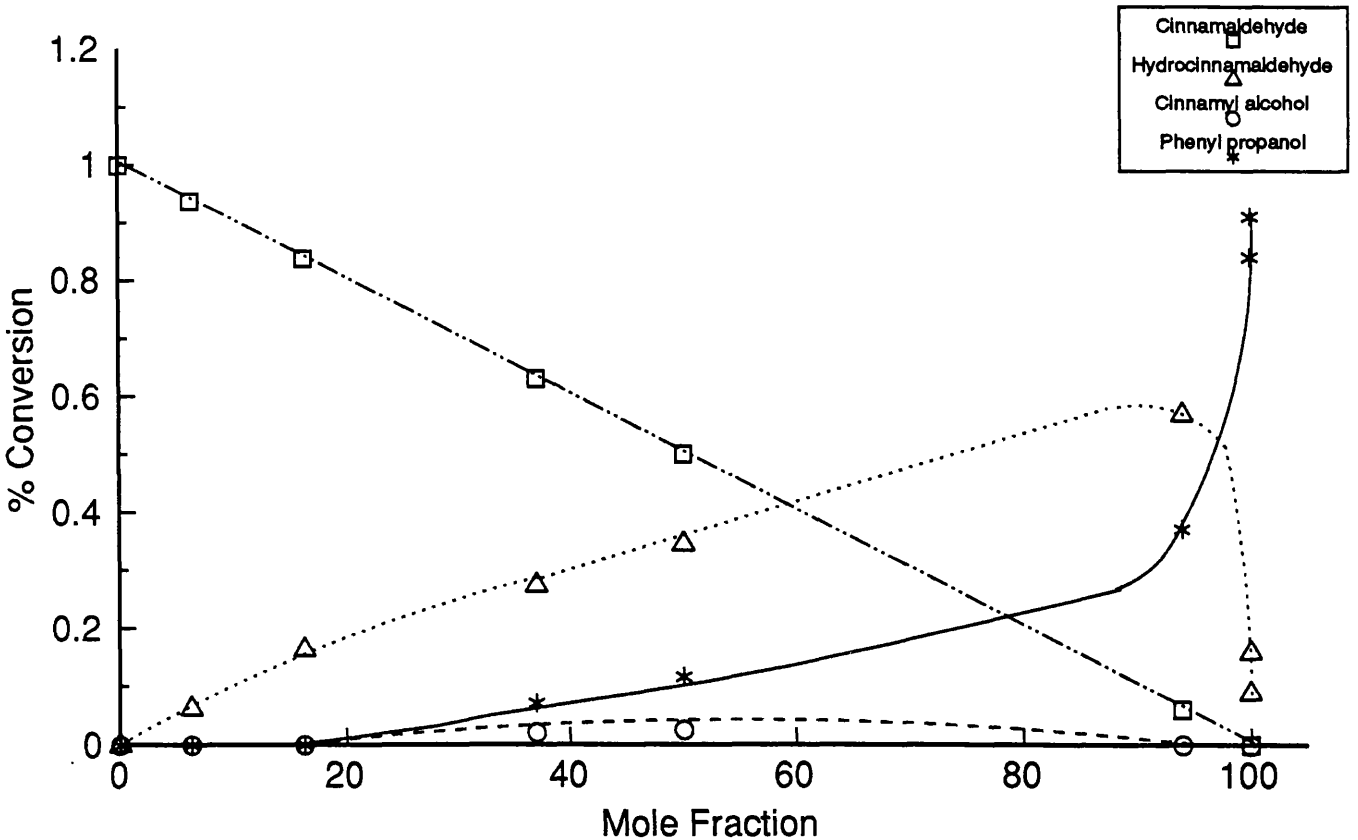

Figure 5.30. % Conversion versus the distribution of products for (CuO/V_2O_5 /PdO /SiO_2)

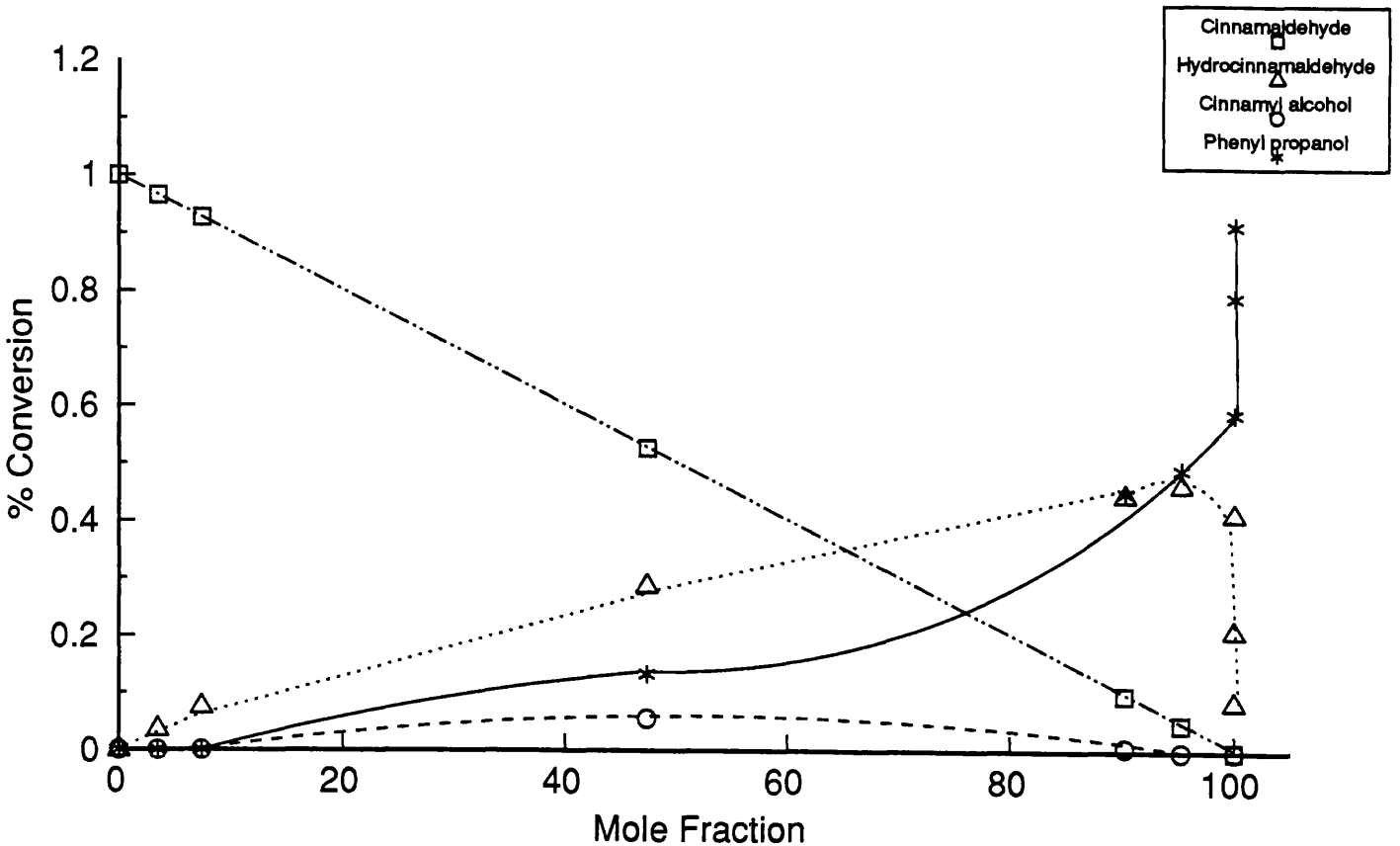

Figure 5.31. % Conversion versus the distribution of products for ($CuO/PdO/SiO_2$ a)

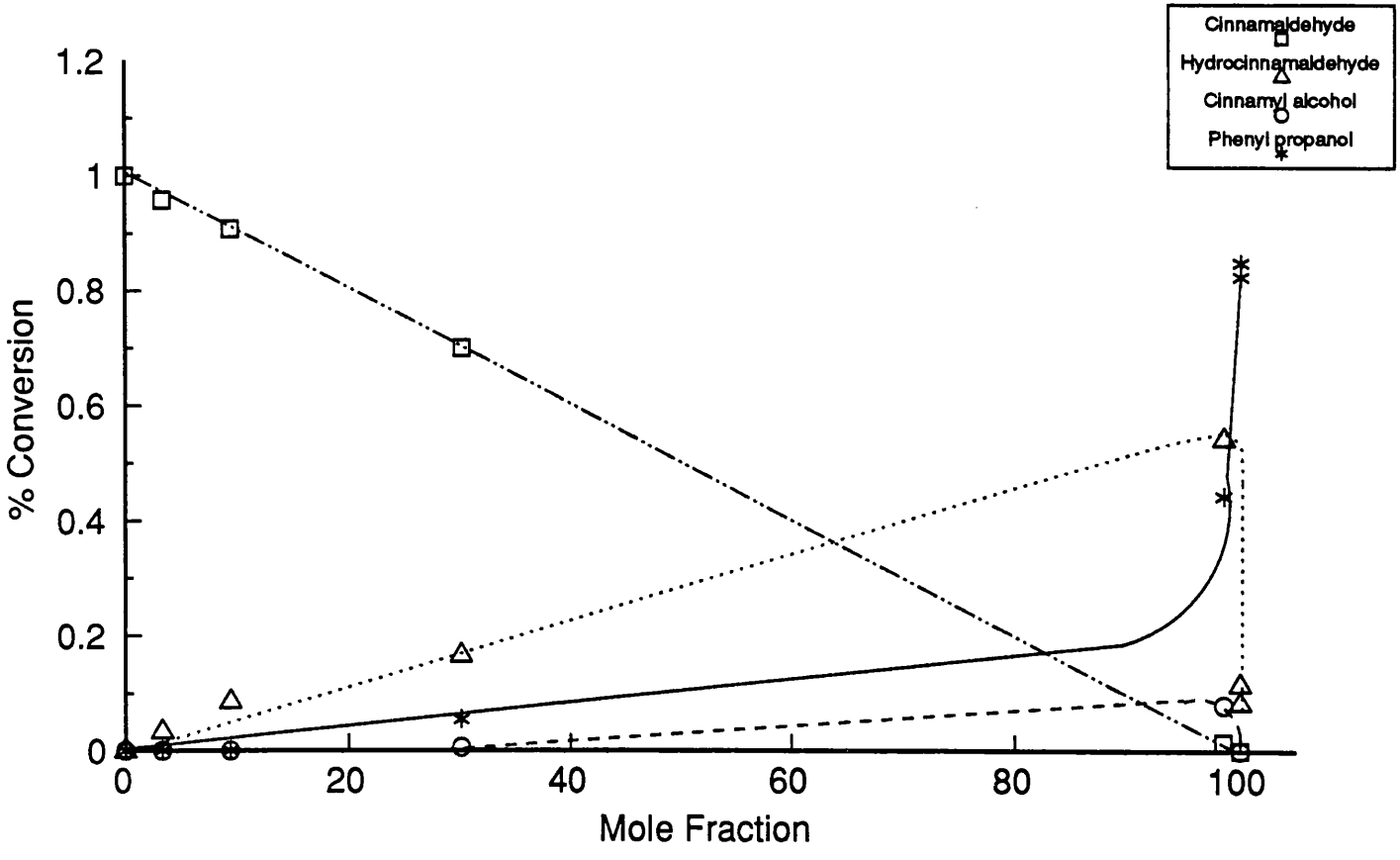

Figure 5.32. % Conversion versus the distribution of products for ($CuO/PdO/SiO_2$ c)

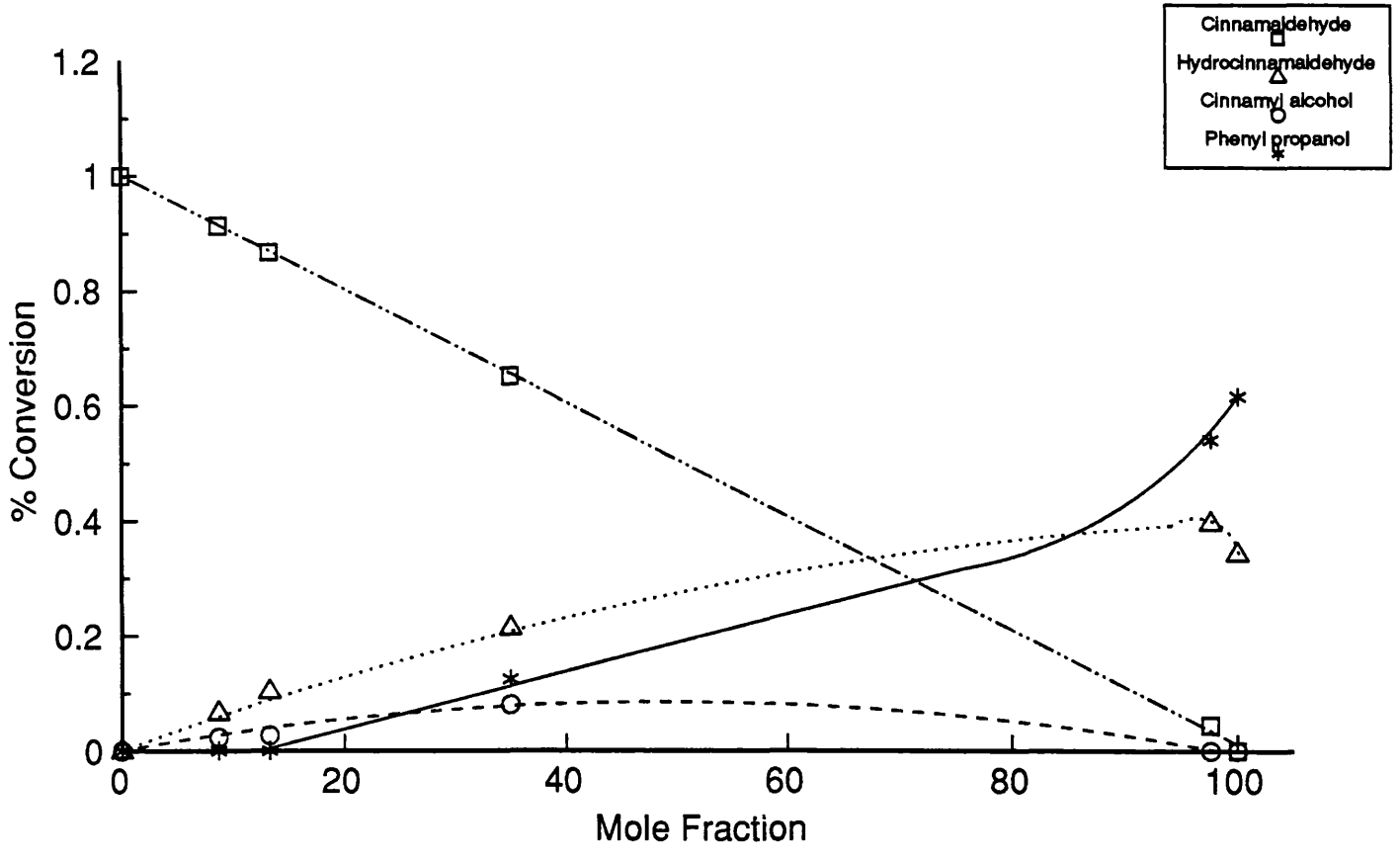

Figure 5.33. % Conversion versus the distribution of products for (CuO /PdO /SiO_2 d)

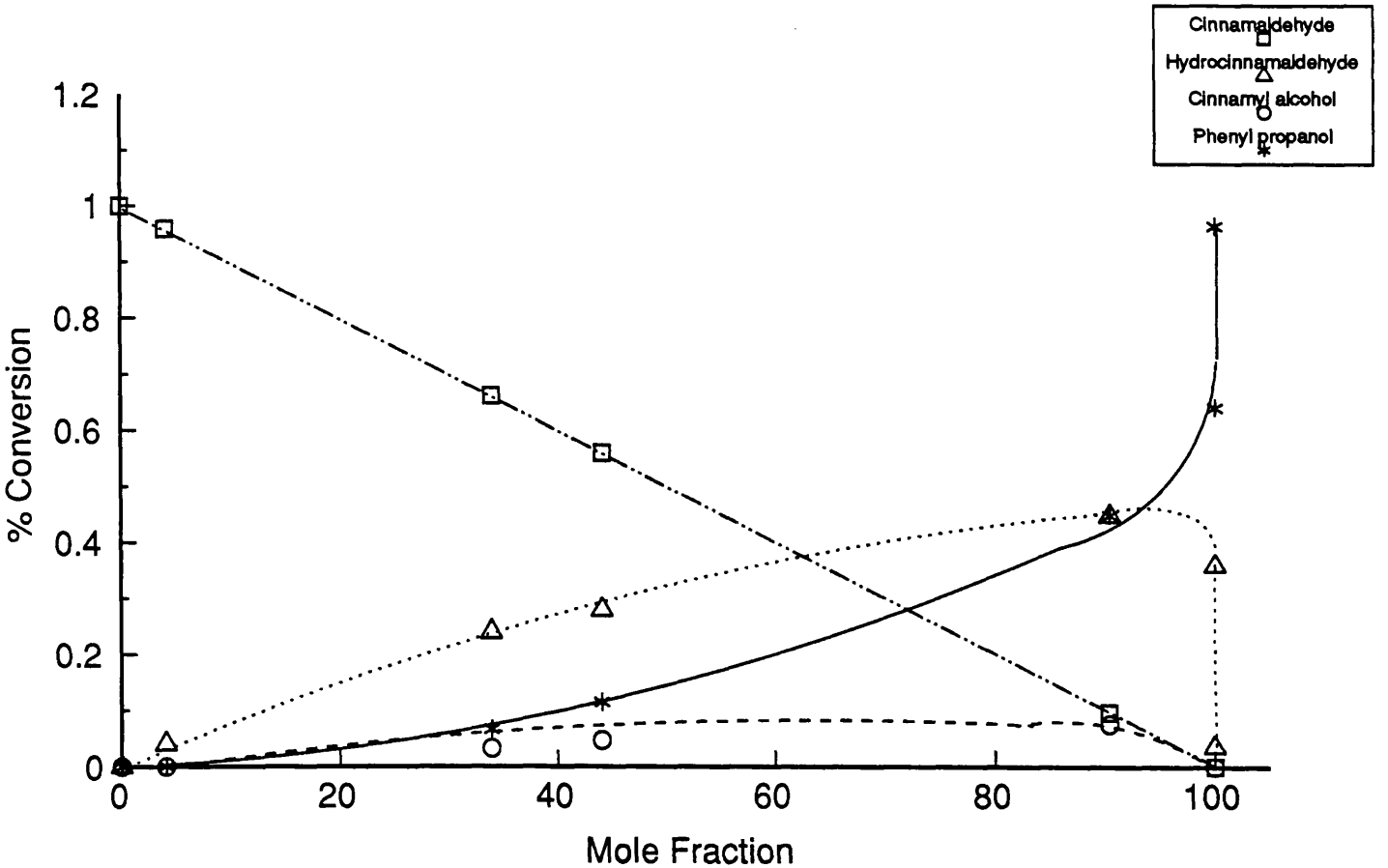

Figure 5.34. % Conversion versus the distribution of products for ($CuO/PdO/SiO_2$ e)

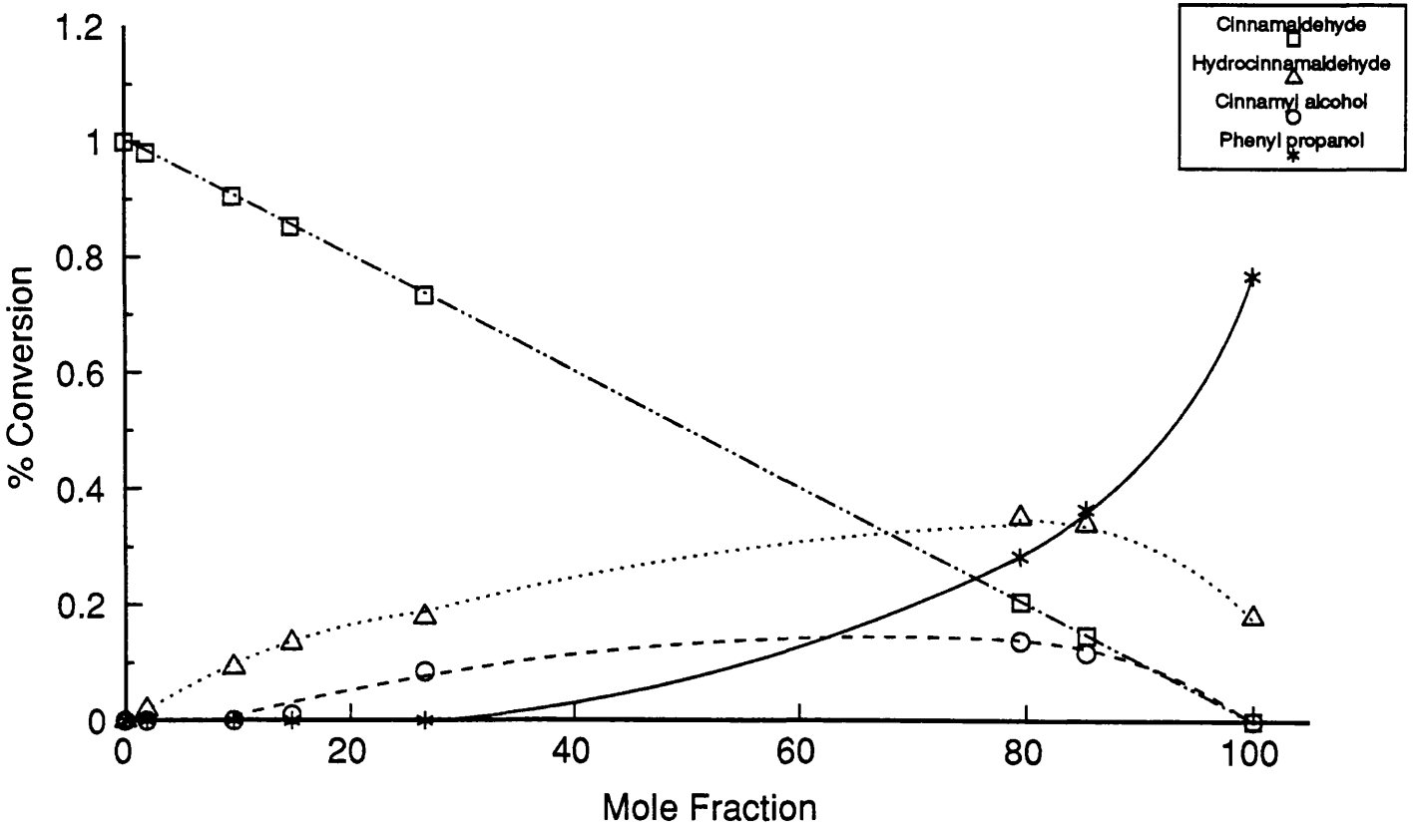

Figure 5.35. % Conversion versus the distribution of products for ($CuO/RuO_2/SiO_2$ a)

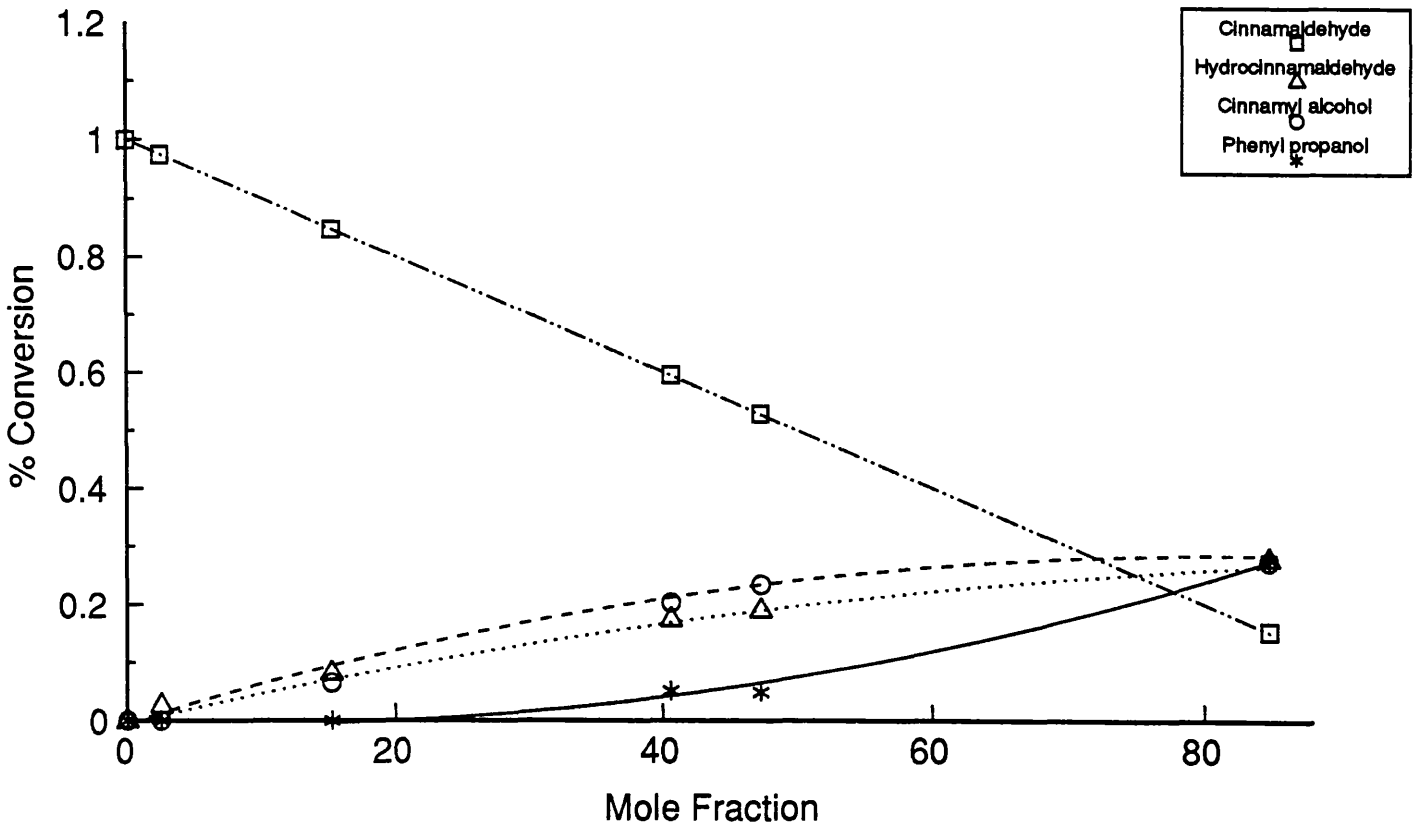

Figure 5.36. % Conversion versus the distribution of products for ($CuO/RuO_2/SiO_2$ b)

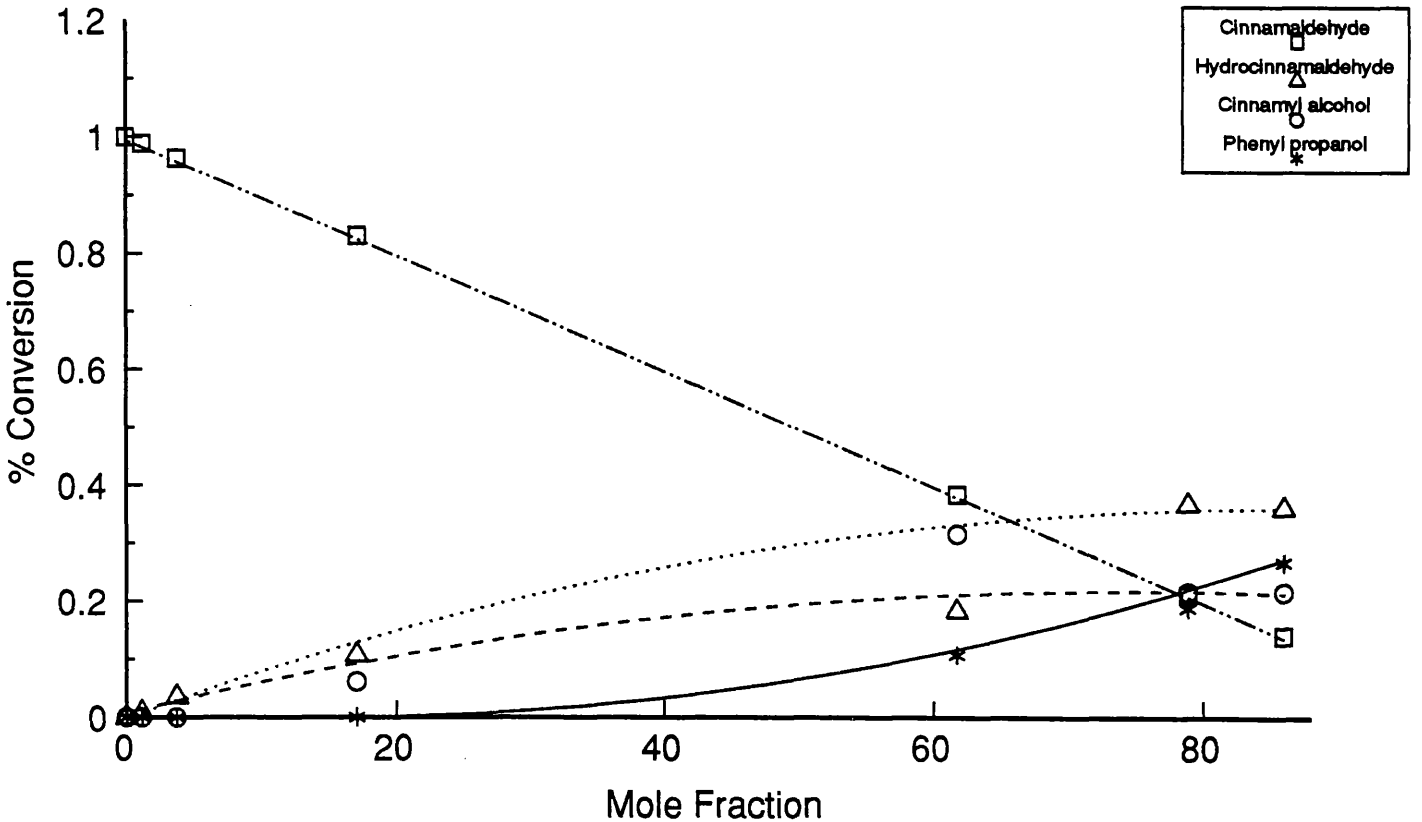

Figure 5.37. % Conversion versus the distribution of products for ($CuO/RuO_2/SiO_2$ c)

Table 5.10 Hydrogenation of 1.98 x 10^{-6} moles of Cinnamaldehyde (ICI CuO/SiO_2/PQ *a*).

Time (hours)	Mole Fraction			
	Cinnam aldehyde	Hydrocinnam aldehyde	Cinnamyl alcohol	Phenyl Propanol
0	1.000	0.000	0.000	0.000
1.5	0.968	0.033	0.000	0.000
4.25	0.880	0.103	0.016	0.000
5.5	0.850	0.110	0.006	0.032
7.25	0.780	0.142	0.015	0.049
10.3	0.710	0.190	0.010	0.081
22.5	0.440	0.329	0.014	0.218
29.25	0.354	0.354	0.008	0.284
42.25	0.177	0.363	0.018	0.412

Table 5.10a Selectivities for Cinnamaldehyde Hydrogenation (ICI CuO/SiO_2/PQ *a*).

% Conversion	Selectivity		
	S_{HCA}	S_{CAL}	$S_{CAL-HCA}$
3.3	100.0	0.0	0.0
11.3	91.2	8.8	0.097
15.0	73.3	4.0	0.054
22.0	64.5	6.8	0.106
29.0	65.5	3.4	0.053
56.0	58.8	2.5	0.043
64.6	54.8	1.2	0.023
82.3	44.1	2.2	0.050

Table 5.11 Hydrogenation of 1.98×10^{-6} moles of Cinnamaldehyde (ICI CuO/SiO_2/Grace *a*).

Time (hours)	Mole Fraction			
	Cinnam aldehyde	Hydrocinnam aldehyde	Cinnamyl alcohol	Phenyl Propanol
0	1.000	0.000	0.000	0.000
0.5	0.986	0.014	0.000	0.000
4.25	0.810	0.155	0.015	0.035
9.0	0.600	0.291	0.030	0.106
19.0	0.220	0.443	0.020	0.328
24.0	0.010	0.482	0.000	0.517
26.0	0.000	0.431	0.000	0.569
48.0	0:000	0.164	0.000	0.828

Table 5.11a Selectivities for Cinnamaldehyde Hydrogenation (ICI CuO/SiO_2/Grace *a*).

% Conversion	Selectivity		
	S_{HCA}	S_{CAL}	$S_{CAL-HCA}$
1.4	100.0	0.0	0.0
19.0	81.6	7.9	0.097
40.0	72.7	7.5	0.103
78.0	56.8	2.6	0.045
99.0	48.7	0.0	0.000
100.0	43.1	0.0	0.000
100.0	16.4	0.0	0.000

Table 5.12 Hydrogenation of 1.98 x 10^{-6} moles of Cinnamaldehyde (ICI CuO/SiO_2/PQ *b*).

Time (hours)	Mole Fraction			
	Cinnam aldehyde	Hydrocinnam aldehyde	Cinnamyl alcohol	Phenyl Propanol
0	1.000	0.000	0.000	0.000
0.67	0.997	0.003	0.000	0.000
5.33	0.960	0.040	0.000	0.000
25.0	0.804	0.135	0.060	0.000
49.75	0.630	0.197	0.104	0.068
54.17	0.580	0.244	0.100	0.070
74.08	0.352	0.272	0.157	0.219
102.83	0.248	0.275	0.163	0.315
123.67	0.229	0.270	0.151	0.349
144.42	0.170	0.274	0.130	0.442

Table 5.12a Selectivities for Cinnamaldehyde Hydrogenation (ICI CuO/SiO_2/PQ *b*).

% Conversion	Selectivity		
	S_{HCA}	S_{CAL}	$S_{CAL-HCA}$
0.3	100.0	0.0	0.000
4.03	100.0	0.0	0.000
19.6	68.9	30.6	0.444
37.0	53.2	28.2	0.530
42.0	58.1	23.8	0.410
64.8	42.0	24.2	0.576
75.2	36.5	21.7	0.595
77.1	35.0	19.6	0.560
83.0	33.0	15.7	0.476

Table 5.13 Hydrogenation of 1.98 x 10^{-6} moles of Cinnamaldehyde (ICI CuO/SiO_2/Grace *b*).

Time (hours)	Mole Fraction			
	Cinnam aldehyde	Hydrocinnam aldehyde	Cinnamyl alcohol	Phenyl Propanol
0	1.000	0.000	0.000	0.000
1.83	0.930	0.070	0.000	0.000
3.83	0.852	0.141	0.007	0.000
7.75	0.653	0.282	0.038	0.026
22.25	0.118	0.581	0.012	0.289
28.0	0.095	0.586	0.000	0.404
42.5	0.000	0.321	0.000	0.679

Table 5.13a Selectivities for Cinnamaldehyde Hydrogenation (ICI CuO/SiO_2/Grace *b*).

% Conversion	Selectivity		
	S_{HCA}	S_{CAL}	$S_{CAL-HCA}$
7.0	100.0	0.0	0.000
14.8	95.3	4.7	0.049
34.7	81.3	11.0	0.135
88.2	65.9	0.0	0.000
90.5	35.5	0.0	0.000

Table 5.14 Hydrogenation of 1.98×10^{-6} moles of Cinnamaldehyde (G.U. CuO/SiO_2).

Time (hours)	Mole Fraction			
	Cinnam aldehyde	Hydrocinnam aldehyde	Cinnamyl alcohol	Phenyl Propanol
0	1.000	0.000	0.000	0.000
2.25	0.971	0.029	0.000	0.000
4.0	0.951	0.049	0.000	0.000
5.5	0.890	0.066	0.041	0.000
24.0	0.521	0.179	0.250	0.050
26.75	0.476	0.190	0.270	0.064
29.75	0.443	0.196	0.282	0.073
35.25	0.362	0.197	0.312	0.092
47.0	0.316	0.215	0.344	0.125
51.0	0.290	0.215	0.357	0.137
70.08	0.199	0.221	0.385	0.195
79.17	0.181	0.218	0.388	0.212

Table 5.14a Selectivities for Cinnamaldehyde Hydrogenation (G.U. CuO/SiO_2).

% Conversion	Selectivity		
	S_{HCA}	S_{CAL}	$S_{CAL-HCA}$
2.9	100.0	0.0	0.000
4.9	100.0	0.0	0.000
11.0	60.0	37.3	0.622
47.9	37.4	52.2	1.396
52.4	36.3	51.5	1.419
55.7	35.2	50.6	1.438
63.8	30.9	48.9	1.582
68.4	31.4	50.3	1.602
71.0	30.3	50.3	1.661
80.1	27.6	48.1	1.743
81.9	22.6	47.4	2.097

Table 5.15 Hydrogenation of 1.98×10^{-6} moles of Cinnamaldehyde (V_2O_5/SiO_2).

Time (hours)	Mole Fraction			
	Cinnam aldehyde	Hydrocinnam aldehyde	Cinnamyl alcohol	Phenyl Propanol
0	1.000	0.000	0.000	0.000
2.0	1.000	0.000	0.000	0.000
6.0	1.000	0.000	0.000	0.000
24.0	1.000	0.000	0.000	0.000
48.0	1.000	0.000	0.000	0.000

Table 5.16 Hydrogenation of 1.98 x 10^{-6} moles of Cinnamaldehyde ($CuO/V_2O_5/SiO_2$).

Time (hours)	Mole Fraction			
	Cinnam aldehyde	Hydrocinnam aldehyde	Cinnamyl alcohol	Phenyl Propanol
0	1.000	0.000	0.000	0.000
5.75	0.969	0.030	0.000	0.000
7.25	0.948	0.043	0.009	0.000
12.0	0.910	0.083	0.008	0.000
18.0	0.812	0.120	0.000	0.069

Table 5.16a Selectivities for Cinnamaldehyde Hydrogenation ($CuO/V_2O_5/SiO_2$).

% Conversion	Selectivity		
	S_{HCA}	S_{CAL}	$S_{CAL-HCA}$
3.1	100.0	0.0	0.000
5.2	83.5	16.5	0.196
9.0	91.7	8.3	0.091
18.8	63.7	0.0	0.000

Table 5.17 Hydrogenation of 1.98 x 10^{-6} moles of Cinnamaldehyde ($CuO/V_2O_5/PdO/SiO_2$).

Time (hours)	Mole Fraction			
	Cinnam aldehyde	Hydrocinnam aldehyde	Cinnamyl alcohol	Phenyl Propanol
0	1.000	0.000	0.000	0.000
0.8	0.937	0.063	0.000	0.000
2.0	0.837	0.163	0.000	0.000
4.5	0.630	0.274	0.021	0.071
5.5	0.500	0.345	0.025	0.117
9.0	0.060	0.569	0.000	0.371
22.0	0.000	0.159	0.000	0.841
22.25	0.000	0.089	0.000	0.911

Table 5.17a Selectivities for Cinnamaldehyde Hydrogenation ($CuO/V_2O_5/PdO/SiO_2$).

% Conversion	Selectivity		
	S_{HCA}	S_{CAL}	$S_{CAL-HCA}$
6.3	100.0	0.0	0.000
16.3	100.0	0.0	0.000
37.0	74.1	5.7	0.077
50.1	68.9	5.0	0.073
94.0	60.5	0.0	0.000
100.0	15.9	0.0	0.000
100.0	8.9	0.0	0.000

Table 5.18 Hydrogenation of 1.98 x 10^{-6} moles of Cinnamaldehyde ($CuO/PdO/SiO_2$ *a*).

Time (hours)	Mole Fraction			
	Cinnam aldehyde	Hydrocinnam aldehyde	Cinnamyl alcohol	Phenyl Propanol
0	1.000	0.000	0.000	0.000
1.25	0.965	0.035	0.000	0.000
2.5	0.926	0.074	0.000	0.000
9.25	0.526	0.286	0.055	0.133
22.0	0.097	0.445	0.007	0.450
24.0	0.047	0.462	0.000	0.491
29.0	0.000	0.412	0.000	0.588
50.0	0.000	0.208	0.000	0.792
70.25	0.000	0.084	0.000	0.916

Table 5.18a Selectivities for Cinnamaldehyde Hydrogenation ($CuO/PdO/SiO_2$ *a*).

% Conversion	Selectivity		
	S_{HCA}	S_{CAL}	$S_{CAL-HCA}$
3.5	100.0	0.0	0.000
7.4	100.0	0.0	0.000
47.4	60.3	11.6	0.192
90.3	49.3	0.7	0.017
95.3	48.5	0.0	0.000
100.0	41.2	0.0	0.000
100.0	20.8	0.0	0.000
100.0	8.4	0.0	0.000

Table 5.19 Hydrogenation of 1.98 x 10^{-6} moles of Cinnamaldehyde ($CuO/PdO/SiO_2$ *c*).

Time (hours)	Mole Fraction			
	Cinnam aldehyde	Hydrocinnam aldehyde	Cinnamyl alcohol	Phenyl Propanol
0	1.000	0.000	0.000	0.000
1.0	0.957	0.033	0.000	0.000
2.0	0.906	0.085	0.006	0.000
4.0	0.699	0.165	0.080	0.054
10.0	0.015	0.542	0.000	0.443
22.0	0.000	0.115	0.000	0.825
24.0	0.000	0.082	0.000	0.849

Table 5.19a Selectivities for Cinnamaldehyde Hydrogenation ($CuO/PdO/SiO_2$ *c*).

% Conversion	Selectivity		
	S_{HCA}	S_{CAL}	$S_{CAL-HCA}$
3.3	100.0	0.0	0.000
9.4	90.4	6.4	0.071
30.1	54.8	0.0	0.000
98.5	54.2	0.0	0.000
100.0	11.5	0.0	0.000
100.0	8.2	0.0	0.000

Table 5.20 Hydrogenation of 1.98 x 10^{-6} moles of Cinnamaldehyde ($CuO/PdO/SiO_2$ *d*).

Time (hours)	Mole Fraction			
	Cinnam aldehyde	Hydrocinnam aldehyde	Cinnamyl alcohol	Phenyl Propanol
0	1.000	0.000	0.000	0.000
1.0	0.913	0.065	0.023	0.000
1.5	0.867	0.102	0.027	0.000
3.67	0.651	0.213	0.080	0.124
9.0	0.045	0.396	0.000	0.542
11.0	0.000	0.342	0.000	0.617

Table 5.20a Selectivities for Cinnamaldehyde Hydrogenation ($CuO/PdO/SiO_2$ *d*).

% Conversion	Selectivity		
	S_{HCA}	S_{CAL}	$S_{CAL-HCA}$
8.7	74.7	26.0	0.350
13.3	76.7	20.3	0.265
34.9	61.0	0.0	0.000
97.6	40.6	0.0	0.000
100.0	34.2	0.0	0.000

Table 5.21 Hydrogenation of 1.98 x 10^{-6} moles of Cinnamaldehyde ($CuO/PdO/SiO_2$ *e*).

Time (hours)	Mole Fraction			
	Cinnam aldehyde	Hydrocinnam aldehyde	Cinnamyl alcohol	Phenyl Propanol
0	1.000	0.000	0.000	0.000
0.67	0.959	0.041	0.000	0.000
5.0	0.661	0.240	0.033	0.066
7.33	0.559	0.279	0.047	0.115
22.0	0.096	0.448	0.076	0.449
27.67	0.000	0.359	0.000	0.641
49.5	0.000	0.036	0.000	0.964

Table 5.21a Selectivities for Cinnamaldehyde Hydrogenation ($CuO/PdO/SiO_2$ *e*).

% Conversion	Selectivity		
	S_{HCA}	S_{CAL}	$S_{CAL-HCA}$
4.1	100.0	0.0	0.000
33.9	70.8	9.7	0.137
44.1	63.3	16.7	0.169
90.4	49.6	8.4	0.169
100.0	35.9	0.0	0.000
100.0	3.6	0.0	0.000

Table 5.22 Hydrogenation of 1.98 x 10^{-6} moles of Cinnamaldehyde ($CuO/RuO_2/SiO_2$ *a*).

Time (hours)	Mole Fraction			
	Cinnam aldehyde	Hydrocinnam aldehyde	Cinnamyl alcohol	Phenyl Propanol
0	1.000	0.000	0.000	0.000
0.5	0.981	0.019	0.000	0.000
1.0	0.904	0.092	0.000	0.000
2.0	0.852	0.134	0.010	0.000
4.0	0.734	0.178	0.084	0.000
24.0	0.205	0.352	0.138	0.284
27.0	0.147	0.340	0.118	0.365
48.0	0.000	0.180	0.000	0.770

Table 5.22a Selectivities for Cinnamaldehyde Hydrogenation ($CuO/RuO_2/SiO_2$ *a*).

% Conversion	Selectivity		
	S_{HCA}	S_{CAL}	$S_{CAL-HCA}$
1.90	100.0	0.0	0.000
9.61	100.0	0.0	0.000
14.77	90.7	6.8	0.075
26.59	66.9	31.6	0.472
79.49	44.3	17.4	0.393
85.27	39.9	13.8	0.346
100.00	0.2	0.0	0.000

Table 5.23 Hydrogenation of 1.98 x 10^{-6} moles of Cinnamaldehyde ($CuO/RuO_2/SiO_2$ *b*).

Time (hours)	Mole Fraction			
	Cinnam aldehyde	Hydrocinnam aldehyde	Cinnamyl alcohol	Phenyl Propanol
0	1.000	0.000	0.000	0.000
1.58	0.974	0.025	0.000	0.000
8.5	0.847	0.080	0.064	0.000
22.0	0.594	0.173	0.202	0.050
24.0	0.527	0.188	0.233	0.048
45.0	0.152	0.276	0.272	0.277

Table 5.23a Selectivities for Cinnamaldehyde Hydrogenation ($CuO/RuO_2/SiO_2$ *b*).

% Conversion	Selectivity		
	S_{HCA}	S_{CAL}	$S_{CAL-HCA}$
2.57	100.0	0.0	0.000
15.29	52.3	41.9	0.801
40.64	42.6	49.7	1.167
47.32	39.7	49.2	1.239
84.78	32.6	32.1	0.985

Table 5.24 Hydrogenation of 1.98 x 10^{-6} moles of Cinnamaldehyde ($CuO/RuO_2/SiO_2$ *c*).

Time (hours)	Mole Fraction			
	Cinnam aldehyde	Hydrocinnam aldehyde	Cinnamyl alcohol	Phenyl Propanol
0	1.000	0.000	0.000	0.000
1.0	0.988	0.008	0.000	0.000
2.0	0.963	0.035	0.000	0.000
6.0	0.830	0.107	0.061	0.000
24.0	0.383	0.183	0.315	0.107
30.5	0.211	0.367	0.216	0.188
48.5	0.141	0.360	0.216	0.267

Table 5.24a Selectivities for Cinnamaldehyde Hydrogenation ($CuO/RuO_2/SiO_2$ *c*).

% Conversion	Selectivity		
	S_{HCA}	S_{CAL}	$S_{CAL-HCA}$
1.16	100.0	0.0	0.000
3.75	100.0	0.0	0.000
17.04	62.8	35.8	0.570
61.70	29.7	51.1	1.721
78.88	46.5	27.4	0.589
85.94	41.9	25.1	0.599

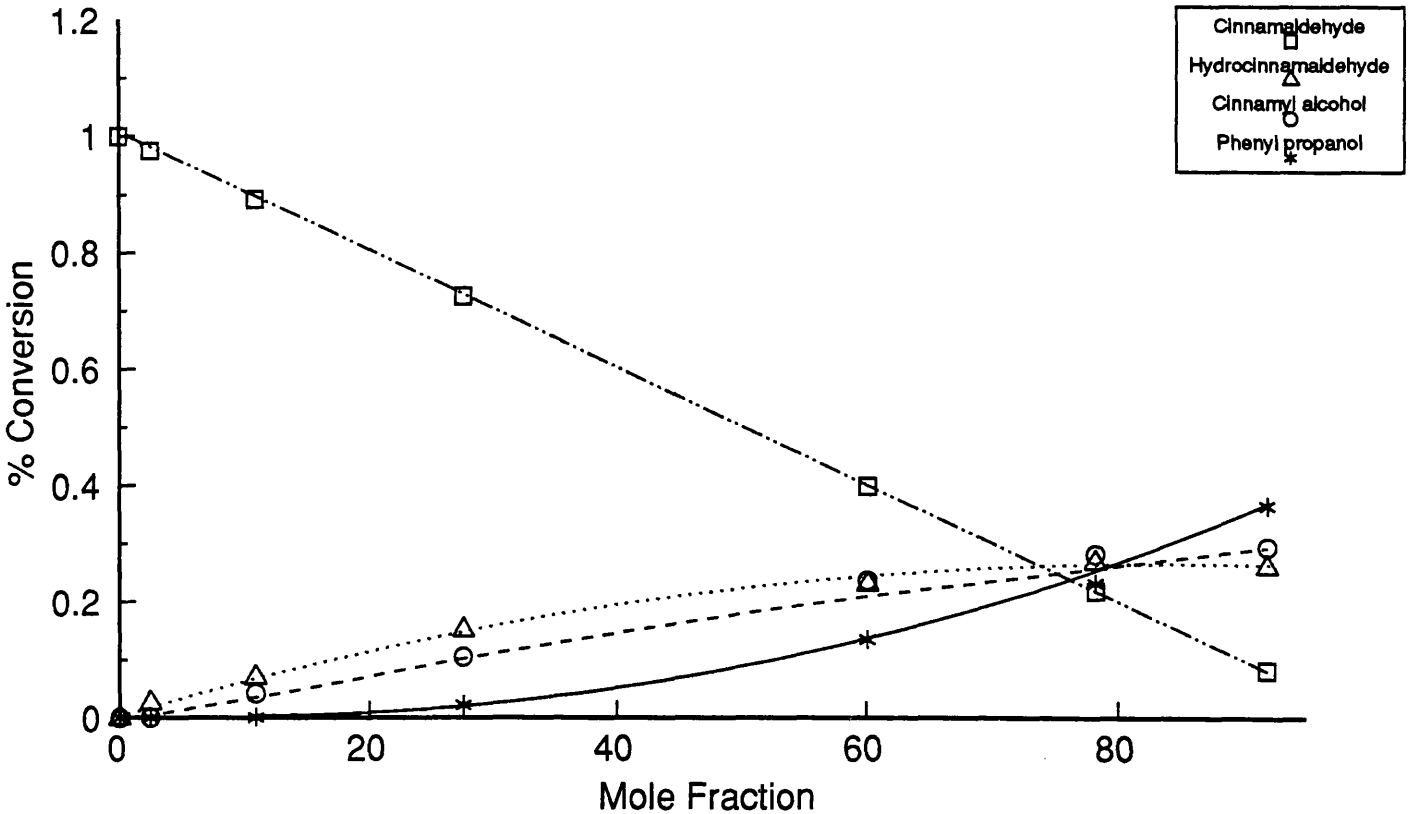

Figure 5.38. % Conversion versus the distribution of products for (G.U. CuO /SiO_2 CIA)

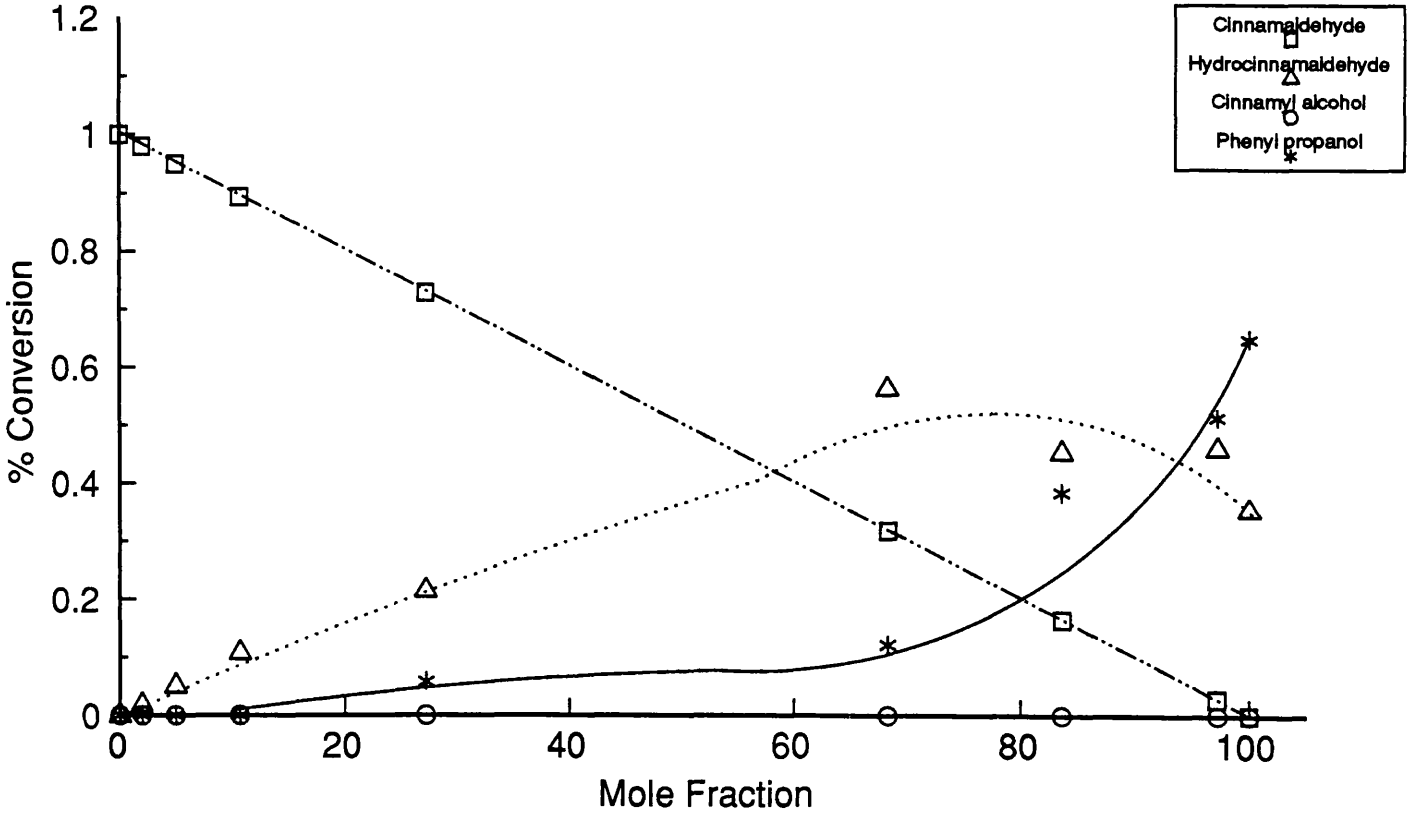

Figure 5.39. % Conversion versus the distribution of products for (G.U. CuO /SiO_2 CIA 623 K)

Table 5.25 Hydrogenation of 1.98×10^{-6} moles of Cinnamaldehyde (G.U. CuO/SiO_2 CIA).

Time (hours)	Mole Fraction			
	Cinnam aldehyde	Hydrocinnam aldehyde	Cinnamyl alcohol	Phenyl Propanol
0	1.000	0.000	0.000	0.000
1.5	0.975	0.025	0.000	0.000
4.75	0.891	0.068	0.041	0.000
11.0	0.724	0.151	0.104	0.021
23.0	0.399	0.231	0.236	0.134
29.0	0.218	0.268	0.282	0.232
36.5	0.081	0.260	0.294	0.365

Table 5.25a Selectivities for cinnamaldehyde hydrogenation (G.U. CuO/SiO_2 CIA).

% Conversion	Selectivity		
	S_{HCA}	S_{CAL}	$S_{CAL-HCA}$
2.5	100.0	0.0	0.000
10.9	62.4	37.6	0.603
27.6	54.7	37.7	0.689
60.1	38.4	39.3	1.023
78.2	34.3	36.1	1.052
91.9	28.3	32.0	1.131

Table 5.26 Hydrogenation of 1.98 x 10^{-6} moles of Cinnamaldehyde (G.U. CuO/SiO_2 CIA 623 K).

Time (hours)	Mole Fraction			
	Cinnam aldehyde	Hydrocinnam aldehyde	Cinnamyl alcohol	Phenyl Propanol
0	1.000	0.000	0.000	0.000
1.17	0.980	0.017	0.000	0.000
1.75	0.950	0.050	Trace	0.000
4.42	0.893	0.107	Trace	0.000
8.42	0.728	0.214	Trace	0.057
20.0	0.317	0.562	0.000	0.121
23.0	0.164	0.453	0.000	0.383
26.0	0.028	0.459	0.000	0.513
30.0	0.000	0.352	0.000	0.648

Table 5.26a Selectivities for Cinnamaldehyde Hydrogenation (G.U. CuO/SiO_2 CIA 623 K).

% Conversion	Selectivity		
	S_{HCA}	S_{CAL}	$S_{CAL-HCA}$
2.0	100.0	0.0	0.0
5.0	100.0	0.0	0.0
10.7	100.0	0.0	0.0
27.2	78.7	0.0	0.0
68.3	82.3	0.0	0.0
83.6	54.2	0.0	0.0
97.2	47.2	0.0	0.0
100.0	35.2	0.0	0.0

Table 5.27 Rate Constants for the Hydrogenation of Cinnamaldehyde.

Catalysts	Rate Constant (moles l^{-1} hr^{-1})
ICI CuO/SiO_2/PQ a	1.9
ICI CuO/SiO_2/Grace a	4.1
ICI CuO/SiO_2/PQ b	0.8
ICI CuO/SiO_2/Grace b	3.9
G.U. CuO/SiO_2	1.9
V_2O_5/SiO_2	0.0
$CuO/V_2O_5/SiO_2$	0.8
$CuO/V_2O_5/PdO/SiO_2$	8.9
$CuO/PdO/SiO_2$ a	4.2
$CuO/PdO/SiO_2$ c	7.7
$CuO/PdO/SiO_2$ d	11.0
$CuO/PdO/SiO_2$ e	4.1
$CuO/RuO_2/SiO_2$ a	3.2
$CuO/RuO_2/SiO_2$ b	1.9
$CuO/RuO_2/SiO_2$ c	2.6
G.U. CuO/SiO_2/CIA	2.6
G.U. CuO/SiO_2/CIA 623 K	3.4

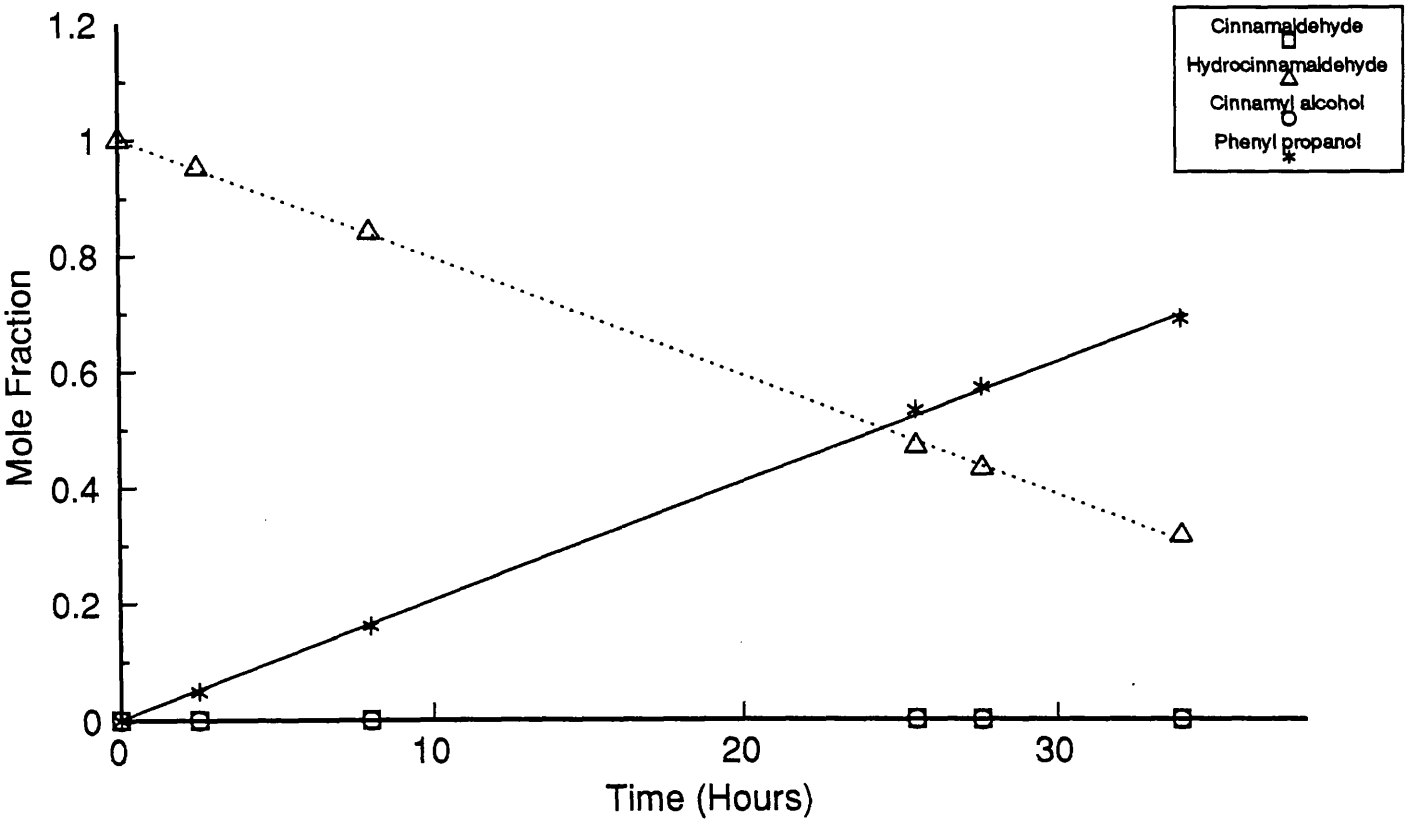

Figure 5.40. Distribution of products versus time for G.U. CuO/SiO_2 from hydrogenation of 2.90×10^{-6} moles of hydrocinnamaldehyde

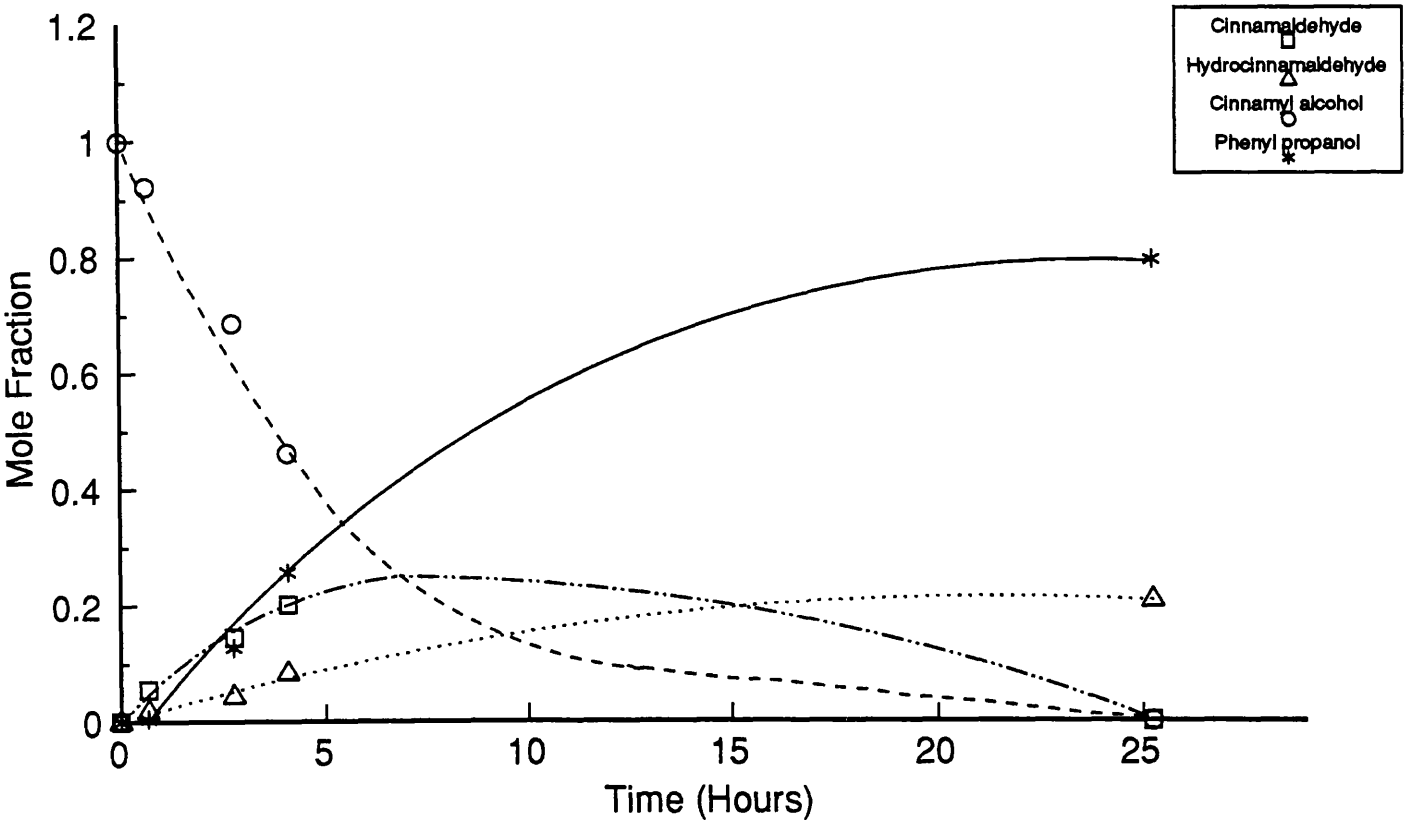

Figure 5.41. Distribution of products versus time for G.U. CuO/SiO_2 from hydrogenation of 3.24×10^{-6} moles of cinnamyl alcohol

Table 5.28 Hydrogenation of 2.90×10^{-6} moles of Hydrocinnamaldehyde (G.U. CuO/SiO_2).

Time (hours)	Mole Fraction			
	Cinnam aldehyde	Hydrocinnam aldehyde	Cinnamyl alcohol	Phenyl Propanol
0	0.000	1.000	0.000	0.000
2.5	0.000	0.952	0.000	0.048
8.0	0.000	0.840	0.000	0.160
25.5	0.000	0.469	0.000	0.531
27.6	0.000	0.430	0.000	0.570
34.0	0.000	0.313	0.000	0.687

Table 5.29 Hydrogenation of 3.24×10^{-6} moles of Cinnamyl Alcohol (G.U. CuO/SiO_2).

Time (hours)	Mole Fraction			
	Cinnam aldehyde	Hydrocinnam aldehyde	Cinnamyl alcohol	Phenyl Propanol
0	0.000	0.000	1.000	0.000
0.67	0.055	0.017	0.922	0.004
2.75	0.144	0.043	0.686	0.127
4.08	0.201	0.083	0.460	0.256
25.25	0.000	0.206	0.000	0.794

Table 5.30 Relative Reaction Rate Constants for the Hydrogenation of Hydrocinnamaldehyde and Cinnamyl Alcohol.

Catalyst	Rate Constant (moles $l^{-1} hr^{-1}$)	
	Hydrocinnam aldehyde	Cinnamyl alcohol
G.U. CuO/SiO_2	2.0	18.7

5.7 REACTION OF CINNAMALDEHYDE WITH DEUTERIUM

Cinnamaldehyde was reacted with deuterium as described in Section 3.4.5. The incorporation of deuterium in the cinnamaldehyde and reaction products was determined by proton and deuterium NMR spectroscopy. The proton and deuterium NMR spectra of the reaction mixture at ≈ 62 % conversion of cinnamaldehyde are shown in Figure 5.42 and 5.44. The mole fractions of each product are listed in Table 5.31.

Table 5.31. Reaction of Cinnamaldehyde with deuterium

% Conversion	Mole Fraction			
	Cinnam aldehyde	Hydrocinnam aldehyde	Cinnamyl alcohol	Phenyl Propanol
61.77	0.382	0.186	0.122	0.310

The experiment was repeated with hydrogen instead of deuterium. The ^1H NMR spectrum for the reaction mixture at ≈ 40 % conversion of cinnamaldehyde is shown in Figure 5.43.

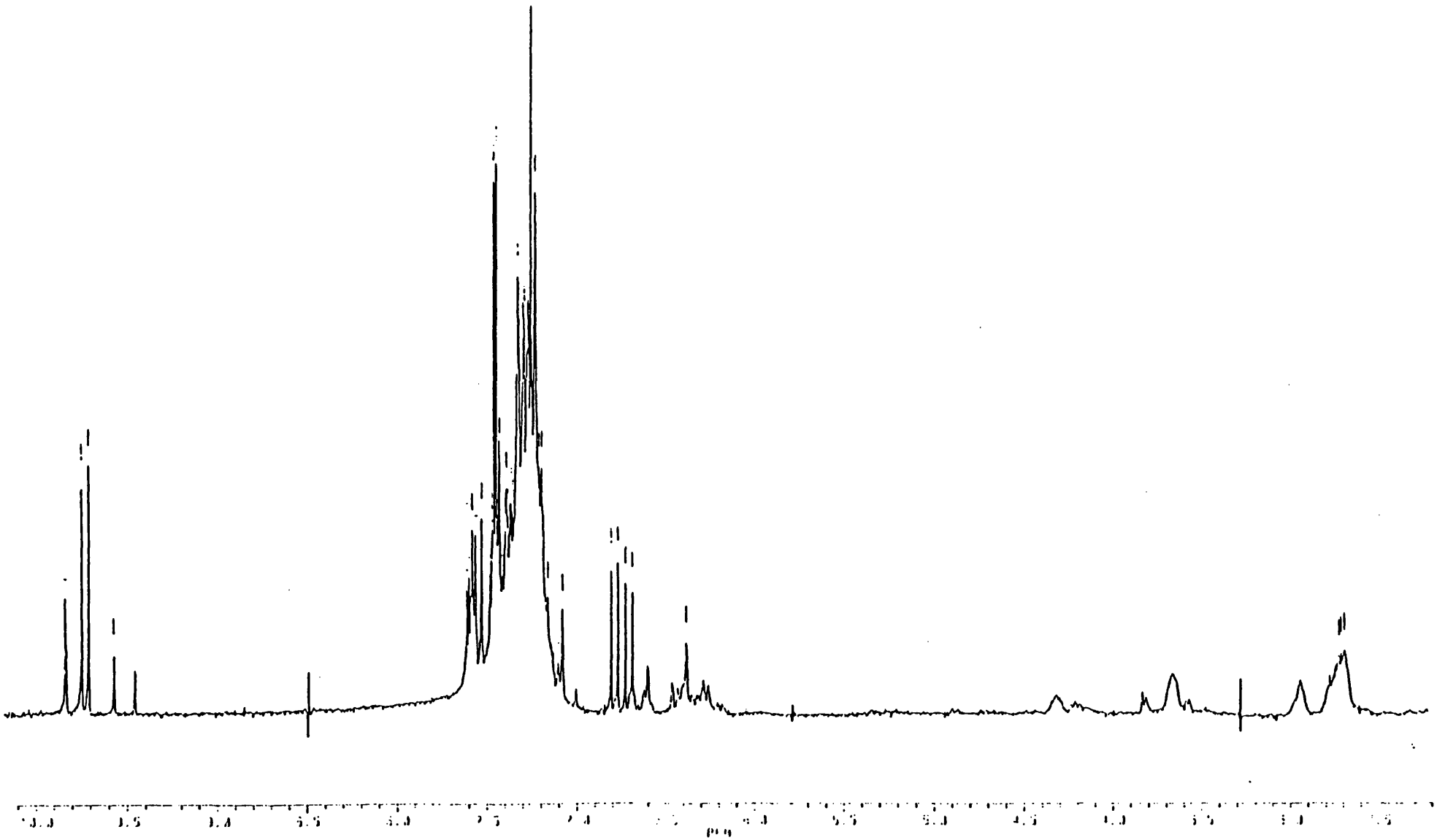

Figure 5.42 ^{1}H NMR Spectrum of Reaction of Cinnamaldehyde with Deuterium.

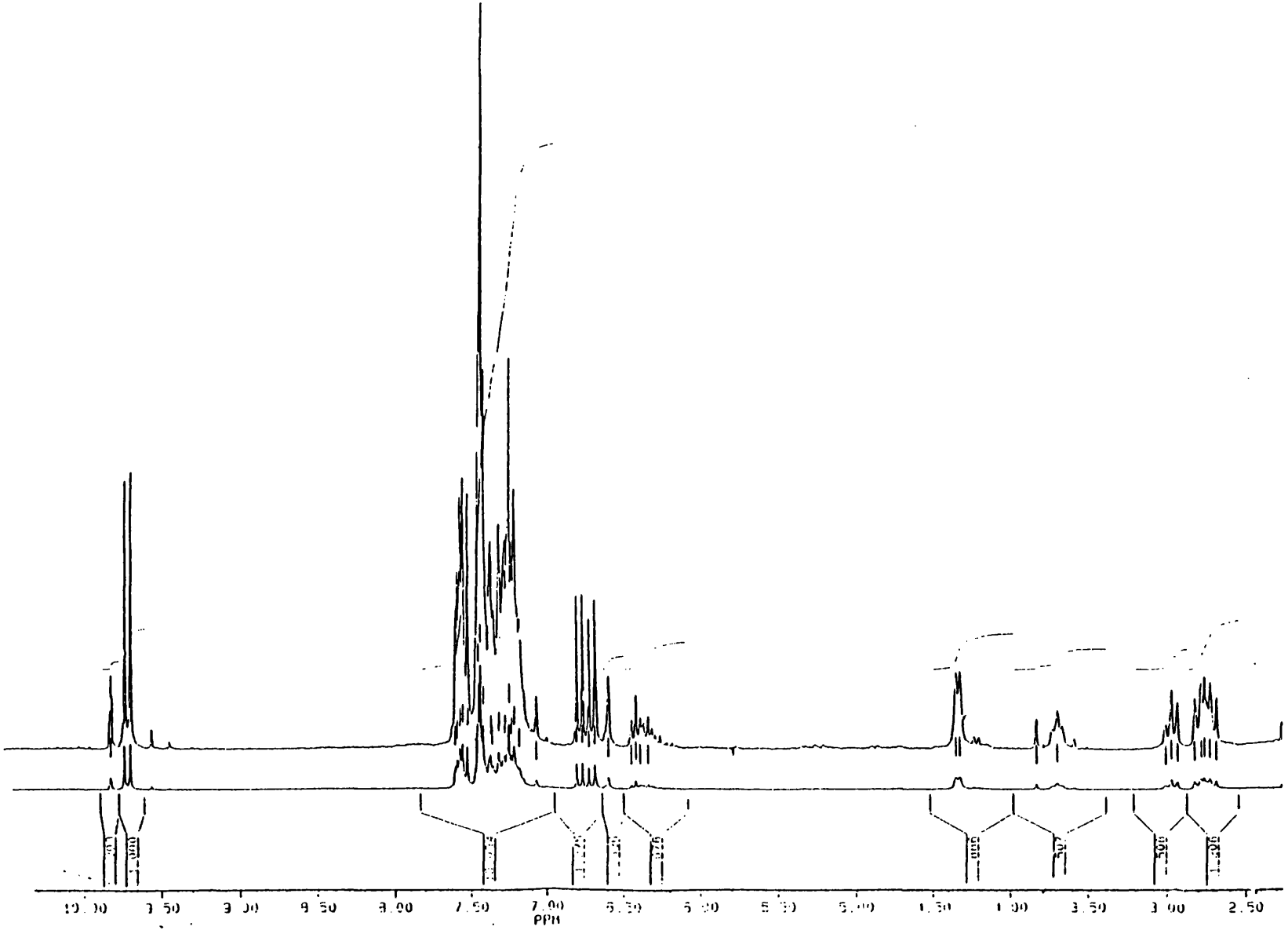

Figure 5.43 ^{1}H NMR Spectrum of Reaction of Cinnamaldehyde with Hydrogen.

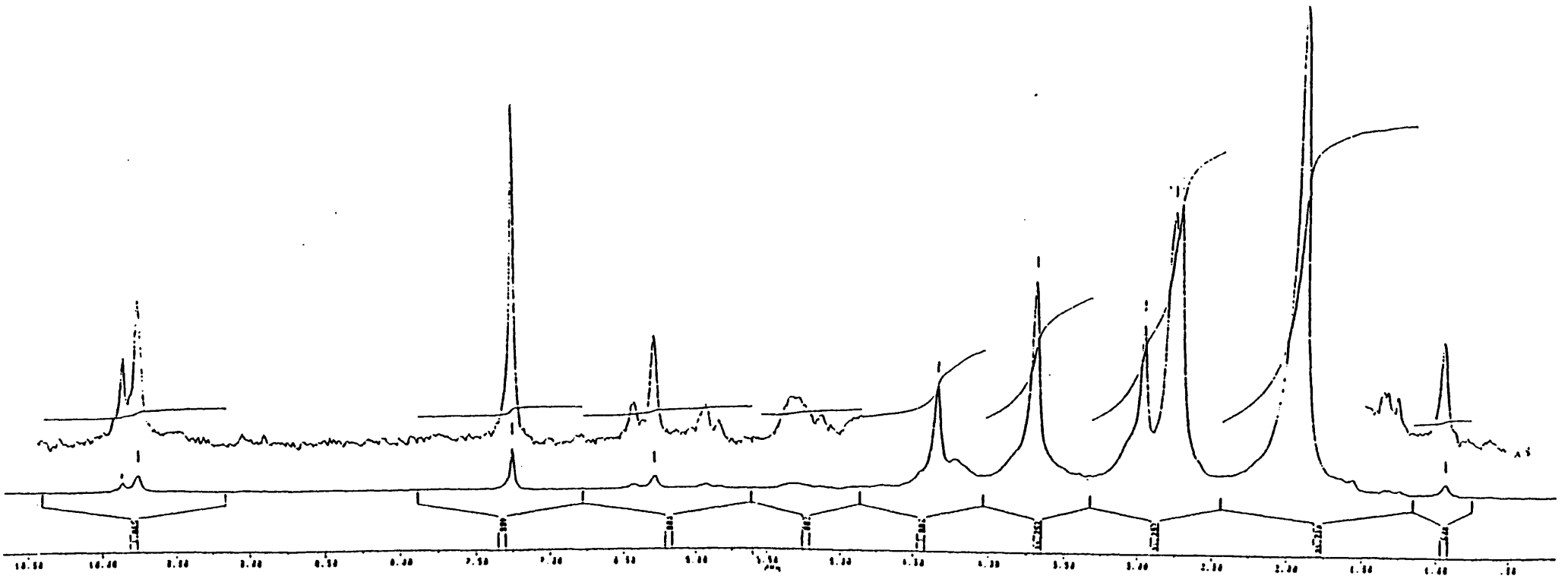

Figure 5.44 ^{2}H NMR Spectrum of Reaction of Cinnamaldehyde with Deuterium.

5.8 TRANSMISSION ELECTRON MICROSCOPY

G.U. CuO/SiO_2 and ICI CuO/SiO_2/PQ *a* were studied by transmission electron microscopy (TEM) after reduction in H_2/N_2 in order to ascertain whether the observed differences in reducibility and catalytic activity could be accounted for by differences in their particle morphologies or particle size distributions. The micrographs are shown in Figures 5.45 and 5.46.

ICI CuO/SiO_2/PQ *a* showed a wide range of particle sizes , from ≈ 10 nm to ≈ 250 nm, under the microscope.

G.U. CuO/SiO_2 contained less very small particles resulting in an overall increase in particle size. Some large clusters, of ≈ 1000 nm, were also observed.